DETERMINATION OF HULL EFFICIENCY PARAMETERS FOR A DEEP SUBMERGENCE HULL FORM

by

HENRY A. MORGAN, JR.

and

WALTER S. SZCZYPINSKI, JR.

DETERMINATION OF HULL EFFICIENCY PARAMETERS FOR A DEEP SUBMERGENCE HULL FORM

by

HENRY ANTHONY MORGAN, JUNIOR, LIEUTENANT, UNITED STATES NAVY

S.B., United States Naval Academy

(1959)

WALTER STANLEY SZCZYPINSKI, JUNIOR, LIEUTENANT, UNITED STATES NAVY

S.B., United States Naval Academy

(1959)

SUBMITTED IN PARTIAL FULFILLMENT

OF THE REQUIREMENTS FOR THE

MASTER OF SCIENCE DEGREE IN MECHANICAL ENGINEERING

AND THE PROFESSIONAL DEGREE, NAVAL ENGINEER

at the

MASSACHUSETTS INSTITUTE OF

TECHNOLOGY

June, 1966

Signature of Authors _____

_____

Department of Naval Architecture and Marine Engineering
May 20, 1966

Certified by _____
Thesis Supervisor

Accepted by _____
Chairman, Departmental Committee
on Graduate Students

DETERMINATION OF HULL EFFICIENCY PARAMETERS

FOR A DEEP SUBMERGENCE HULL FORM

by

Henry A. Morgan, Jr., Lt., U.S.N.

Walter S. Szczypinski, Jr., Lt., U.S.N.

Submitted to the Department of Naval Architecture and Marine Engineering in partial fulfillment of the requirements for the degree of Master of Science in Mechanical Engineering and the professional degree, Naval Engineer.

ABSTRACT

The objective of this thesis is the experimental determination of the wake fraction (w) and the thrust deduction factor (t) for a deep submergence hull form. The development of a model with a length to diameter ratio of 1.97 was based on potential flow theory using superposition of sources and sinks on a uniform fluid stream. This hull form was tested in a propeller tunnel with both an open and a shrouded propeller. The shroud design was based on fundamental circulation theory utilizing concepts developed by Dr. J. D. van Manen.

Wake fraction is obtained by conducting a velocity survey in the plane of the propeller behind the model. The thrust deduction factor is determined from the results of three distinct tests which provided the thrust and drag acting on the model. The hull efficiency (e_h) is computed from the ratio (1-t)/(1-w).

Test results for the model with an open propeller are: w = .302, t = .271, e_h = 1.05. These results compare favorably with those published for model tests on submarines and bodies of revolution. The test results for the model in the shrouded condition are: w = -0.191, t = 0.198, e_h = 0.669.

Since the hull efficiency alone does not offer a totally conclusive comparison of the shrouded and unshrouded conditions, the respective propulsion coefficients (P.C.) are evaluated for this purpose. For the two specific systems analyzed, the propulsive coefficient was found to be lower in the shrouded condition. This is attributed to light propeller loading, large clearance between blade tips and nozzle wall, and the restricted fluid flow around the model within the test chamber.

Thesis Supervisor: S. Curtis Powell

Title: Associate Professor of Marine Engineering

ACKNOWLEDGEMENTS

Without the encouragement, advice, and recommendations of many people, this work would not have been possible. In particular, the authors are sincerely grateful to the following persons:

Professor S. Curtis Powell, who as thesis advisor, provided the guidance and counsel so necessary for the successful completion of the investigation.

Mr. James W. Mavor, Jr. (Woods Hole Oceanographic Institution), good friend and naval architect, whose administrative liaison between the authors and the Woods Hole Oceanographic Institution made this entire project possible.

Professor Andrew A. Fejar (Director, Department of Mechanical and Aerospace Engineering, Illinois Institute of Technology), friend and tutor par excellence, who indelibly influenced this work in its early stages.

Professor Justin E. Kerwin, whose guidance and instruction in propeller theory and Kort nozzle theory proved invaluable.

Professor Neal A. Brown, whose instruction and advice on the physical concept of open-jet theory is deeply appreciated.

Mr. James Sullivan (Woods Hole Oceanographic Institution), teacher and pattern maker, who turned and built the model body and nozzle. His efforts reflect only the highest quality of workmanship.

Mr. Kim David Saunders (Rose Polytechnical Institute), close friend and fellow student, who aided in preparing the source-sink computer program.

Miss Louise E. Carella, who tirelessly and efficiently typed the manuscript.

We wish to acknowledge the M.I.T. Computation Center and the Woods Hole Oceanographic Institution Computation Center for the use of their facilities. In addition, we are grateful to the Graphic Arts Department of W.H.O.I. for their excellent services.

TABLE OF CONTENTS

LIST OF FIGURES

LIST OF TABLES

CHAPTER I

INTRODUCTION

The last three years have seen a greatly expanded interest and activity in the field of manned deep submersibles, a part of which stemmed directly from the tragic loss of the submarine THRESHER. More recently, the operational success of the deep-submergence research vehicle ALVIN has heightened the emphasis on the exploration of the ocean depth.

Although submarine technology has developed markedly during the post-World War II era, the limitations and problems encountered at extremely deep depths require a comparatively more sophisticated technology. The extreme pressures and currents experienced at these depths necessitate improved naval architectural and engineering applications, especially with regard to the hull forms.

Unlike the conventional submarine, the length to diameter ratio of a deep-submergence hull form is in the vicinity of 2.5, an area where only limited experimental work has been undertaken. Consequently, the hull efficiency parameters applied in the design of a deep-diving vehicle are generally the same as those employed for submarines which are designed to operate at considerably more shallow depths. As a result, the wake fraction and thrust deduction factors used in deep-submersible design reflect estimates based on conventional submarines experience.

In light of these facts, it was concluded that an experimental analysis of a deep-submergence body and propeller combination would yield necessary data for determining the actual hull efficiency parameters over a limited speed range. With this motivation, an appropriate hull form was developed and a series of tests were devised.

The experimental tests and analysis were performed on the model with two distinct screw* configurations - an open propeller and a shrouded** propeller.

The wake fraction, thrust deduction factor, and related conclusions resulting from this project may prove useful in the expanding technology associated with the field of deep-submergence.

---

* The words screw and propeller are used interchangeably throughout this thesis.

** The words shroud and nozzle are used interchangeably throughout this thesis. They infer a Kort nozzle which is fixed to the hull, as opposed to the concept of a cylinder attached to and rotating with the propeller.

CHAPTER II

TEST PROCEDURE

General

The hydrodynamic study which led to the determination of the hull efficiency parameters may be divided into two principal categories:

1. the development of the model, including the hull form, propellers, and shroud.
2. the experimental investigation of the hydrodynamic flow about the model in the propeller test tunnel.

Presented in this section are the assumptions, theories, and procedures used in the design of the complete model and its installation for testing in the M.I.T. Propeller Tunnel. The series of tests conducted on the model with both open and shrouded propeller are also described in detail.

Model Development

A. Body

The development of an appropriate model for testing purposes was governed by three independent requirements. These factors were the similarity of hull form to an actual deep-submersible, compatibility of the model with the testing facility, and the feasibility of applying proven mathematical techniques in the development.

In order to fulfill the initial requirement that the model shape be similar to an existing or proposed deep submergence vehicle

the deep diving submarine, ALVIN, belonging to the Woods Hole Oceanographic Institution was selected as a prototype. ALVIN was designed with a length to diameter ratio of 2.6 and a stern propeller diameter to body diameter ratio of 0.53. Based on this parent hull form, the following criteria were established:

$$2.0 \leq \left[{}^{L}/_{D} \right]_{Model} \leq 3.0$$

and

$$0.40 \leq \left[\frac{\text{Prop. Diameter}}{\text{Body Diameter}} \right]_{Model} \leq 0.80$$

Next the physical dimensions of the propeller tunnel test facility at M.I.T. were closely studied. The inlet and exit nozzles to the test chamber are 20 inches in diameter and emerge into an open test chamber of 60 inch diameter. The open jet flow in this section traverses 26 inches. Review of tunnel records indicated that best test results were obtained for propellers of about 12 inch diameter and that unsatisfactory results were common for propellers of less than six-inch diameter. Consequently, the tunnel dimensions led to establishment of the following limitations:

1. Model length not to exceed 24 inches. Insertion of a propeller behind the body would extend overall length by 3 to 5 inches.
2. Model diameter limited to a maximum of 13 inches.
3. $6 \leq$ Propeller diameter (inches) ≤ 14.

In order to satisfy all the criteria and limitations established to this point, numerous combinations of model dimensions were graphically outlined. Consideration of the aforementioned requirements coupled with

ease of fabrication and installation led to the selection of the following target characteristics:

Body Length - 24 inches

Body Diameter - 12 inches

Propeller Diameter - 8 inches

Since it was envisaged that ideal velocity flow patterns would prove useful in this thesis, it was decided to develop the proposed body of revolution by stringing sources and sinks of suitable strength along the body axis and superposing a uniform flow parallel to that axis.

Although a three dimensional flow is generally complicated to analyze, the axisymmetric form of the body reduces the problem to a specialized case, which has been previously solved in the field of applied hydrodynamics by Milne-Thomson (17).

Combining a uniform stream along the horizontal axis with a point source of strength m and a combination point and line sink of total strength m, yields the following stream function:

$$\psi = -\frac{1}{2}UW^2 - \frac{A}{C}m\left[\sqrt{(X-B)^2+W^2} - \sqrt{(X-B-C)^2+W^2}\right] + \frac{mX}{\sqrt{X^2+W^2}} - (1-A)m\,\frac{X-B}{\sqrt{(X-B)^2+W^2}} \qquad (1)$$

where:

ψ = Stream Function

U = Uniform Free Stream Velocity

$\frac{1}{2}UW^2$ = Uniform Flow Stream Function Parallel to the X-axis in the positive direction

$\frac{mX}{\sqrt{X^2 + W^2}}$ = point source of strength m at the origin

A = dimensionless fraction denoting a percentage of total sink strength

B = distance from point source (origin) to point sink

C = length of the line sink

$(1-A)m \frac{X-B}{\sqrt{(X-B)^2 + W^2}}$ = point sink of strength $(1-A)m$ located at coordinates $(B,0)$

$\frac{A}{C} m \left[\sqrt{(X-B)^2 + W^2} - \sqrt{(X-B-C)^2 + W^2} \right]$ = line sink of strength Am and length C located between coordinates $(B,0)$ and $(B+C,0)$.

This development is illustrated below where P represents a locus of points on the periphery of the body.

FIGURE 1

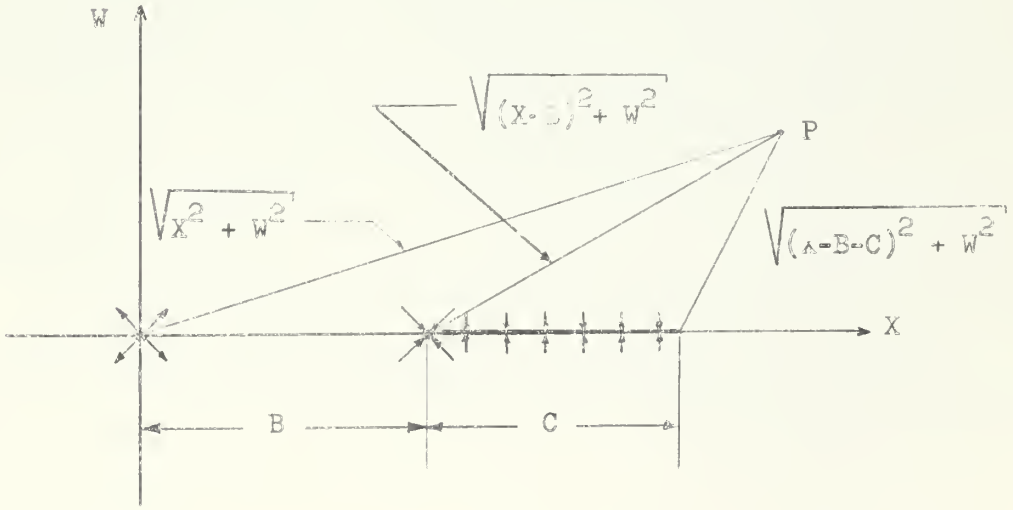

The model shape is formed only for the zero streamline. Upon dividing equation (1) through by m and setting $\psi = 0$, it becomes:

$$\frac{X}{\sqrt{X^2 + W^2}} - \frac{A}{C}\left[\sqrt{(X-B)^2 + W^2} - \sqrt{(X-B-C)^2 + W^2}\right]$$

$$- \frac{(1-A)(X-B)}{\sqrt{(X-B)^2 + W^2}} - \frac{1}{2}\left(\frac{U}{m}\right) W^2 = 0 \qquad (2)$$

Setting the four equation constants $\frac{U}{m}$, A, B, and C equal to 2.22, 0.5, 2.00 and 1.75 respectively reduces equation (2) to:

$$\frac{X}{\sqrt{X^2 + W^2}} - 0.286\left[\sqrt{(X-2.0)^2 + W^2} - \sqrt{(X-3.75)^2 + W^2}\right]$$

$$- \frac{0.5\ (X-2.0)}{\sqrt{(X-2.0)^2 + W^2}} - 1.11\ W^2 = 0 \qquad (3)$$

A graphical representation of this equation yields a body shape (Figure II) that meets the prescribed hull parameters resulting in a final length to diameter ratio of 1.97. This equation was solved by the body development computer program described Appendix B.

B. Unshrouded Propeller

The selection of the propeller used in the unshrouded tests was based on naval engineering assumptions, availability of a suitable standard stock propeller, and the requirement that the propeller be of eight-inch diameter.

FIGURE II

Model Hull Form Profile

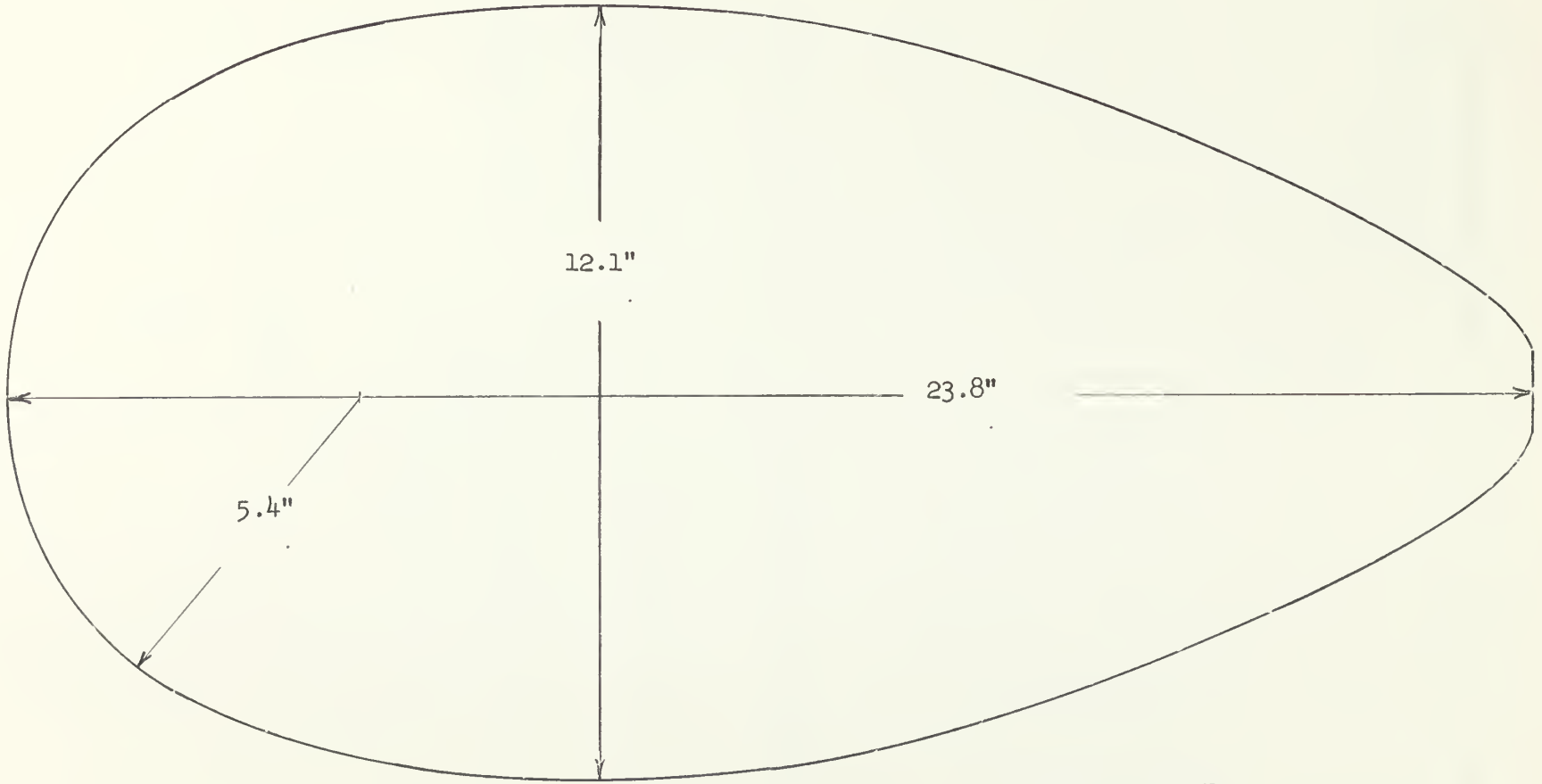

Scale - 1:2.7

Assumed parameters which led to the selection of the test propeller were as given below:

$$C_D \text{ (body)} = 0.25$$

$$1 - t = 0.90$$

$$1 - w = 0.80$$

An approach common to the field of propeller design was then followed. Using non-dimensional quantities, the standard propeller curves are entered and an operating curve developed to indicate optimum efficiency. The general method is related in the following paragraphs.

Model drag is a function of V_c^2 and is expressed as:

$$R = \frac{1}{2} \rho S C_D V_c^2 \tag{4}$$

The Taylor wake fraction, w, is defined by the equation:

$$1 - w = \frac{V_o}{V_c} \tag{5}$$

The thrust deduction factor, t, is defined by the equation:

$$1 - t = \frac{R}{T} \tag{6}$$

Combining these three equations and solving for thrust:

$$T = \frac{C_D \rho S V_o^2}{2 (1 - t)(1 - w)^2} \tag{7}$$

Since by definition:

$$K_t = \frac{T}{\rho n^2 D^4} \tag{8}$$

and

$$J = \frac{V_o}{nD} \tag{9}$$

Appropriate algebraic substitution leads to the non-dimensional expression:

$$\frac{K_t}{J^2} = \frac{C_D S}{2 (1 - t)(1 - w)^2 D^2} \qquad (10)$$

Substituting the cross-sectional area of the model body, S = .817 sq. ft., previously determined together with the assumed parameter values yields the following result:

$$\frac{K_t}{J^2} = 0.398$$

The curve of this parabolic equation was superposed on a type B.3.35 propeller curve in reference (19). At each intersection of the K_t/J^2 curve with the family of K_t and K_q versus J curves the propeller efficiencies were noted for each pitch ratio. The highest propeller efficiencies were observed in the range:

$$0.8 \leq \frac{P}{D} \leq 1.1$$

On this basis, a standard stock propeller with the following characteristics was selected for the unshrouded tests:

Number of blades	3
Diameter	8 inches
Uniform P/D	1.0
Mean Width Ratio	0.31
Hub Diameter	1.375 inches

C. Shrouded Propeller

Design of the propeller used in the shrouded condition was based primarily upon conclusions and recommendations presented in several papers by J. D. van Manen. In order to retain as much similarity as practicable to the open propeller, yet satisfy the basic requirements for a suitable nozzle propeller, only minimum modifications were made to the open propeller characteristics. The fact that the system of nozzle and screw must form an integral unit as indicated by van Manen (13), was a governing factor in insuring that the final propeller design be adaptable to a shrouded configuration.

Since an eight-inch diameter propeller operated with satisfactory results in an open-water unshrouded test, the same diameter was retained. In addition, from van Manen and Superina (14) it was concluded that neither the radial pitch distribution of the screw nor the section shape of the propeller blades have a large effect on the efficiency of the shrouded propeller. It was also noted that a propeller with uniform pitch ratio and flat face sections did not show appreciable drawbacks with respect to efficiency or cavitation. Consequently, a uniform pitch ratio was incorporated in the propeller design.

In addition to the eight-inch diameter and uniform pitch ratio, a wide blade tipped propeller, commonly called a Kaplan type, was decided upon. Theoretically, this design prevents cavitation, and practically, it is more readily adaptable to the contour of a cylindrical nozzle wall

than the round tip propeller. This feature is significant since it permits attainment of smaller clearances between the full blade tip and the nozzle inner wall; thereby improving the overall system efficiency by reducing tip losses.

The general characteristics of the shrouded screw are presented below:

Type of blade sections: Wide tip; flat face; circular arc back

Number of blades: 3

Diameter: 8 inches

Uniform P/D : 1.0

Mean Width Ratio: 0.31

Hub Diameter: 1.375 inches

D. Shroud

Since the shrouded propeller design was completed and it had been established that the nozzle and propeller must form an integral unit, it was necessary that the nozzle design be thoroughly compatible with the selected propeller. Reference was made to numerous sources in order to find methods of incorporating the qualities of system compatibility, hydrodynamic soundness and structural durability in the final nozzle design.

Summarized from reference (14) are the following practical design characteristics which a nozzle should possess:

(a) An axial cylindrical part at the inner side at the location of the screw.

(b) A slightly diverging section behind the screw for improving astern efficiency and facilitating removal of the screw.

(c) An angle (α_i) of approximately 10 degrees between the outer nozzle wall at the tail and the shaft centerline axis.

(d) A minimum thickness - length ratio of about 0.15.

(e) A variation of diffuser - angle from 3.5 to 6.5 degrees and a variation in camber ratio from 0.05 to 0.09 in order to prevent serious loss in efficiency.

In addition, since it was expected that the shrouded propeller on a deep submergence vehicle would undergo at least moderately heavy loading, the choice of a relatively large length-diameter ratio was indicated in each of the references consulted. However, based upon an experimental investigation of propellers in nozzles as reported by Solovev (22) it was concluded that the length-diameter ratio should be no greater than 0.7. Based upon van Manen's satisfactory test results on nozzles with a length-diameter ratio of 0.5, a nozzle with ℓ/D equal to 0.7 could be expected to have a reasonable efficiency under heavy load conditions and properties under the free running condition which were not appreciably inferior to those of a shorter profile. Moreover, this ratio contributed fewer mechanical difficulties in fitting the shroud to the model as will be discussed in a later section of this thesis.

Reference (22) also indicated that the distance from the leading edge of the nozzle to the propeller plane should not exceed 0.35D. This latter criterion was confirmed in reference (12), where this distance was given as $\frac{1}{2}\ell \cos \alpha_i$. Substituting the accepted values for length-diameter ratio of 0.7 and angle α_i of 10°, results in the following:

$$\frac{1}{2}\ell \cos \alpha_i \approx 0.35D$$

Furthermore, the propeller should be located at the narrowest section of the nozzle with a minimum clearance between the tip of the propeller blade and the inside of the nozzle in order to realize minimum tip vortex losses. Although the optimum recommended clearance is about 0.01 of the diameter, in practice, the magnitude of this clearance generally ranges from 5 to 10 millimeters.

Additional parameters which are considered significant in the design of a nozzle are the outlet coefficient, F_o/F, and the inlet coefficient, F_i/F_P. F_i and F_o are the inlet and outlet nozzle area respectively, and F_P is the nozzle area at minimum nozzle diameter. According to the experimental data given in reference (22), the value of the outlet coefficient should be chosen within the limits of 1.0 to 1.10, and the inlet coefficient within the range of 1.30 to 1.65.

In order to incorporate into the shroud-propeller system the aforementioned design criteria, procedures advocated in several publications were analyzed and considered. The method which led to most nearly fulfilling all the design requirements discussed was the practical

"optimimum" solution of the "screw plus nozzle" combination proposed by van Manen in reference (10).

The reference propeller employed in this method has both uniform pitch and flat face sections similar to the shroud propeller designed and described in the previous section. Hence, the compatibility of the actual nozzle and screw system was considered adequate in this regard.

The general arrangement of the "optimum" nozzle exhibits two design features which are uncommon to standard nozzle profiles. The outside of the nozzle wall is straight and the trailing edge is thicker. In reference (13) it was noted that no considerable differences in performance were noted if the outer profile of a nozzle were made straight. Moreover, the operating curves of a nozzle with increased trailing edge thickness showed no appreciable drop in efficiency compared to a standard thin trailing edge.

Figure III given below identifies the nomenclature used in the shroud development. In Table I are presented the non-dimensional ordinates for the "optimum" nozzle design as developed by van Manen (10).

FIGURE III

Definition of Nozzle Dimensions

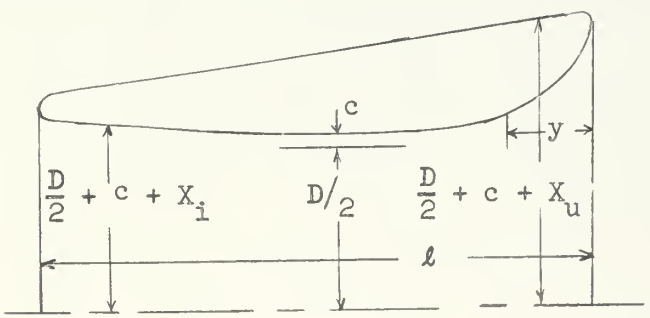

TABLE I

Non-Dimensional Ordinates for "Optimum" Nozzle

y/ℓ	0	1.25	2.50	5.0	7.5	10	15	20	25
Xi/ℓ	18.75	14.66	12.80	10.87	8.00	6.34	3.87	2.17	1.10
Xu/ℓ	-----	20.72	21.07	20.80		Straight Line			
y/ℓ	30	40	50	60	70	80	90	95	100
Xi/ℓ	0.48	Circular Cylinder			0.29	0.82	1.45	1.86	2.36
Xu/ℓ		Straight Line							$\pm$6.36

Selecting a length-diameter ratio of 0.7, the length of nozzle profile is fixed at 5.6 inches to enclose the 8 inch diameter propeller. The clearance between the blade tip and the inner wall of the nozzle was set at 3/16 inch. Although this distance is excessive relative to the desired clearance, the alignment of the screw within the nozzle and the tunnel torque shaft vibration indicated this clearance to be the smallest practically acceptable.

With these three parameters fixed, offsets for the shroud profile were calculated based on the "optimum" nozzle method and are presented in Table II. The actual nozzle profile is shown to scale in Figure IV.

Details of the final nozzle design are presented below:

ℓ	= 5.6 in.	ℓ/D	= 0.700
D	= 8.0 in.	F/ℓ	= 0.057
f	= 0.438 in.	s/ℓ	= 0.162
s	= 0.906 in.	F_o/F_P	= 1.030
c	= 0.188 in.	F_i/F_P	= 1.265
α_i	= 10^o		

The shroud was attached to the body by three brass mounting fins spaced at 120^o intervals around the body and shroud outer profiles. These fins were machined to a reasonable faired hydrofoil shape comparable to actual support bars extensively used for hull-shroud interconnections. An illustration of the mounting fin shape and method of attachment to the hull form is shown in Figure V.

TABLE II

Actual Nozzle Ordinates

y	0	.700	.140	.280	.420	.560	.838	1.12	1.40
X_i	1.02	.820	.816	.607	.448	.355	.217	.122	.0615
X_u	----	1.18	1.165		Straight Line				
y	1.68	2.24	2.80	3.36	3.92	4.48	5.04	5.32	5.6
X_i	.0268	Circular Cylinder			.0162	.0459	.0812	.104	.132
X_u		Straight Line							.356

FIGURE IV

Actual Nozzle Profile

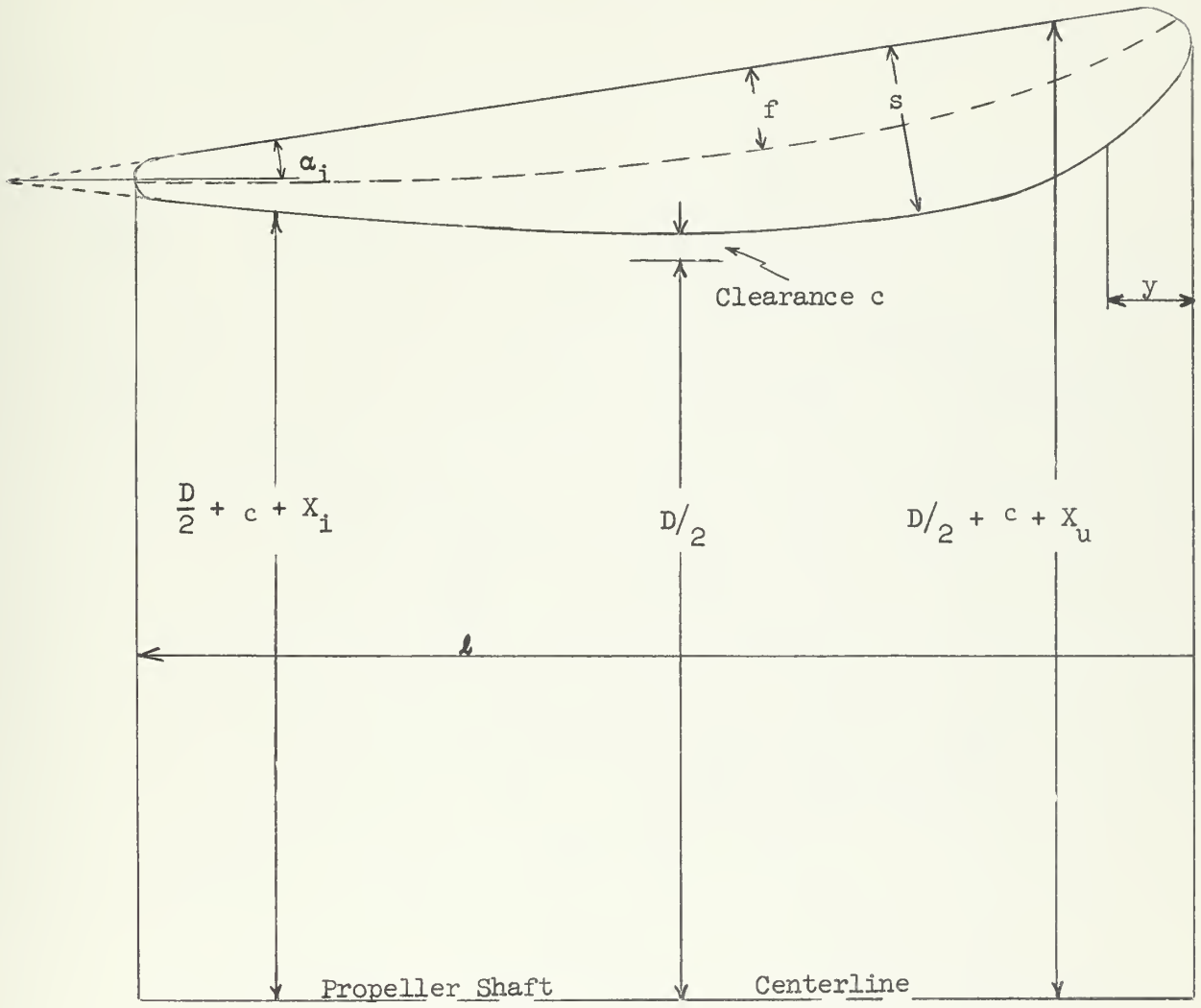

Principal Dimensions

$D/_2$ = 4.00 inches

ℓ = 5.60 inches

c = 0.188 inches

FIGURE V

Shroud Support Assembly

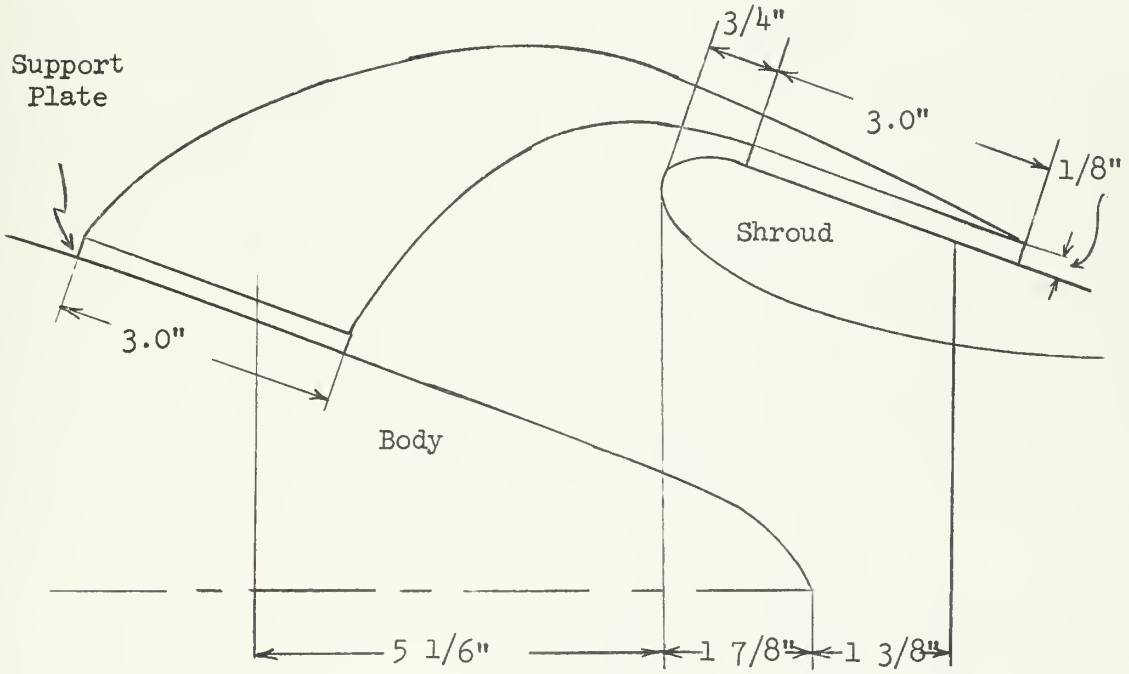

Side View

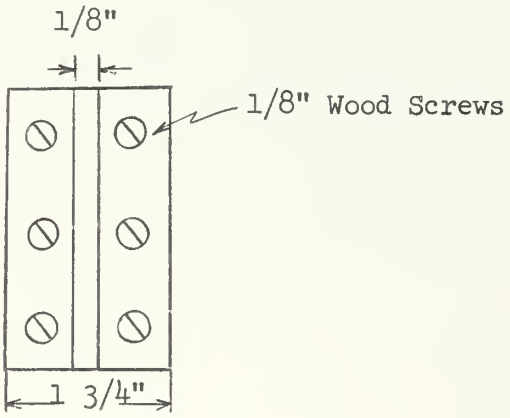

Support Plate Detail

Open-Water Propeller Test

The two propellers used in the unshrouded and shrouded tests respectively were initially subjected to open-water propeller tests. These tests adhered to the standard propeller tunnel test procedures employed at the Massachusetts Institute of Technology.

The testing chamber was vacant except for the propeller shaft. A torque sleeve was passed over the shaft and coupled to it securely with a brass key. Next, the propeller was mounted on a tapered shaft extension which screwed into the propeller shaft. This arrangement insured a snug fit of the propeller against the torque sleeve to which it was also pinned. Just forward of the propeller a hub fairing was mounted on a short protrusion of the propeller shaft extension and held in place with an Allen screw. This assembly is shown in Figure VI.

With the propeller installed, the tunnel was flooded and the propeller was rotated at an average speed of 1200 RPM. The water velocity controlled by an impeller pump was varied from 0 to 15 feet per second in incremental steps. At each velocity the thrust, torque, water pressure, and propeller RPM were recorded. In addition, zero readings of thrust and torque plus water temperature and atmospheric pressure were recorded. This information was transferred to data cards which were included in a computer program* devised to determine the faired offsets of K_t, K_q, and e_p as a function of J.

* Refer to Appendix C

FIGURE VI

PROPELLER ASSEMBLY

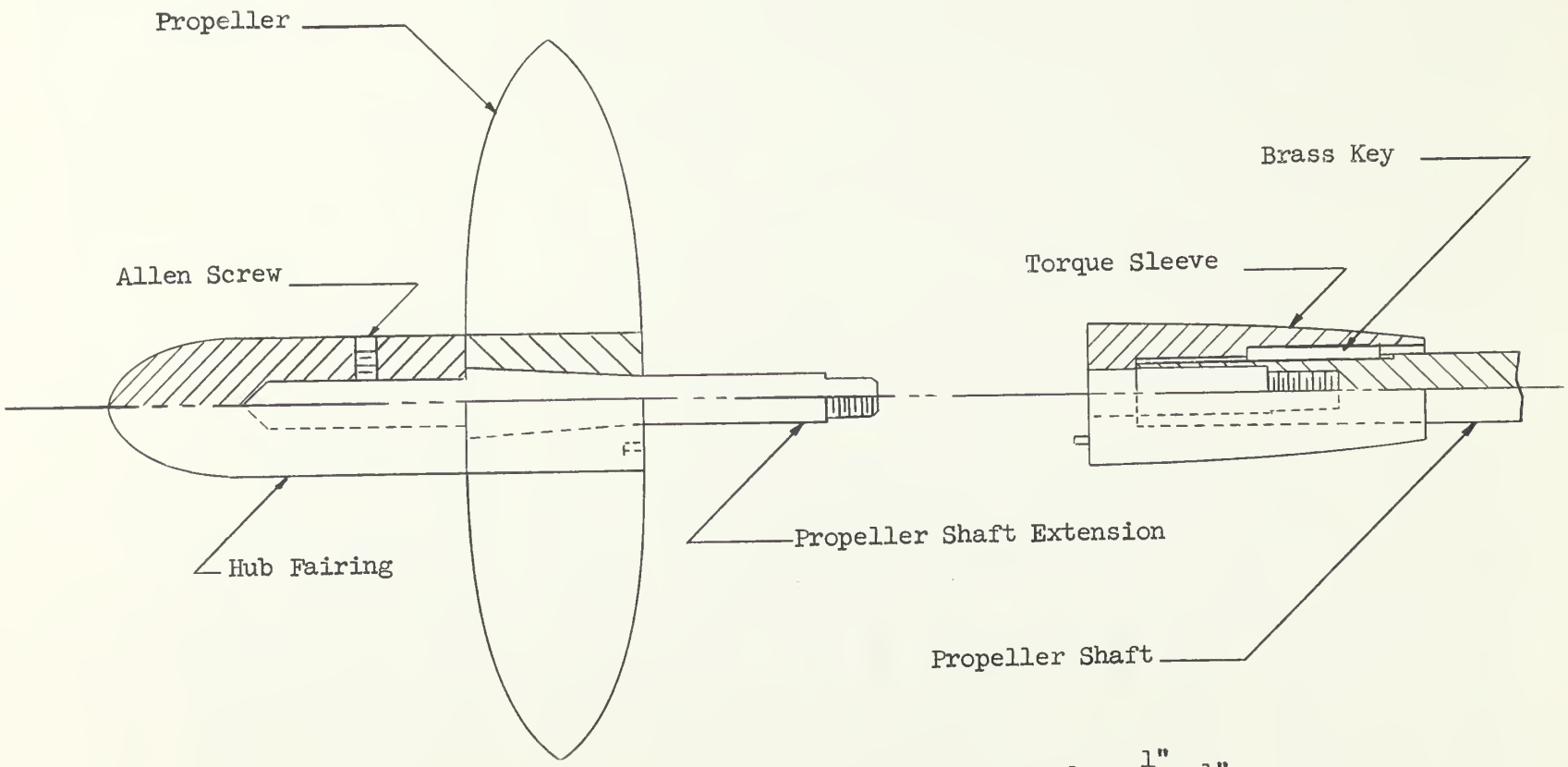

Scale: $\frac{1"}{2} = 1"$

Velocity Survey

As indicated by equation (5), the Taylor wake fraction is a function of V_o, the average velocity of the water in the plane of the propeller disc normal to the direction of flow and V_c, the effective free stream velocity of the test model. The purpose of the velocity survey is to experimentally determine these two parameters.

During this test, the body was mounted in a manner identical to that described in the previous section. The water flow past the stationary hull form was varied from 0 to 12 feet per second.

As the flow was altered, the propeller tunnel velocity, V_v, was measured forward of the body by reading a bromo-benzene gage which recorded the pressure differential at two pressure taps within the tunnel inlet nozzle. At each recorded V_v, a velocity survey was conducted astern of the body in the vertical plane of the propeller. This was accomplished by measuring the water velocity in incremental steps moving radially outward from the body center line axis. A calibrated pitot tube* was used for this purpose. A sketch of the general model arrangement is shown in Figure VII.

For the test employing the open propeller, this survey was conducted out to a radius of ten inches, being terminated at the periphery of the tunnel exit nozzle. With the shroud attached to the body, an identical test procedure was followed. However, in this case, the survey was limited between the body center line axis and the shroud inner wall, a distance of approximately four inches.

*Refer to Appendix D

The data, which included the velocities V_v and V_o and the corresponding radial distances at which they were measured, was used in the wake fraction analysis for both the unshrouded and shrouded propeller conditions.

FIGURE VII

VELOCITY SURVEY ARRANGEMENT

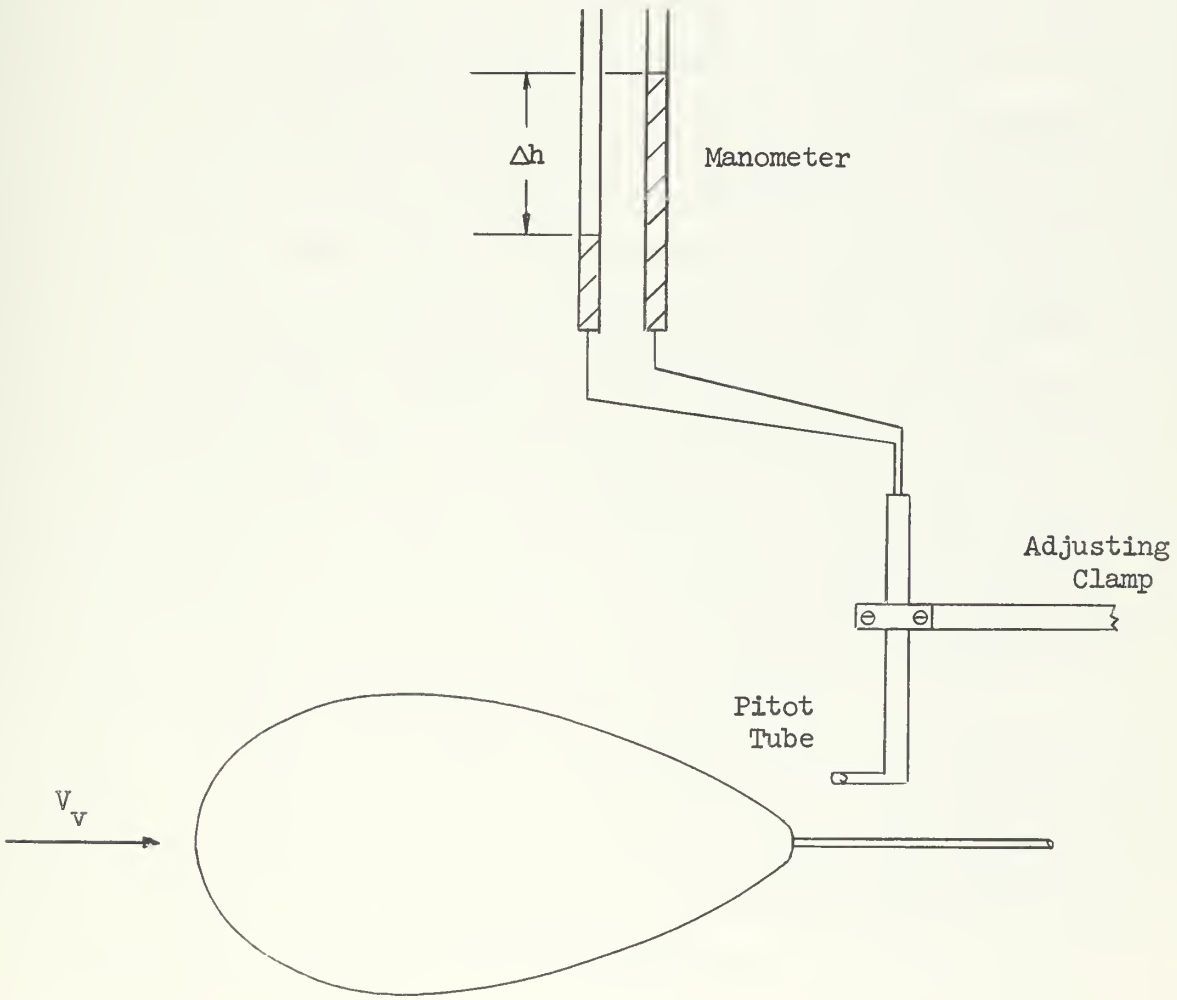

Model Drag Test

Normally a model drag test is conducted in a towing tank in which a model is towed at a specified speed. In this case, the model drag is measured by a dynamometer attached to a towing assembly. However, in the propeller tunnel this is not possible. The body must be kept stationary and the water must be made to flow past the body. It is evident that the results will be equivalent.

In order to conduct this test, it was necessary to mount the body in the test chamber in a manner such that it remained parallel to the flow, yet maintained freedom sufficient for small axial movement thereby permitting accurate drag measurements. This arrangement was effected by using six cables extending normal to the center line axis of the body. These cables were run through three 3/4 inch square iron bars, which were mounted between the tunnel nozzles and attached to their outer peripheries. Each bar was fitted with two adjusting screws through which a cable from the body was passed and then secured by cable clamps that rested on these screws. The other end of each cable was attached to a 1/4 inch iron closed marine type eye bolt by a standard nico-press splicing process. The eye bolts were inserted into countersunk holes and screwed into the body.

Three of the cables were located 120 degrees apart in a plane normal to the center line and seven inches aft of the most forward point of the model. In a similar manner, the remaining three cables were mounted ten inches aft of the forward group.

Figure VIII shows the general body mounting arrangement. Section A - A' of this figure is reproduced in larger scale in Figure IX.

Into the stern of the body and concentric with its center line axis was inserted a two inch long, 3/4 inch O.D. brass tube. This tube serves two purposes. First, it acts as a guide for the propeller shaft extension which supports the body in the fore and aft direction. Secondly, a 5/8 inch thrust bearing is supported in the forward most part of this guide tube.

The thrust bearing serves to transmit the drag developed on the model body to the propeller shaft extension without a transmission of torque. This requirement is mandatory since the propeller shaft must be rotating for accurate thrust measurements.

The fluid flow velocity past the body was regulated by a rheostat control on the propeller tunnel impeller pump. At each selected flow rate, the drag force developed on the body was measured. It was then possible to determine the functional relationship between drag and velocity through analysis.

Propeller Test with Body Disturbing Flow

In order to examine the performance of the propeller operating behind the model, the support arrangement described in the drag test section was slightly modified. Two cables were nico-pressed to a single 1/4 inch closed eye bolt. This bolt was aligned with the body center line axis and inserted into the forward end of the body. The cables were led forward and passed through two pre-drilled holes (180° apart) in the periphery of the tunnel inlet nozzle.

FIGURE VIII

GENERAL BODY MOUNTING ARRANGEMENT

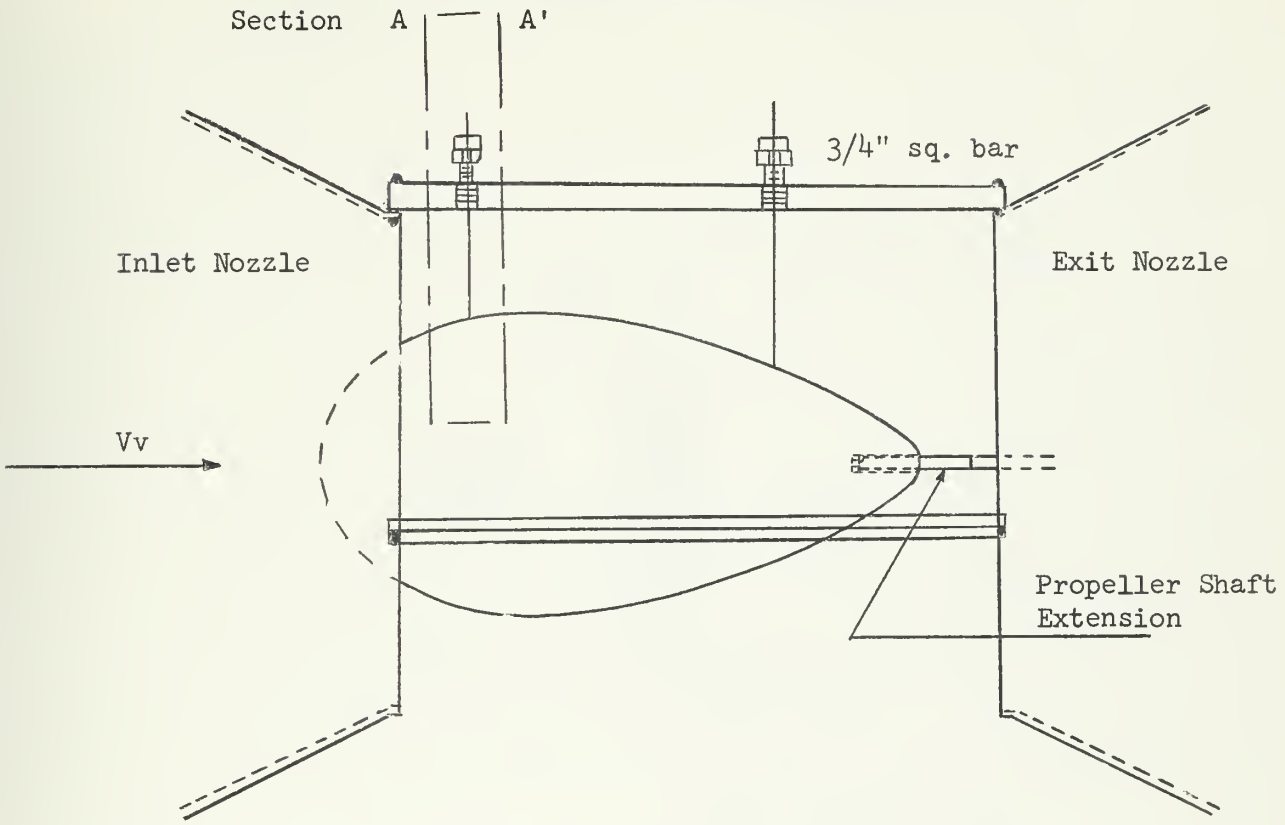

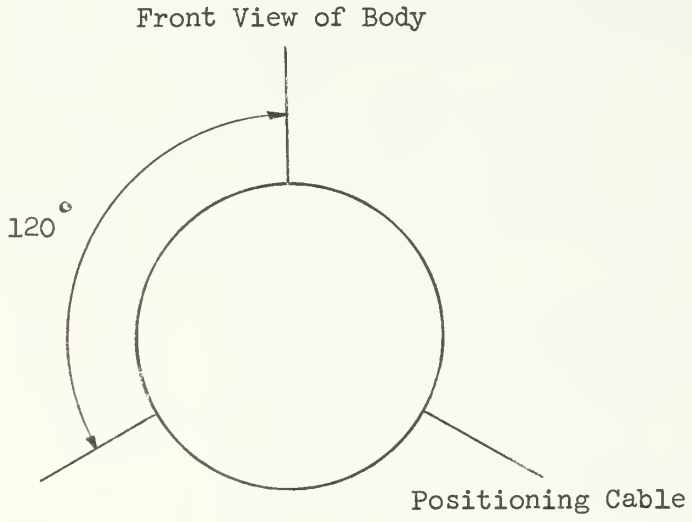

FIGURE IX

SECTION A - A' OF GENERAL BODY MOUNTING ARRANGEMENT

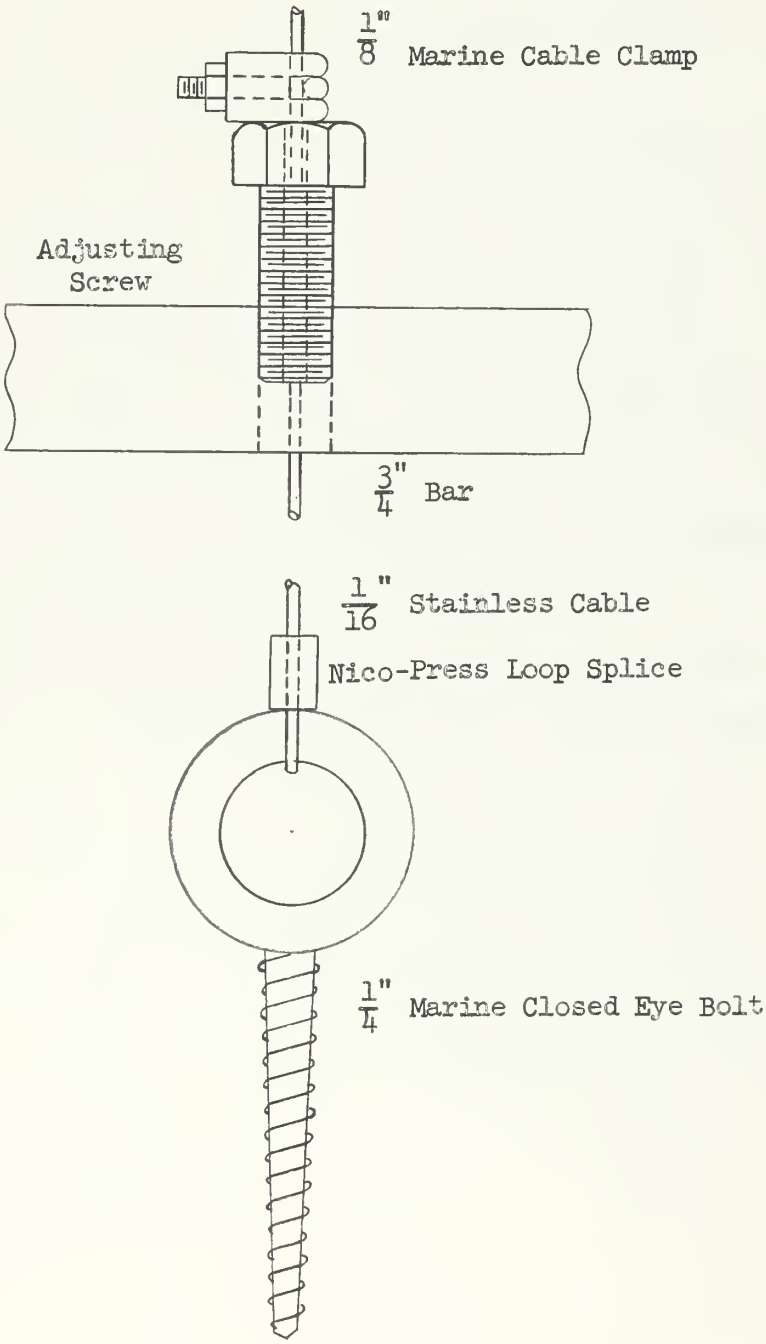

Each cable end was then attached to one extremity of a medium size turnbuckle, the other end of which was permanently secured to a flange protruding from the outer periphery of the tunnel inlet nozzle. The two turnbuckles were adjusted to exert sufficient tension on the wires to pull the body forward about one inch and thereby prevent it from seating on the propeller shaft extension.

Since the model was not in contact with the propeller shaft, it served only to alter the fluid flow passing through the propeller. Hence, the test procedure and data reduction were essentially identical to that described in the section on the open-water propeller test. With the model in this position, the thrust coefficient differs from that of the open-water test due to the body disturbing the flow, while the torque coefficient remains virtually unchanged due to non-contact between body and propeller shaft extension.

The reduced data from this test is used for the thrust deduction analysis of both the open and shrouded propeller configurations.

Operating Point Test

The purpose of this test was to determine the shaft revolution rate at the optimum operating condition for each fluid velocity. The body mounting arrangement was similar to that described in the drag test procedure. The only modification was the attachment of the propeller to the propeller shaft extension, which was inserted into the body stern and rested freely in the model thrust bearing.

Initially, the tunnel was operated at zero impeller velocity. The shaft revolution rate was varied from about 300 to 40 RPM. The voltmeter readings and pan weights, which indicated the thrust exerted, were recorded at each RPM. This data was used to determine the value of thrust at zero RPM; that is, the inherent thrust produced as a result of the tunnel propeller shaft configuration.

Next, the fluid flow rate was varied from 2 to 12 feet per second. At each selected fluid velocity, the shaft revolution rate was controlled over a range of RPM values. At each specified RPM, the corresponding thrust values were recorded. These thrust values combined with the zero thrust reading over the associated RPM range were then analyzed to determine the propeller operating point at each speed. This investigation is explained in the Thrust Deduction Section of Chapter III.

CHAPTER III

TEST ANALYSIS

Wake Fraction

The calculation of the Taylor wake fraction for both the unshrouded and shrouded model configuration is based on data obtained during the respective velocity survey tests.

As indicated in Chapter II, the fact that the body was positioned within the limited confines of the test chamber required that the incoming free stream velocity be adjusted to compensate for this restriction. The development of this concept* indicates that the effective free stream velocity, V_c, is related to the propeller tunnel velocity V_v, by the expression:

$$V_c = k\, V_v \qquad (11)$$

For each effective free stream velocity there exists a family of velocities in the plane of the propeller which vary as a function of the distance from the center line axis of the body. The tabulation and illustration of this average velocity, V_o, plotted versus the respective distance from the axis are presented in Figures XIV-XXIII of Chapter IV. Since the propeller radius is four inches, an analysis of the velocity distribution within an eight-inch diameter disc, concentric with the body center line axis, results in an average V_o.

---

* Refer to Appendix E

The averaging process leading to this result is illustrated in Figure X, which shows the propeller disc divided into a series of concentric discs and a general plot of the velocity in the propeller plane versus the radial distance.

FIGURE X

VELOCITY PROFILE IN THE PROPELLER PLANE

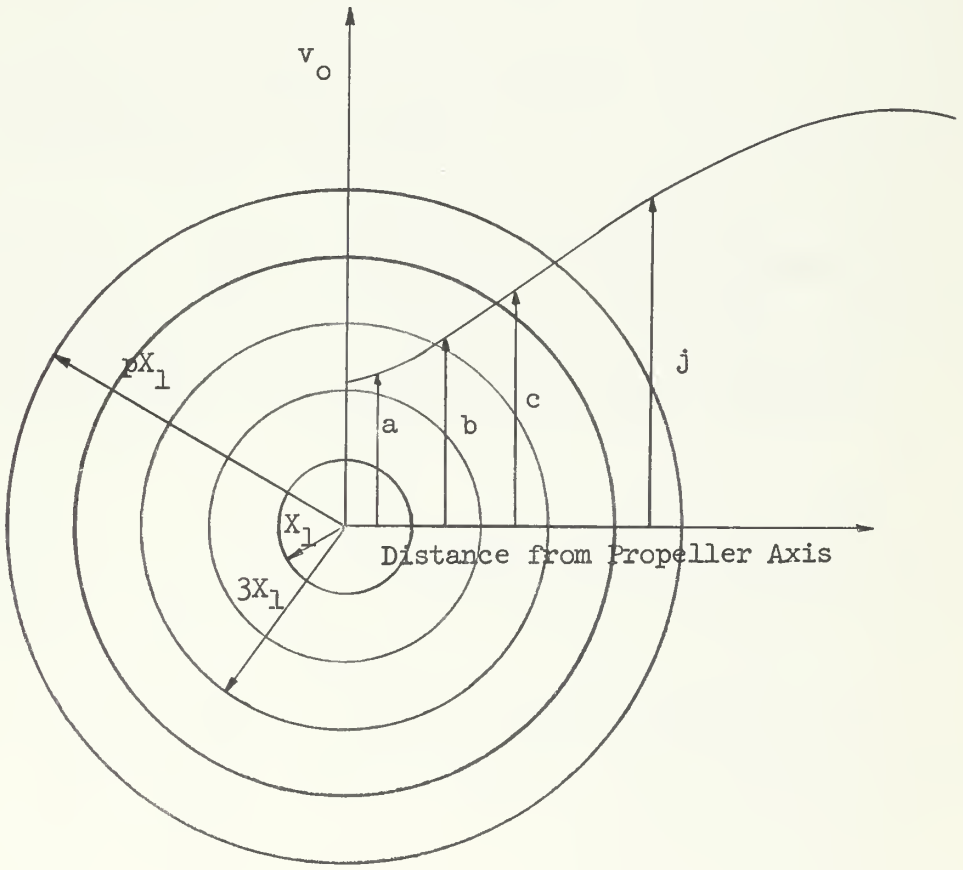

For each concentric disc, the mean velocity, $v_o(a,b,c,d,.....j)$, is read graphically and weighed proportionately with its respective disc area. This process may be represented by the relation:

$$(p^2 X_1^2 \pi)\, v_o = X_1^2 \pi a + \left[(2X_1)^2 - X_1^2\right] \pi b + \left[(3X_1)^2 - (2X_1)^2\right] \pi c + ... + \left[(pX_1)^2 - ((p-1)X_1)^2\right] \pi j \qquad (12)$$

Reducing this equation to:

$$p^2 V_o = a + 3b + 5c + 7d + ... + (2p-1)j \qquad (13)$$

the average velocity in the propeller disc becomes:

$$V_o = \frac{a + 3b + 5c + ... + (2p-1)j}{p^2} \qquad (14)$$

Consequently, with the velocity in the propeller plane known at the corresponding effective free stream velocity, the Taylor wake fraction, w, is determined and represented by the common expression:

$$(1-w) = \frac{V_o}{V_c} \qquad (5)$$

A graphical representation of the quantity (1-w) plotted with respect to V_c is presented in Chapter IV.

The preceding analysis procedure used to determine the wake fraction over a selected speed range is identical for both the unshrouded and shrouded model condition.

Thrust Deduction

The thrust deduction factor, t, was previously defined by the relation:

$$(1-t) = \frac{R}{T} \tag{6}$$

To determine this factor for the deep submergence hull form, the compilation and analysis of data from three of the previously described tests is required. The actual operating RPM of the propeller at each specified flow velocity is determined from the operating point test. Thrust is deduced through analysis of the propeller test with body disturbing flow. The drag test yields the resistance force at each corresponding flow velocity.

Based upon the propeller tunnel geometry a free body diagram (Figure XI) is constructed of the actual forces acting on the body while undergoing the operating point test. Equilibrium equations are then developed as the basis for analytical determination of the thrust deduction factor.

The basic equilibrium equation may be written as:

$$Y - R = \left[3\, W_a - W_f + \frac{VMU}{C_o} \right] + K \tag{15}$$

where the quantity in brackets is designated:

$$P = \left[3\, W_a - W_f + \frac{VMU}{C_o} \right] \tag{16}$$

Hence, equation (15) may now be written:

$$Y - R = P + K \tag{17}$$

FIGURE XI

FREE BODY DIAGRAM - OPERATING POINT TEST

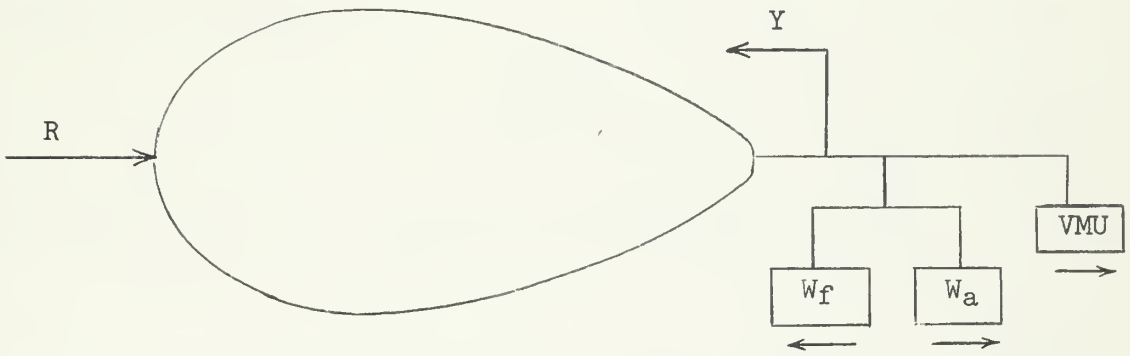

Positive Direction (←—)

Definition of symbols used in conjunction with the above figure:

C_o = conversion factor (see Appendix F) (VMU/lb_f)

K = constant thrust developed at zero velocity (lb_f)

Y = propeller thrust developed (lb_f)

R = body drag (lb_f)

W_f = weight acting to create CCW moment (lever arm = 1) (lb_f)

W_a = weight acting to create CW moment (lever arm = 3) (lb_f)

VMU = voltmeter thrust readings (VMU)

Applying the boundary conditions:

When the propeller tunnel velocity, V_v, equals zero and the propeller is stationary (N = 0), the expression (Y - R) = 0 and P = P_o. Thus, equation (17) becomes:

$$0 = P_o + K \tag{18}$$

and equation (16) becomes:

$$P_o = \left[3 W_a - W_f + \frac{VMU}{C_o} \right]_o \tag{19}$$

Substituting equation (18) into equation (17) gives:

$$Y - R = P - P_o \tag{20}$$

The data recorded for the segment of the operating point test during which the impeller velocity was set to zero is now converted to pound force units through equation (16) for each specific RPM. The calculated values of P are plotted along the ordinate axis versus the corresponding N (RPM) value along the abscissa. Extrapolating this curve to N = 0, the value at which it intersects the ordinate is defined as P_o in accordance with equation (19). Because adjustment of the measuring apparatus was necessary during the conduct of the experiment, the P_o value used for the analysis of the operating point test at V_v = 3 ft/sec and the value used for the succeeding velocities are based on different sets of data. The tables of data from which the corresponding P_o values result are presented in Appendix J.

For each selected fluid velocity, the voltmeter readings and pan weights recorded at each RPM are also converted to pound force units as previously described in order to yield a value of P corresponding to each N. Algebraically combining these values of P with the constant value P_o in accordance with equation (20) yields a value of $(P - P_o)$ for each value of N over the range tested.

Plotting $(P - P_o)$ with respect to N produces a curve which intersects the abscissa at the actual operating RPM for the specified fluid velocity. These operating point curves are presented in Chapter IV.

With these operating values of N and V_v, the advance coefficient, J, is found from the previously defined identity:

$$J = \frac{V_o}{nD} \tag{9}$$

where: $V_o = k V_v (1-w) = V_c (1-w)$

$n = N/60$

Hence, equation (9) is written in the form:

$$J = \frac{V_c (1-w)}{(N/60) D} \tag{21}$$

Using the value of wake fraction determined in the preceding section of this chapter, and designating the combined constants in equation (21) as C_1, the equation is reduced to:

$$J = C_1 \left(\frac{V_c}{N}\right) \tag{22}$$

Theoretically, the propeller operates at a constant advance coefficient. The operating RPM is plotted versus the corresponding V_c. By a method of least squares curve fitting, the resulting plot, a line of constant slope, intersects the coordinate axis at the origin. This curve is presented in Chapter IV and the associated mathematical analysis is outlined in Appendix H.

Using the N picked off the faired curve at any of the corresponding selected velocities, the constant value of J is calculated. With this value of the advance coefficient, the K_t versus J corrected curve resulting from the test with body disturbing flow is entered to pick off the corresponding value of propeller thrust coefficient.

Therefore, all the parameters of equation (23) are known. This permits solution for the thrust at each selected velocity.

$$T_c = \rho n^2 D^4 K_t \qquad (23)$$

By combining constants, this equation is reduced to:

$$T_c = C_2 N^2 K_t \qquad (24)$$

Now, substituting the values of N across the range of selected velocities generates values of thrust for the combination of model and supporting cables. The excess thrust required to overcome the cable drag,* R_{mdc}, is subtracted from the combined thrust to yield the thrust, T, exerted on the hull form alone.

With the thrust known, the next logical step is to analyze the drag test and to determine the body resistance. During this test the

---

* Refer to Appendix G

total combined model hull form and cable drag had been measured at each selected velocity. In order to find the body resistance alone, the cable drag is subtracted from the total drag. The resulting body drag may be expressed as:

$$R = f(\rho S V) \tag{26}$$

From fundamental fluid dynamics the drag is as previously given:

$$R = \frac{1}{2} C_D \rho S V_c^2 \tag{4}$$

This drag resistance is plotted versus its respective effective free stream velocity and a curve is fitted to the data points using the method of least squares.* This method results in the determination of the coefficients a_1, a_2, a_3 from the general parabolic equation:

$$y = a_1 + a_2 x + a_3 x^2 \tag{27}$$

where y and x represent dummy variables for the body drag and effective free stream velocity, respectively. The coefficients a_1 and a_2 approach zero, thereby reducing equation (27) to:

$$y = a_3 x^2 \tag{28}$$

Therefore, with all parameters known, the constant drag coefficient is found from the relation:

$$a_3 = \frac{1}{2} \rho S C_D \tag{29}$$

Hence, the drag test yields a significant hull parameter, C_D, as well as the body resistance as a function of velocity.

---

* Refer to Appendix H

With the thrust and drag of the body known at each corresponding effective free stream velocity, equation (6) is solved for the thrust deduction factor in the case of the unshrouded model configuration.

For the shrouded model configuration, the thrust produced by the nozzle must be added to the propeller thrust to yield the total thrust for the propeller-nozzle system. Since the nozzle profile design is based on the van Manen "optimum system", the operating curves derived from open water tests conducted on this family of nozzles are used to determine the nozzle thrust coefficient. The nozzle K_t versus J curve of reference (10) is given in Figure XIII of Chapter IV.

Entering this curve with the previously determined value of J, the constant nozzle thrust coefficient is found. Assuming the difference between the open water nozzle thrust and the thrust with the nozzle aft of the test body to be comparatively small, the thrust produced by the shroud at each test velocity is given by:

$$T_n = K_{tn} \rho n^2 D^4 \qquad (30)$$

With the total system thrust for the propeller and shroud known at each corresponding effective free stream velocity, equation (6) may be solved to yield the thrust deduction factor for the shrouded model configuration.

The plots of the average (1-t) with respect to the effective free stream velocities for the respective model configuration are presented in Chapter IV.

Hull Efficiency

With the wake fraction and the thrust deduction factor known for each model configuration, the hull efficiency, e_h, may be computed from the expression:

$$e_h = \frac{1-t}{1-w} \tag{31}$$

This particular element of efficiency represents a measure of the recovery by the propeller of the energy dissipated by the hull in creating the wake.

CHAPTER IV

RESULTS

The following results were obtained by experiments conducted at the Massachusetts Institute of Technology propeller tunnel with the testing procedure and analysis described in preceding chapters of this thesis.

Open-water propeller performance curves for the unshrouded and shrouded screws are given in Figures XII and XIII. Plots of the water velocity in the plane of the propeller (v_o) measured with respect to the radial distance from the body centerline axis for each selected free stream velocity are given in Figures XIV through XXIII. The resulting wake fraction at each corresponding effective free stream velocity is presented in Figure XXIV for the unshrouded and the shrouded model configuration.

The resistances of the model plotted with respect to the effective free stream velocity for each propeller condition are given in Figures XXV and XXXIV. A series of curves which provide operating propeller RPM at each test velocity are presented in Figures XXVI through XXXI and Figures XXXV through XL. Plots of the operating RPM versus the effective free stream velocity as described in the thrust deduction analysis are given in Figures XXXII and XLI. General propeller performance curves for the body disturbing flow test are presented in Figures XXXIII and XLII. The nozzle thrust coefficient curve for the shrouded configuration is included in Figure XIII. The computed thrust

deduction factor at each corresponding effective free stream velocity is presented in Figure XLIII for the shrouded and unshrouded model configuration. The hull efficiency is plotted with respect to the effective free stream velocity in Figure XLIV.

A concise tabulation of significant results for the unshrouded and shrouded model condition are presented in Tables III through VI at the end of this chapter.

FIGURE XII

PROPELLER TEST, UNSHROUDED

(OPEN WATER)

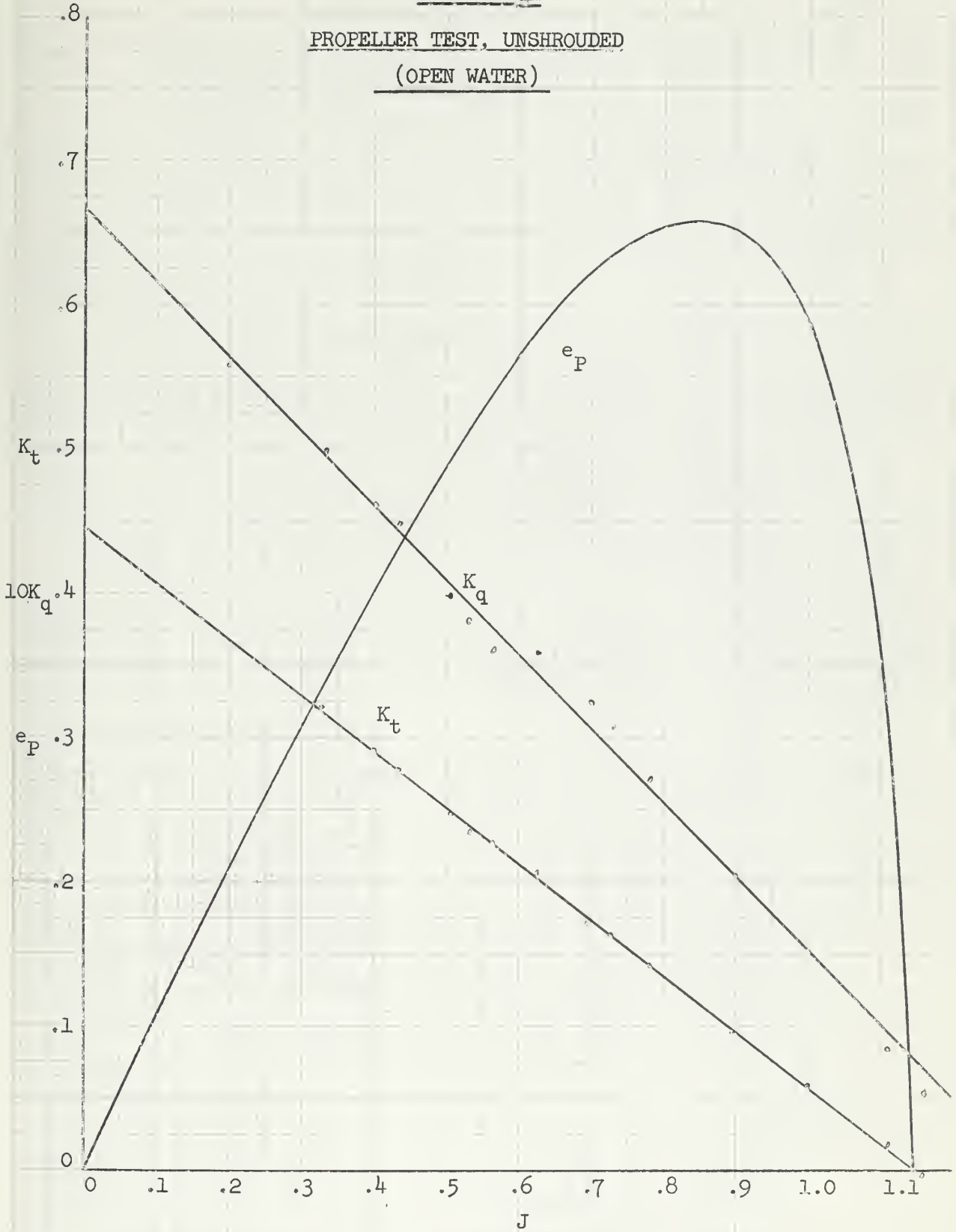

FIGURE XIII

OPEN WATER PROPELLER TEST

KAPLAN PROPELLER AND NOZZLE

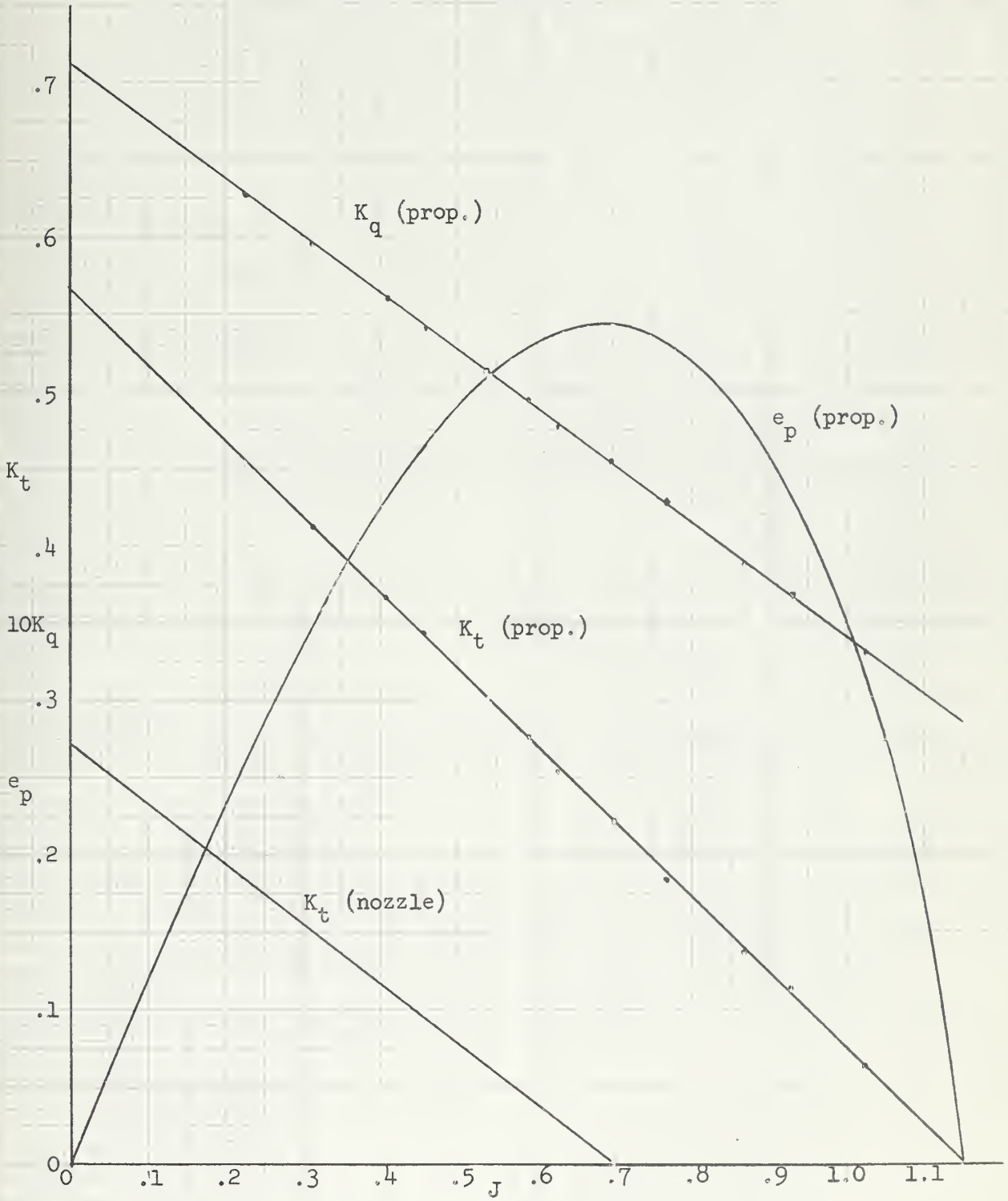

FIGURE XIV

VELOCITY SURVEY IN PLANE OF THE PROPELLER

(UNSHROUDED)

V_v = 4.0 ft/sec

V_c = 3.89 ft/sec

V_o = 2.70 ft/sec

1-w = .695

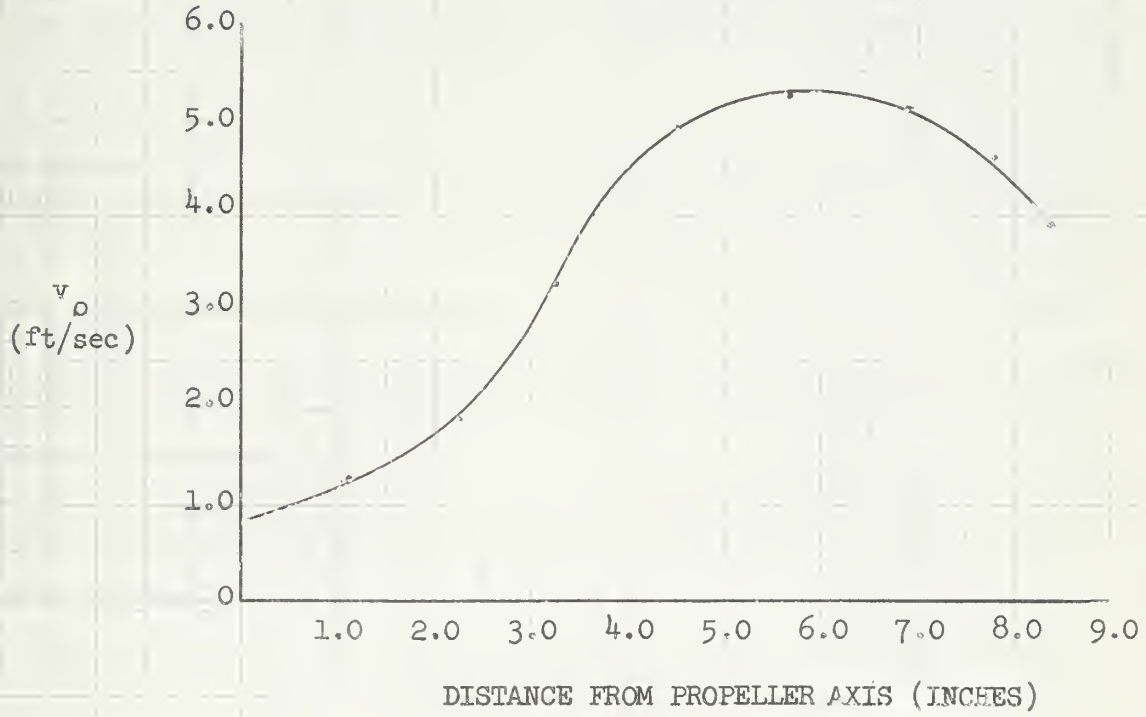

FIGURE XV

VELOCITY SURVEY IN PLANE OF THE PROPELLER

(UNSHROUDED)

V_v = 6.00 ft/sec

V_c = 5.83 ft/sec

V_o = 4.08 ft/sec

1-w = .700 ft/sec

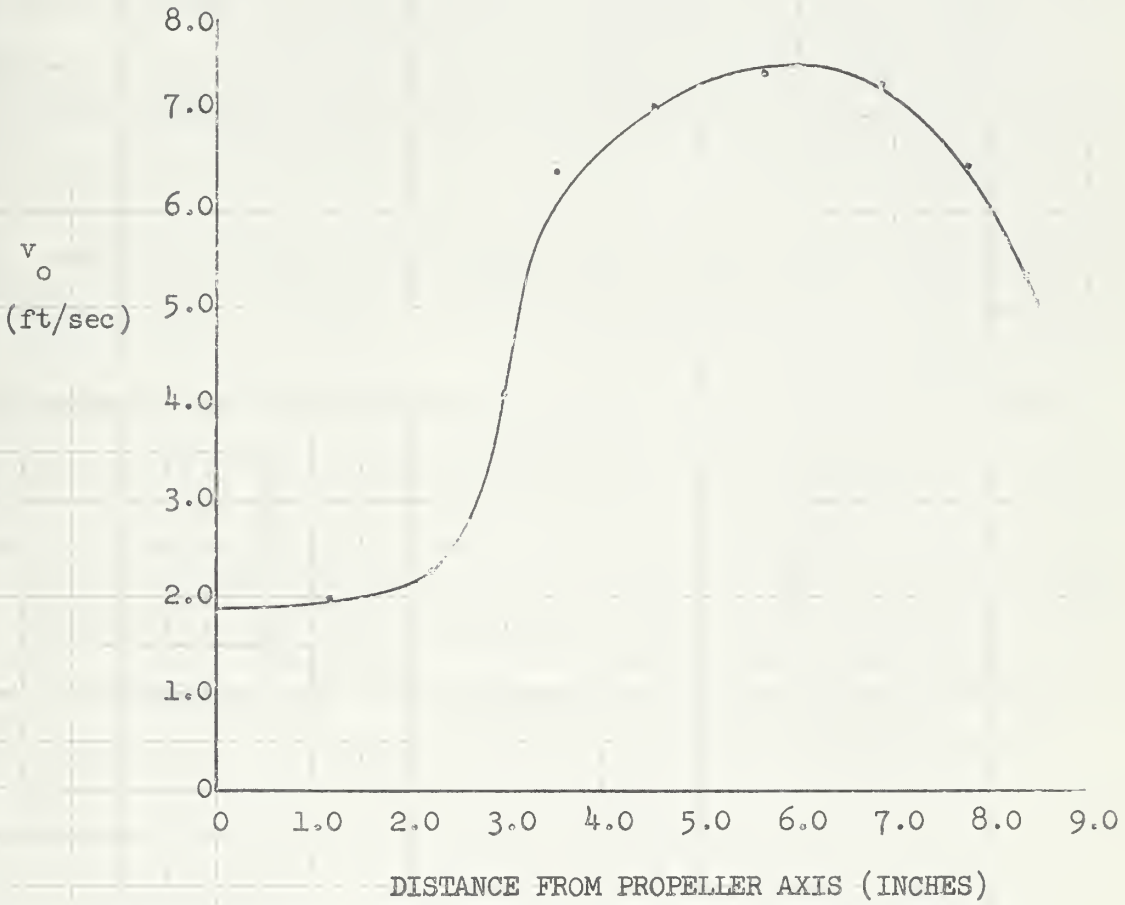

FIGURE XVI

VELOCITY SURVEY IN THE PLANE OF THE PROPELLER

(UNSHROUDED)

V_v = 8.0 ft/sec

V_c = 7.77 ft/sec

V_o = 5.52 ft/sec

1-w = .710

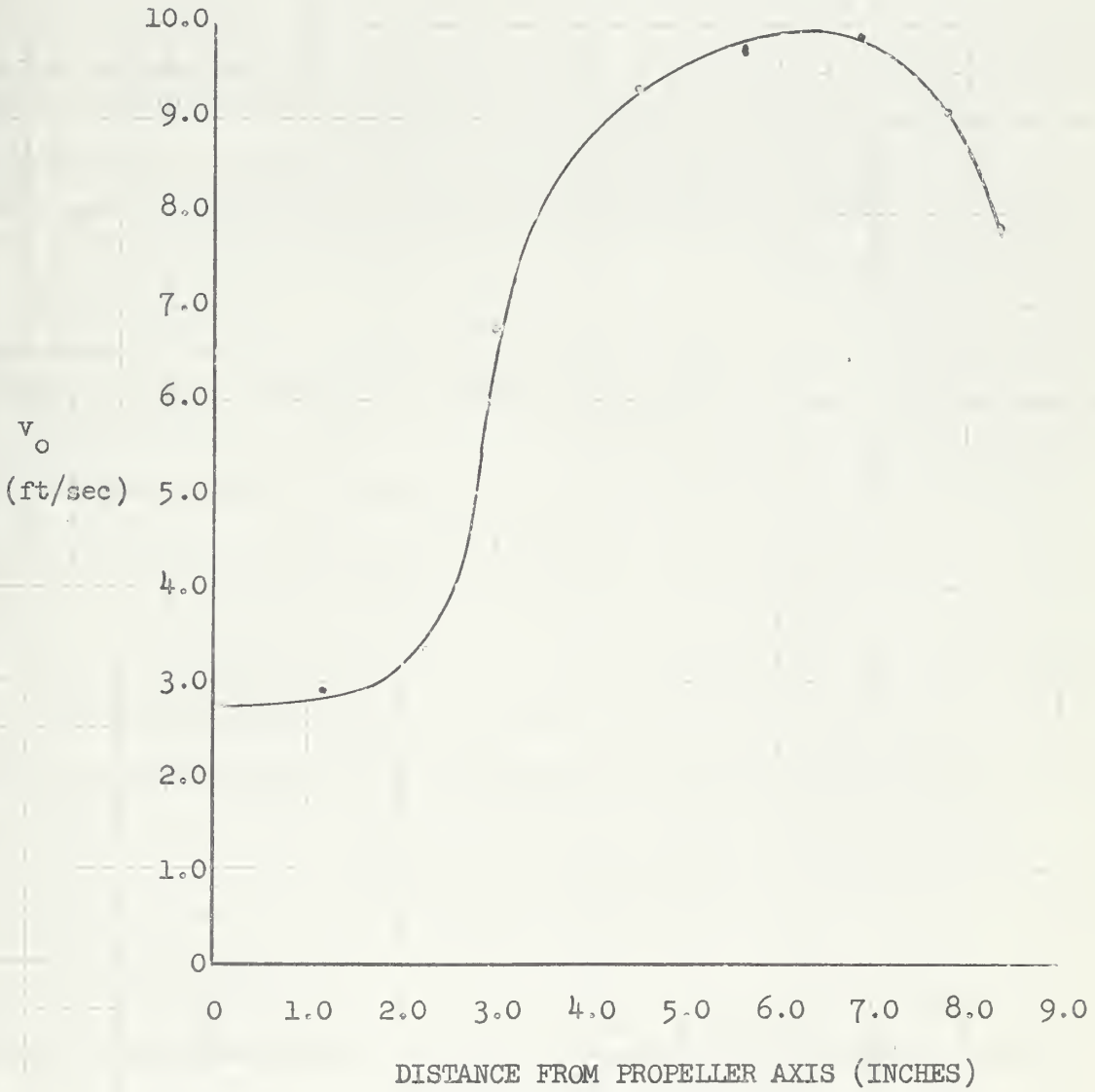

FIGURE XVII

VELOCITY SURVEY IN PLANE OF THE PROPELLER

(UNSHROUDED)

V_v = 10 ft/sec

V_c = 9.72 ft/sec

V_o = 6.85 ft/sec

1-w = .705

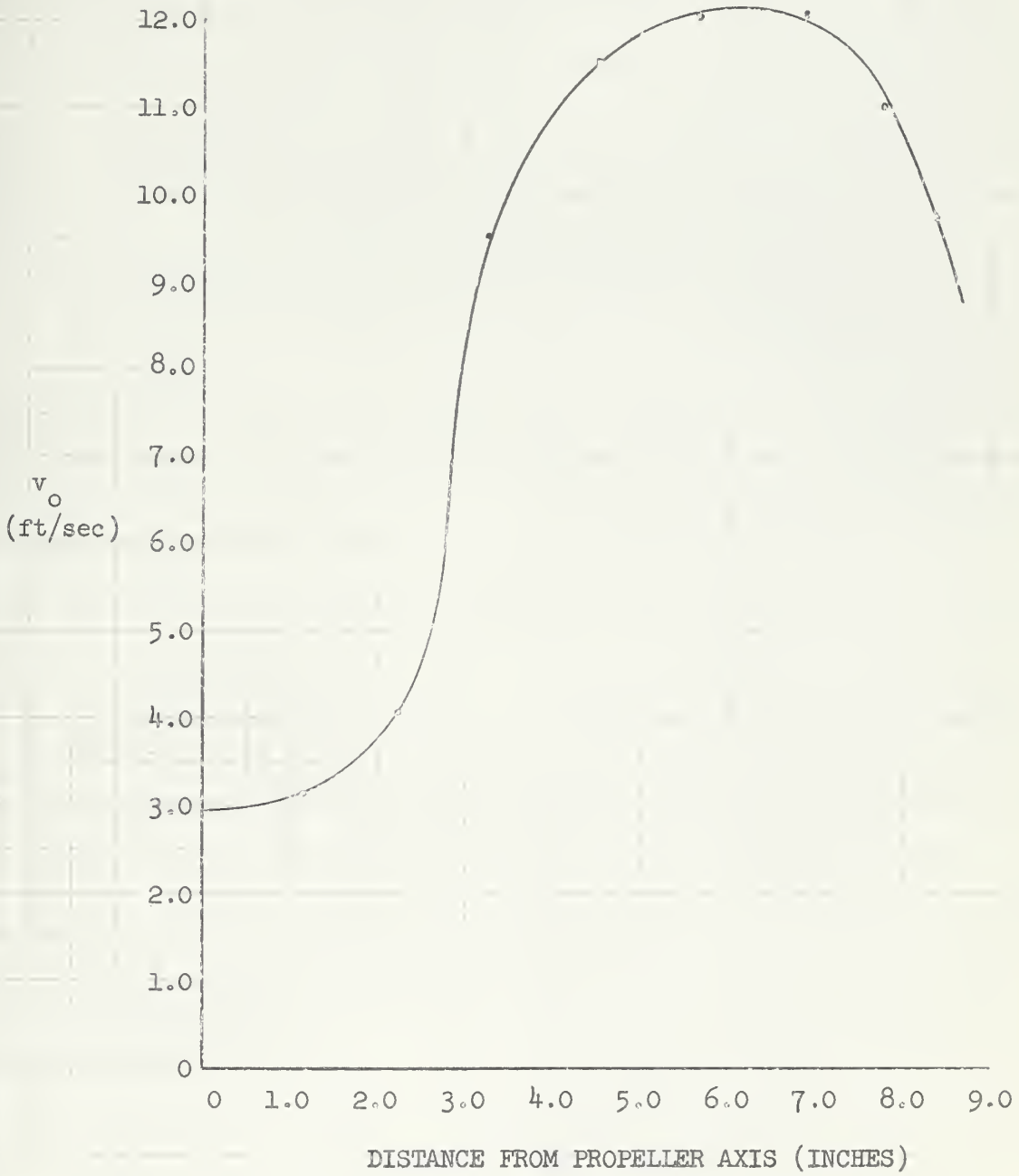

FIGURE XVIII

VELOCITY SURVEY IN PLANE OF PROPELLER

(UNSHROUDED)

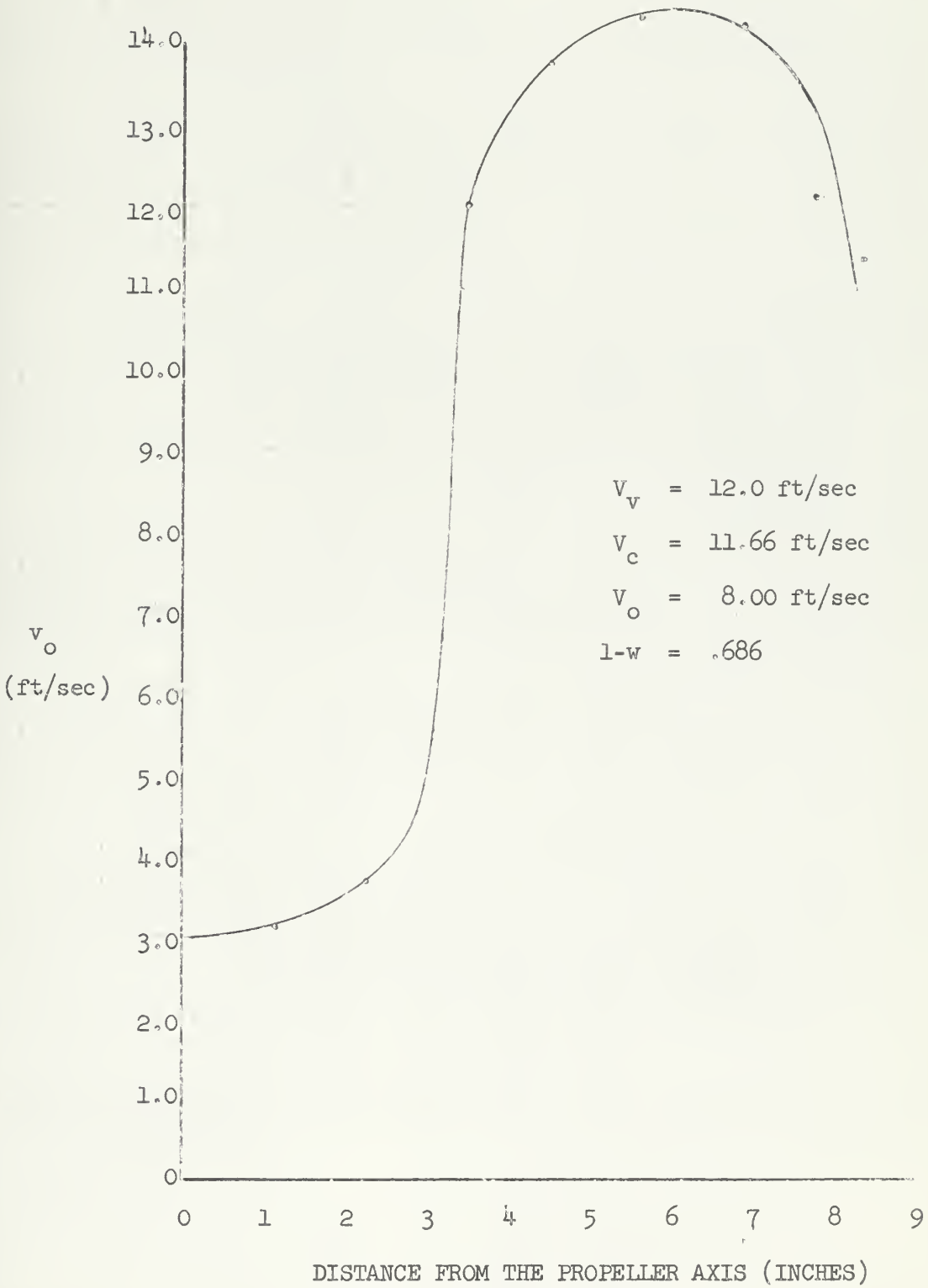

FIGURE XIX

VELOCITY SURVEY IN THE PLANE OF THE PROPELLER
(SHROUDED)

V_v = 4.00 ft/sec

V_c = 3.89 ft/sec

V_o = 4.64 ft/sec

1-w = 1.195

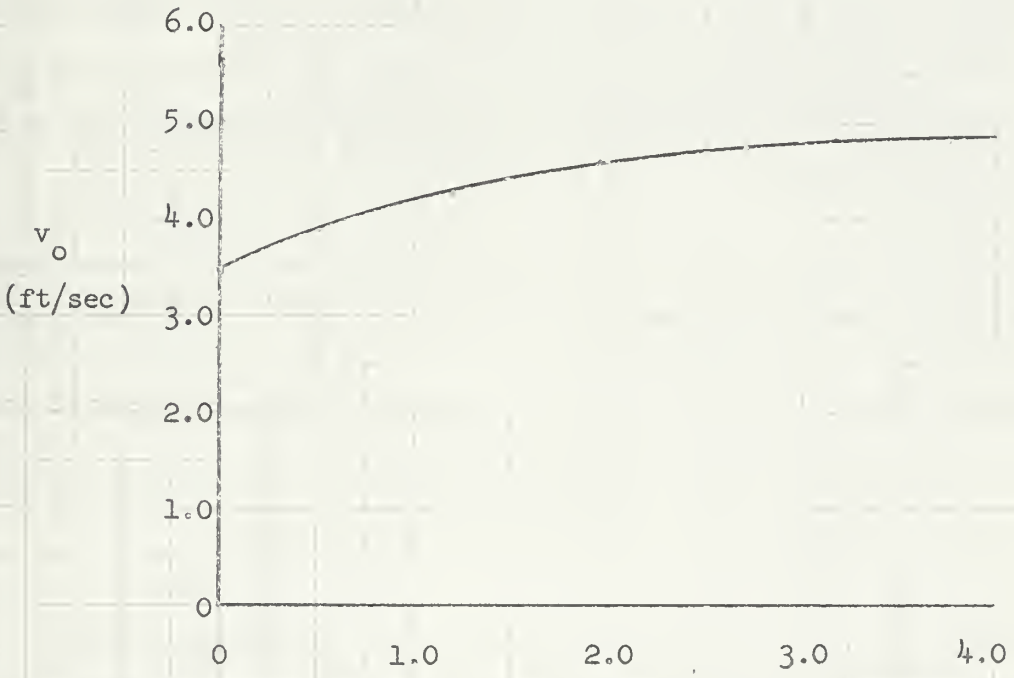

FIGURE XX

VELOCITY SURVEY IN THE PLANE OF THE PROPELLER

(SHROUDED)

V_v = 6.00 ft/sec

V_c = 5.83 ft/sec

V_o = 7.04 ft/sec

1-w = 1.205

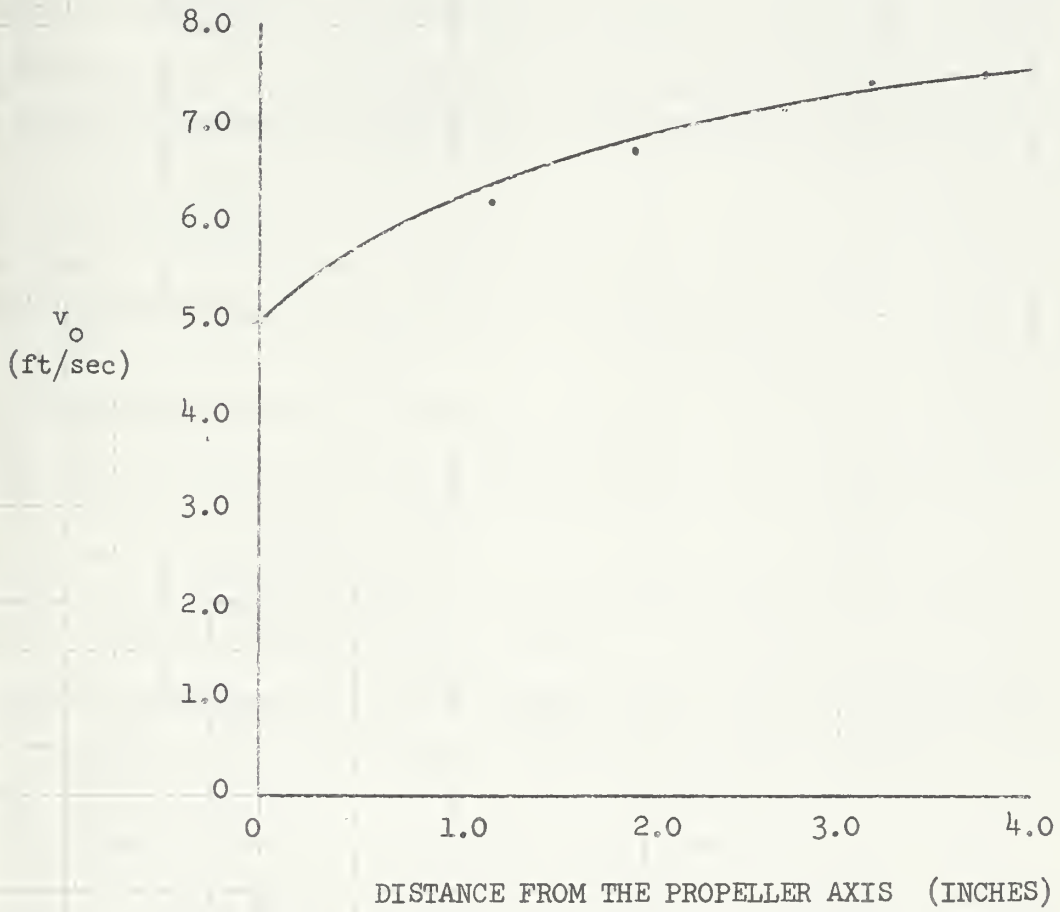

FIGURE XXI

VELOCITY SURVEY IN THE PLANE OF THE PROPELLER

(SHROUDED)

V_v = 8.00 ft/sec

V_c = 7.78 ft/sec

V_o = 9.30 ft/sec

1-w = 1.195

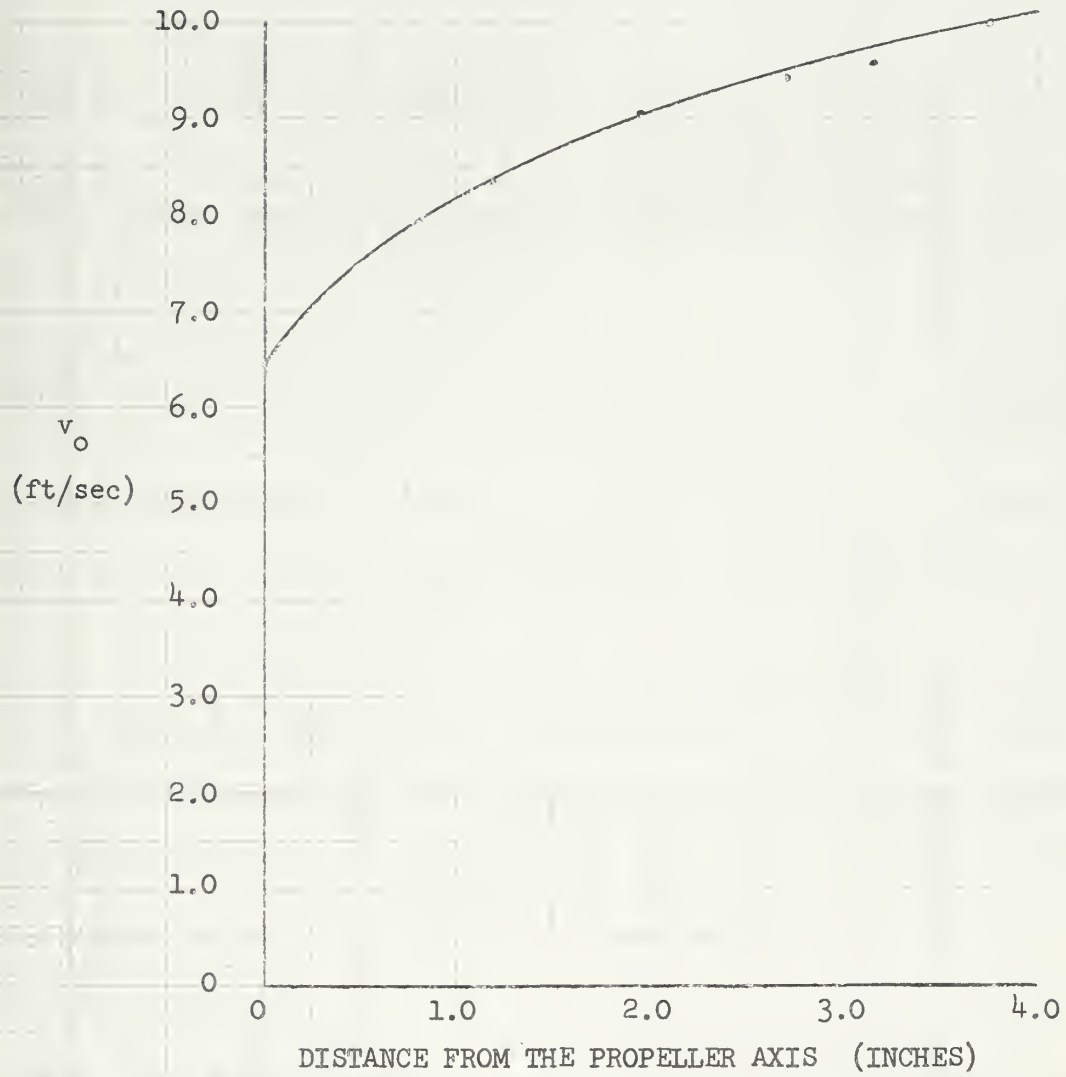

FIGURE XXII

VELOCITY SURVEY IN THE PLANE OF THE PROPELLER

(SHROUDED)

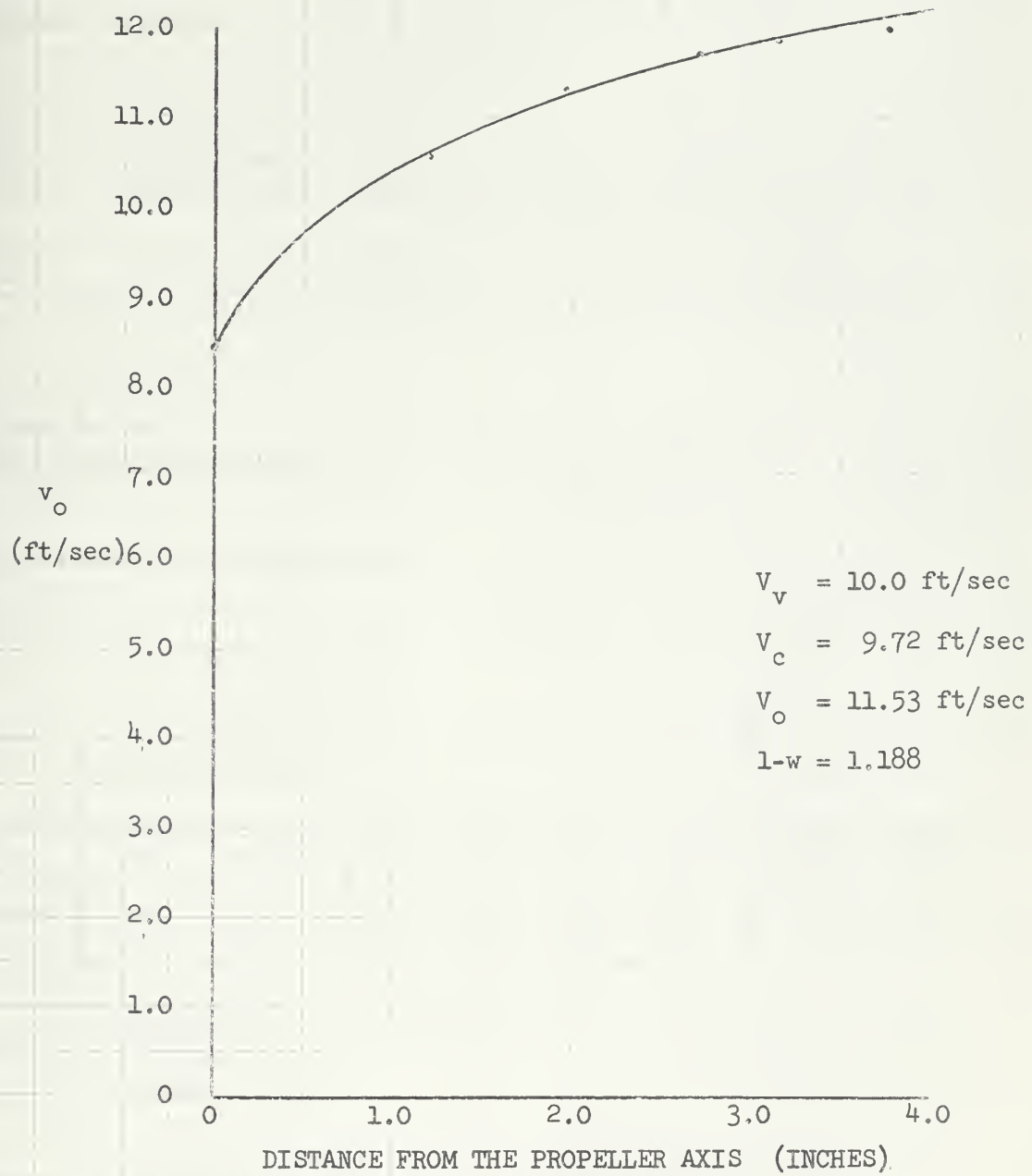

FIGURE XXIII

VELOCITY SURVEY IN THE PLANE OF THE PROPELLER

(SHROUDED)

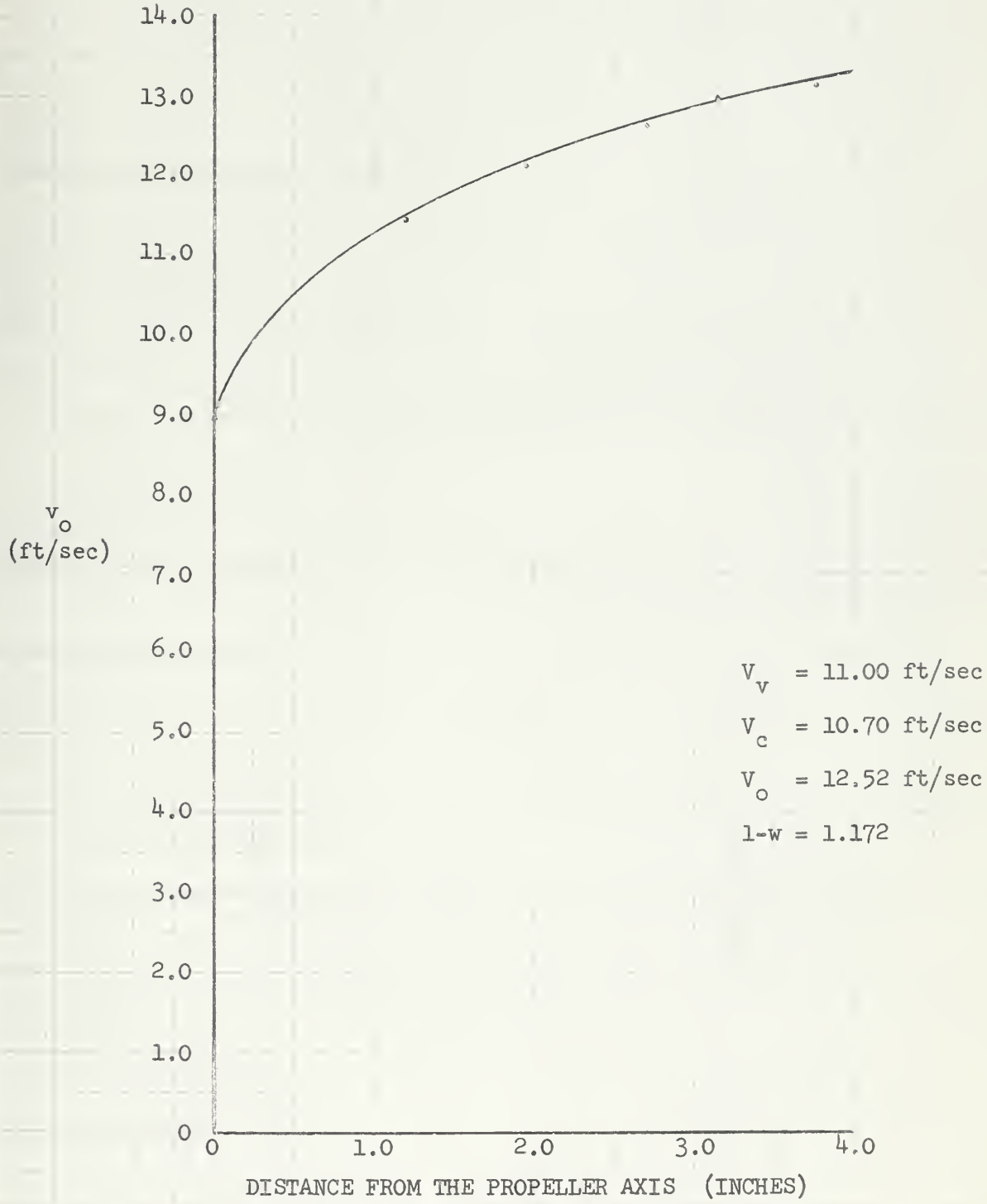

FIGURE XXIV

COMPILATION OF WAKE FRACTION

vs

EFFECTIVE FREE STREAM VELOCITY

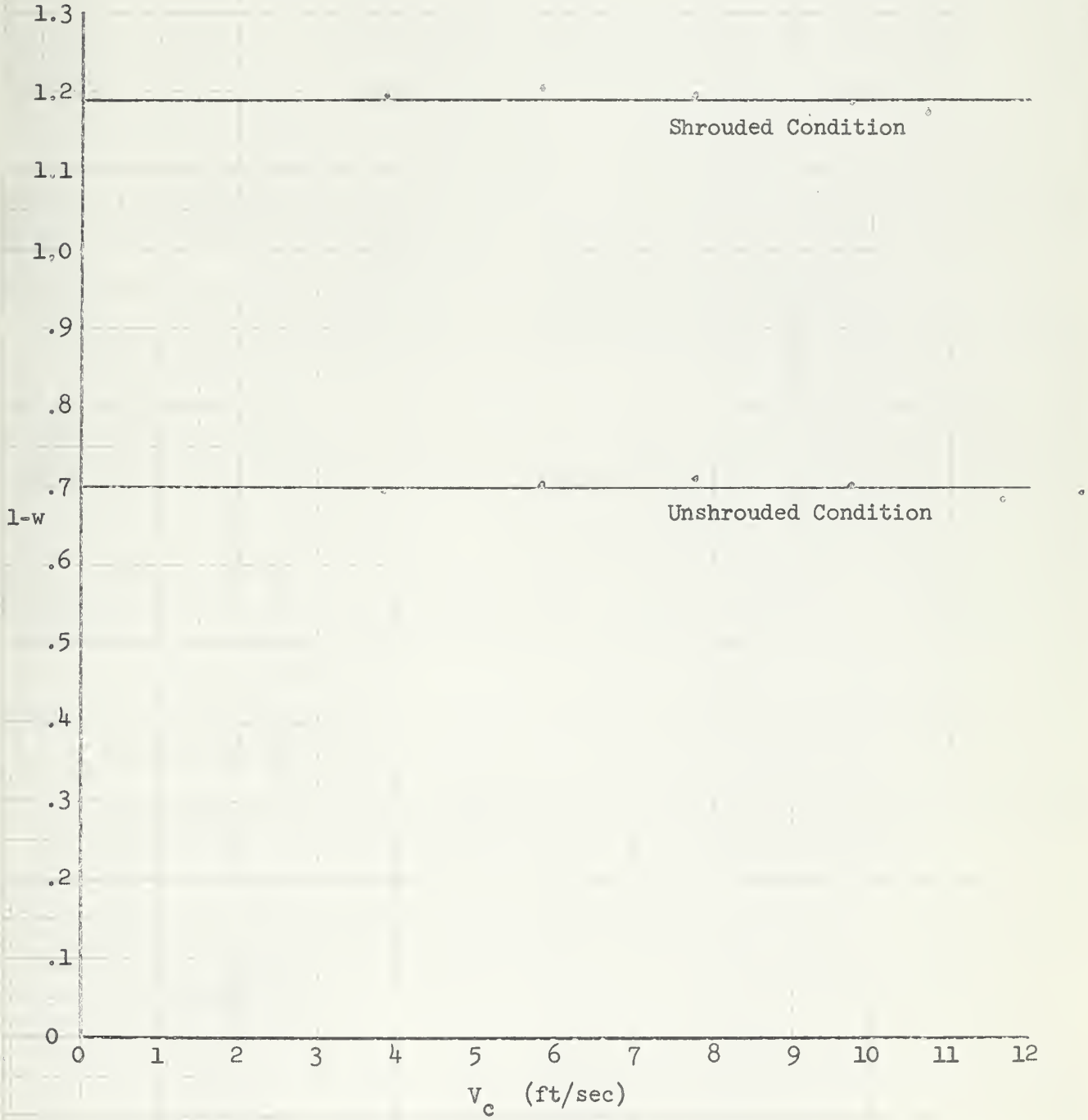

FIGURE XXV

MODEL DRAG CURVE, UNSHROUDED

FIGURE XXVI

OPERATING POINT TEST

ZERO POINT EXTRAPOLATION - UNSHROUDED CONDITION

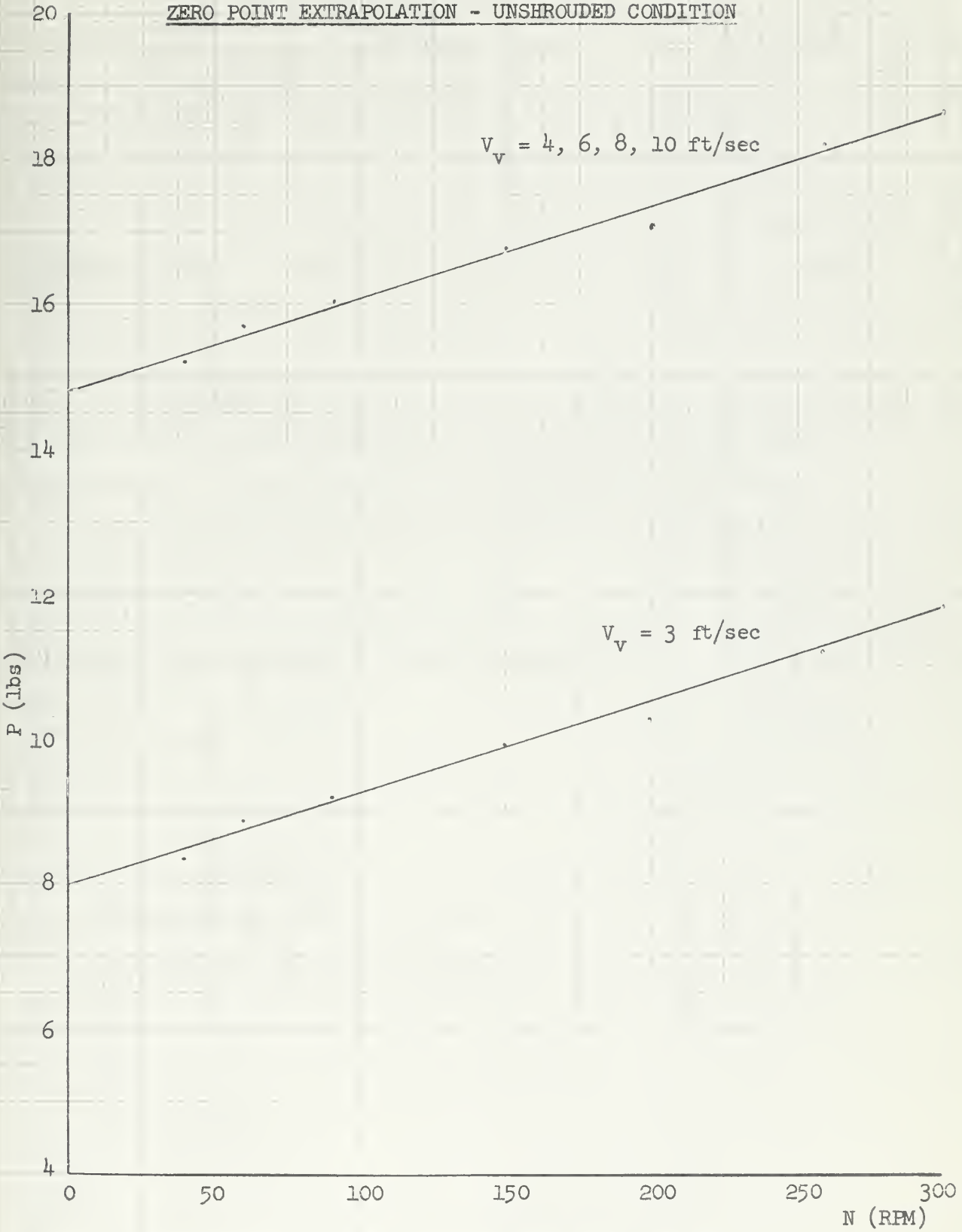

FIGURE XVII

OPERATING POINT TEST

UNSHROUDED CONDITION

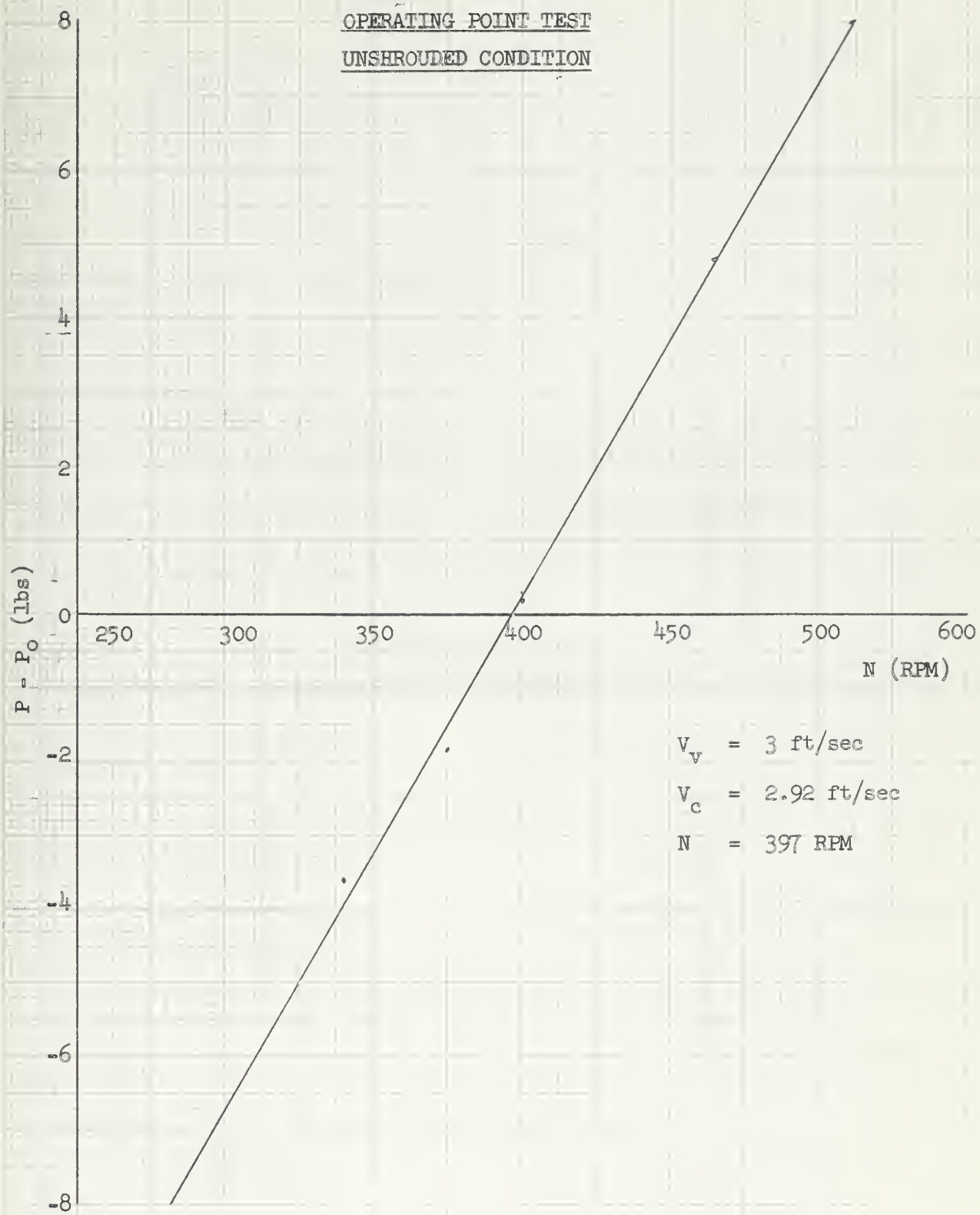

FIGURE XVIII

OPERATING POINT TEST

UNSHROUDED CONDITION

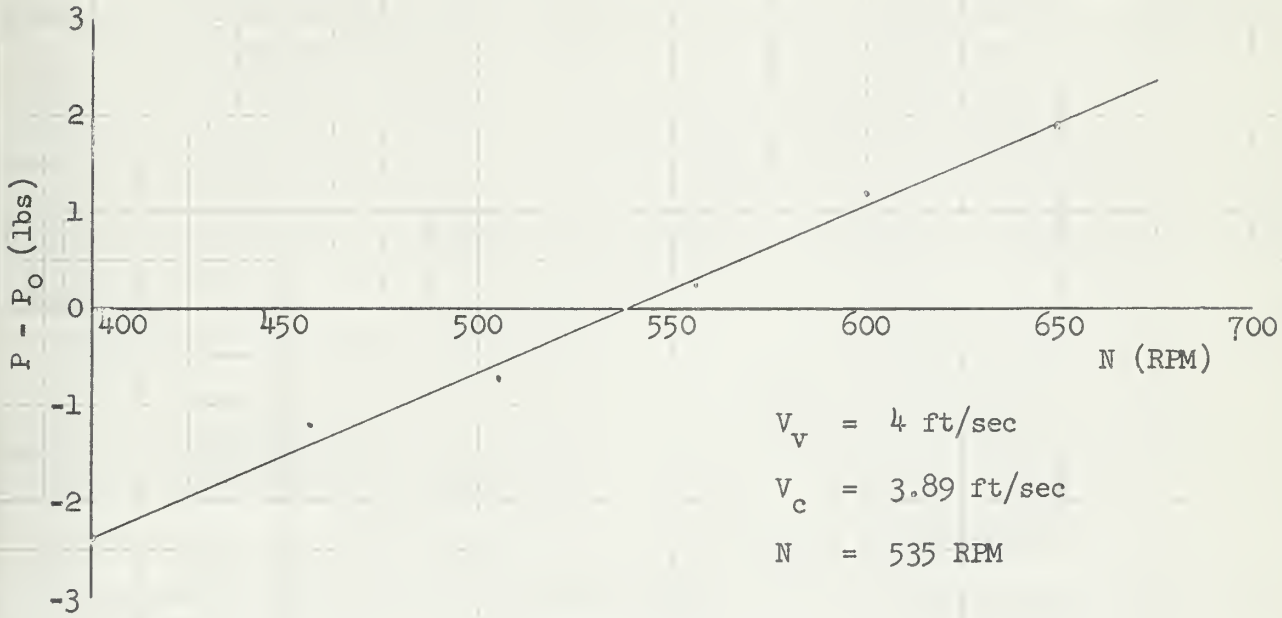

V_v = 4 ft/sec

V_c = 3.89 ft/sec

N = 535 RPM

FIGURE XXIX

OPERATING POINT TEST

UNSHROUDED CONDITION

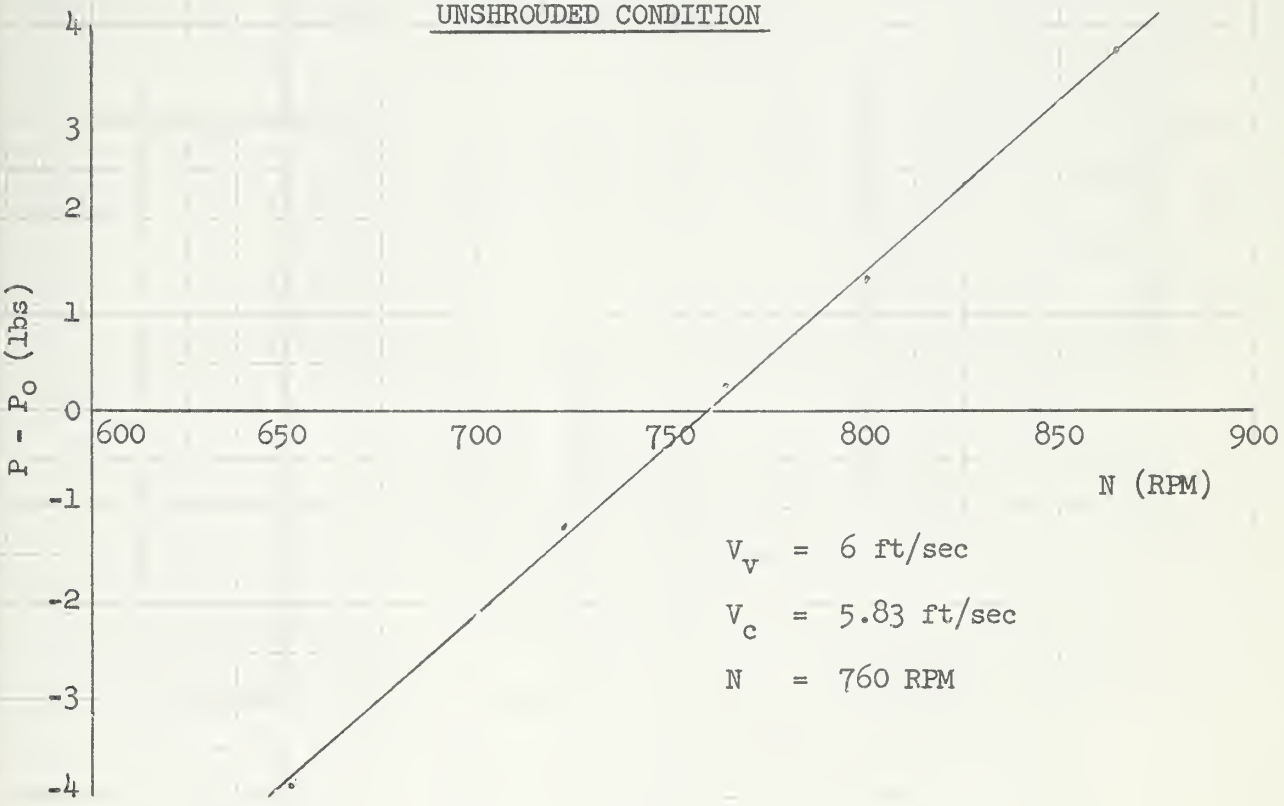

V_v = 6 ft/sec

V_c = 5.83 ft/sec

N = 760 RPM

FIGURE XXX

OPERATING POINT TEST

UNSHROUDED CONDITION

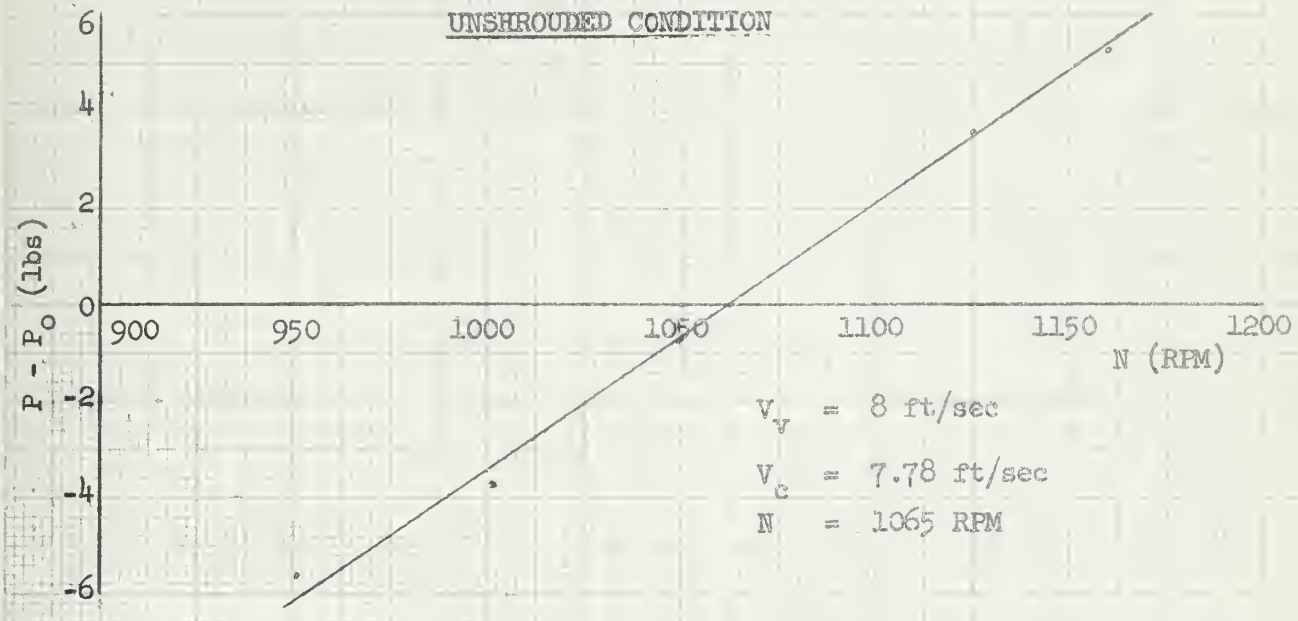

V_v = 8 ft/sec

V_c = 7.78 ft/sec

N = 1065 RPM

FIGURE XXXI

OPERATING POINT TEST

UNSHROUDED CONDITION

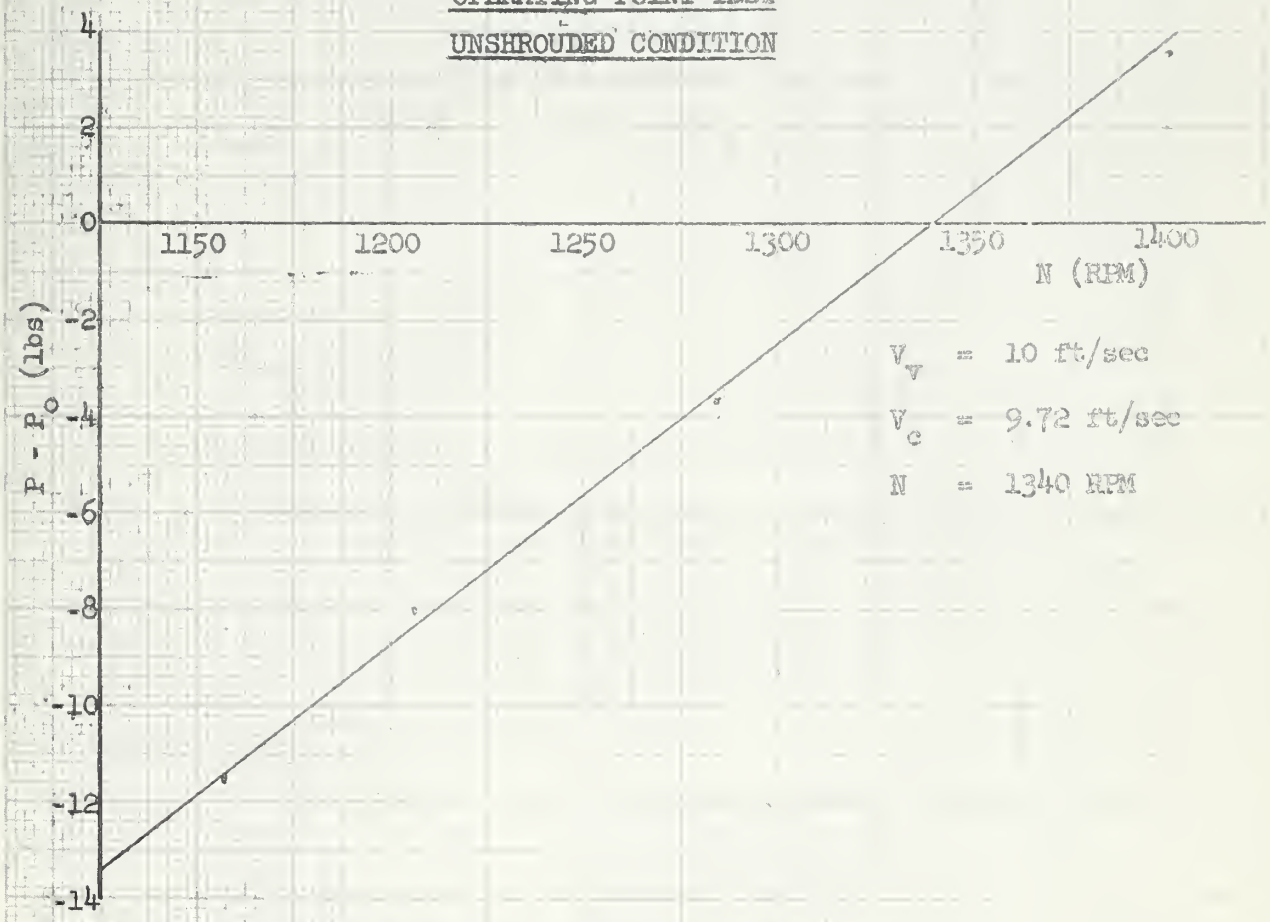

V_v = 10 ft/sec

V_c = 9.72 ft/sec

N = 1340 RPM

FIGURE XXXII

COMPILATION OF OPERATING POINT DATA

(UNSHROUDED CONDITION)

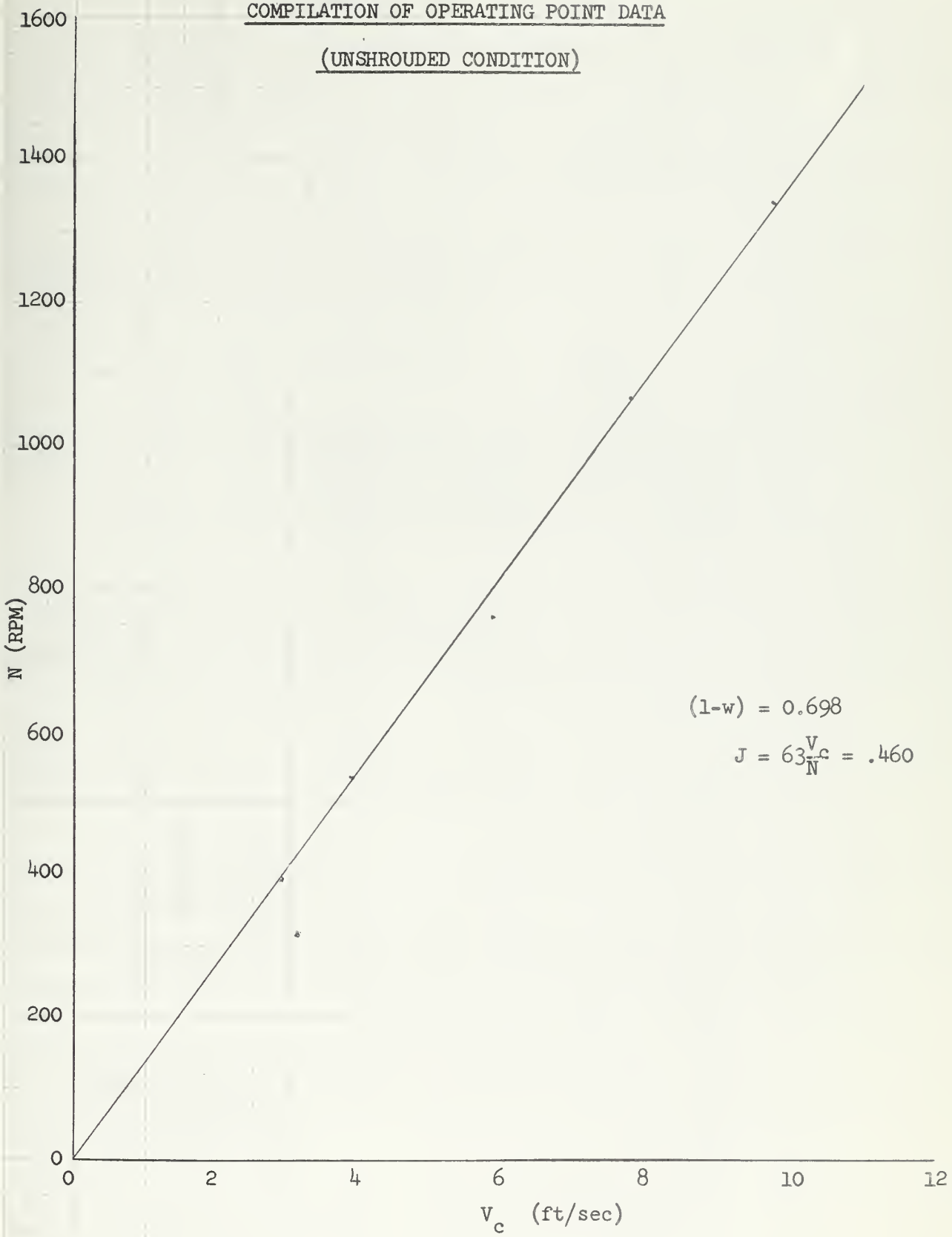

FIGURE XXXIII

PROPELLER TEST, UNSHROUDED

(WITH BODY DISTURBING FLOW)

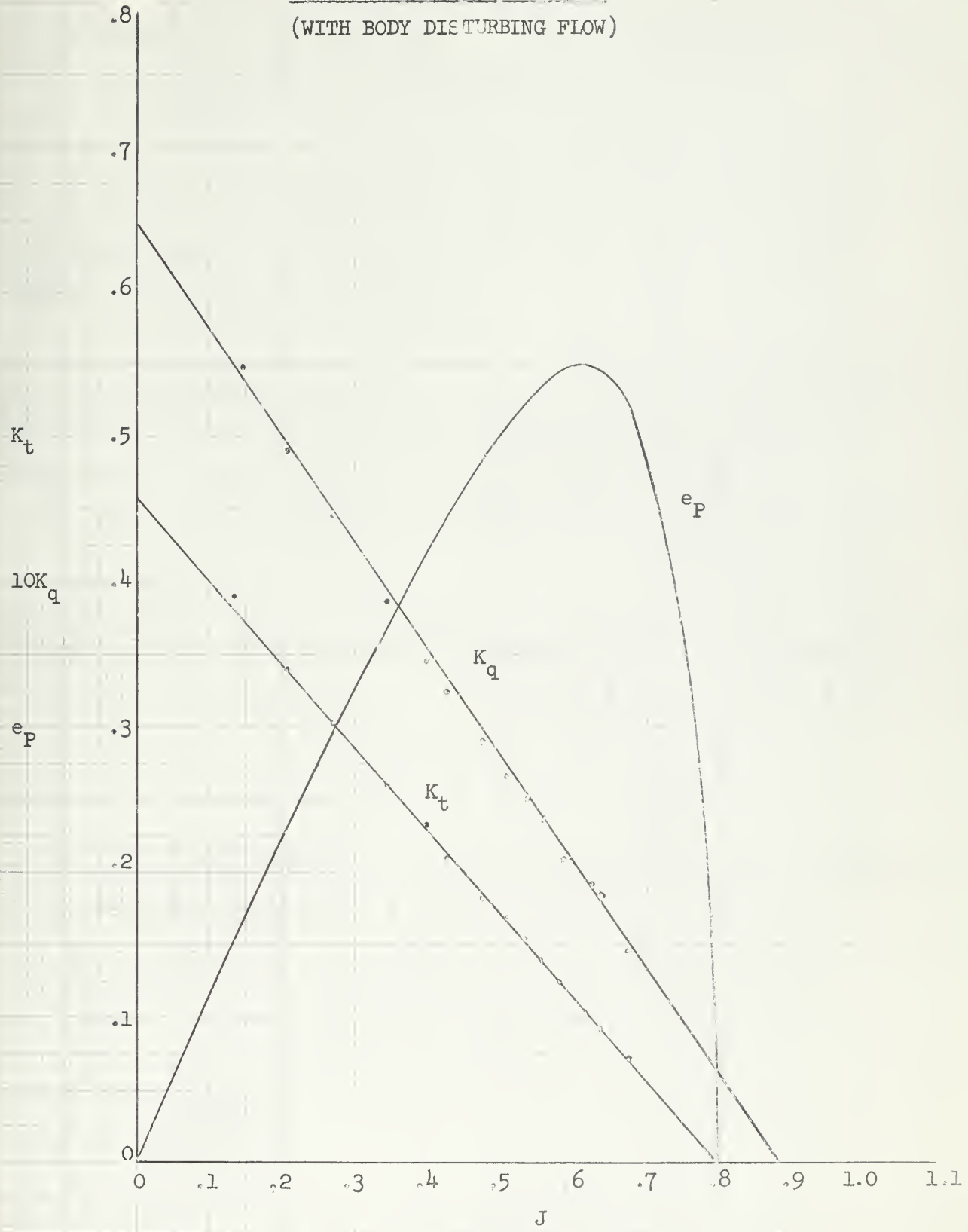

FIGURE XXXIV

MODEL DRAG CURVE, SHROUDED

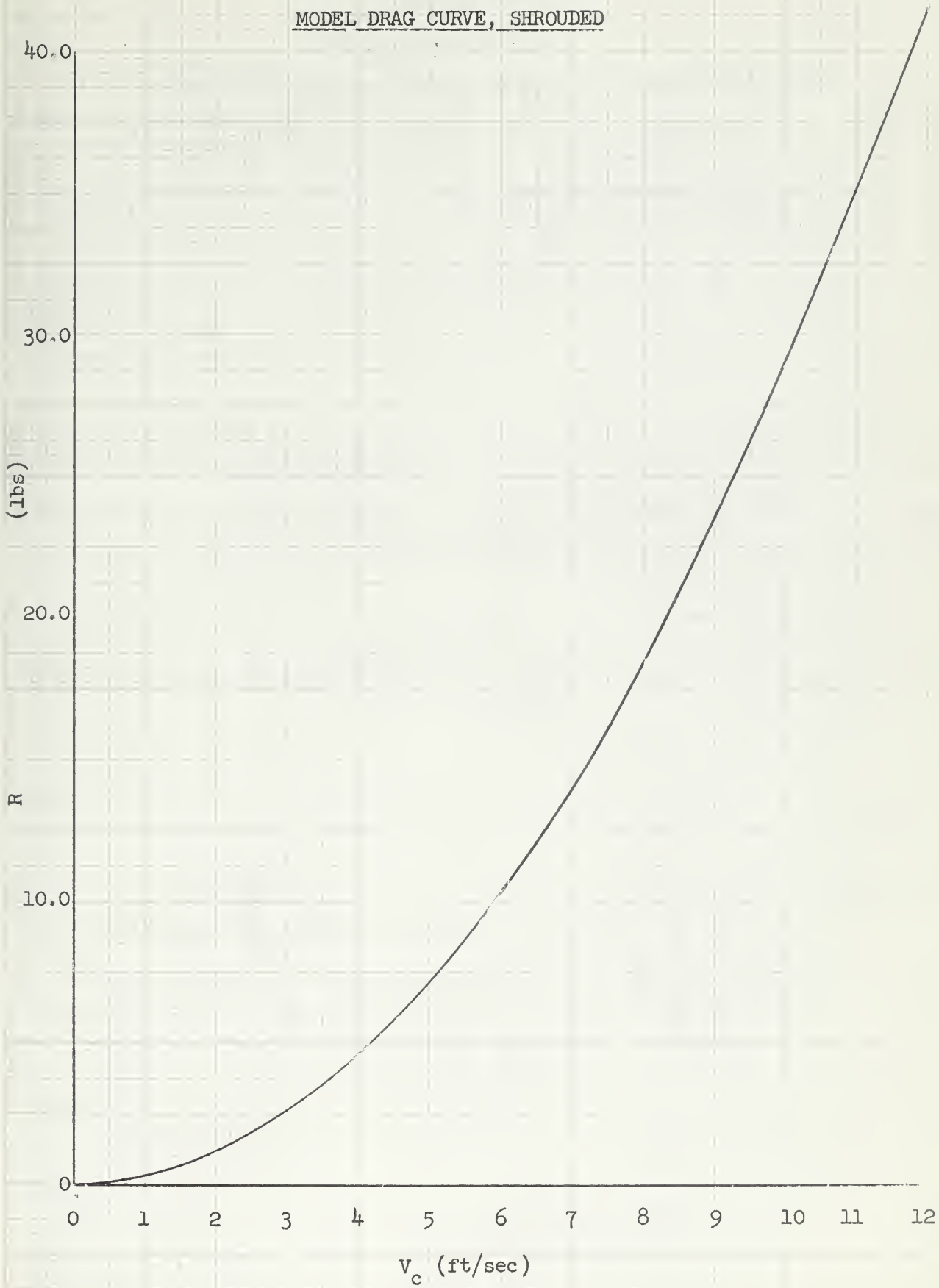

FIGURE XXXV

OPERATING POINT TEST

ZERO POINT EXTRAPOLATION - SHROUDED CONDITION

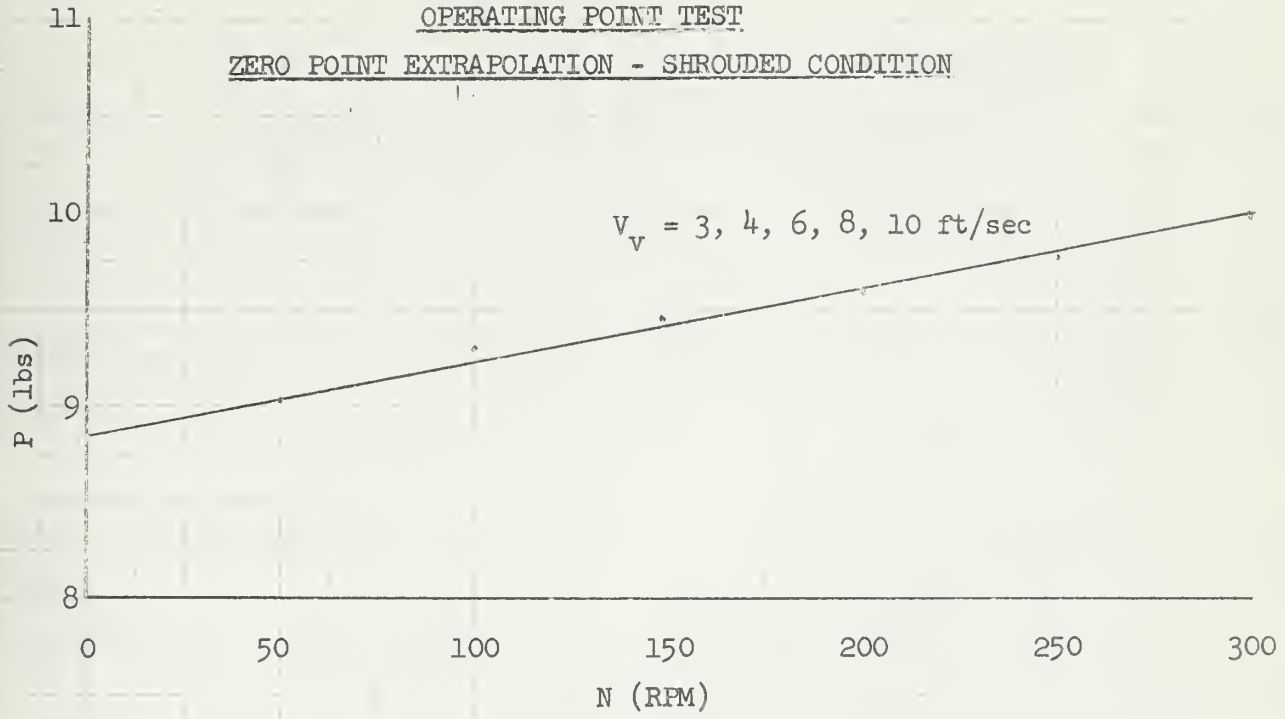

FIGURE XXXVI

OPERATING POINT TEST

SHROUDED CONDITION

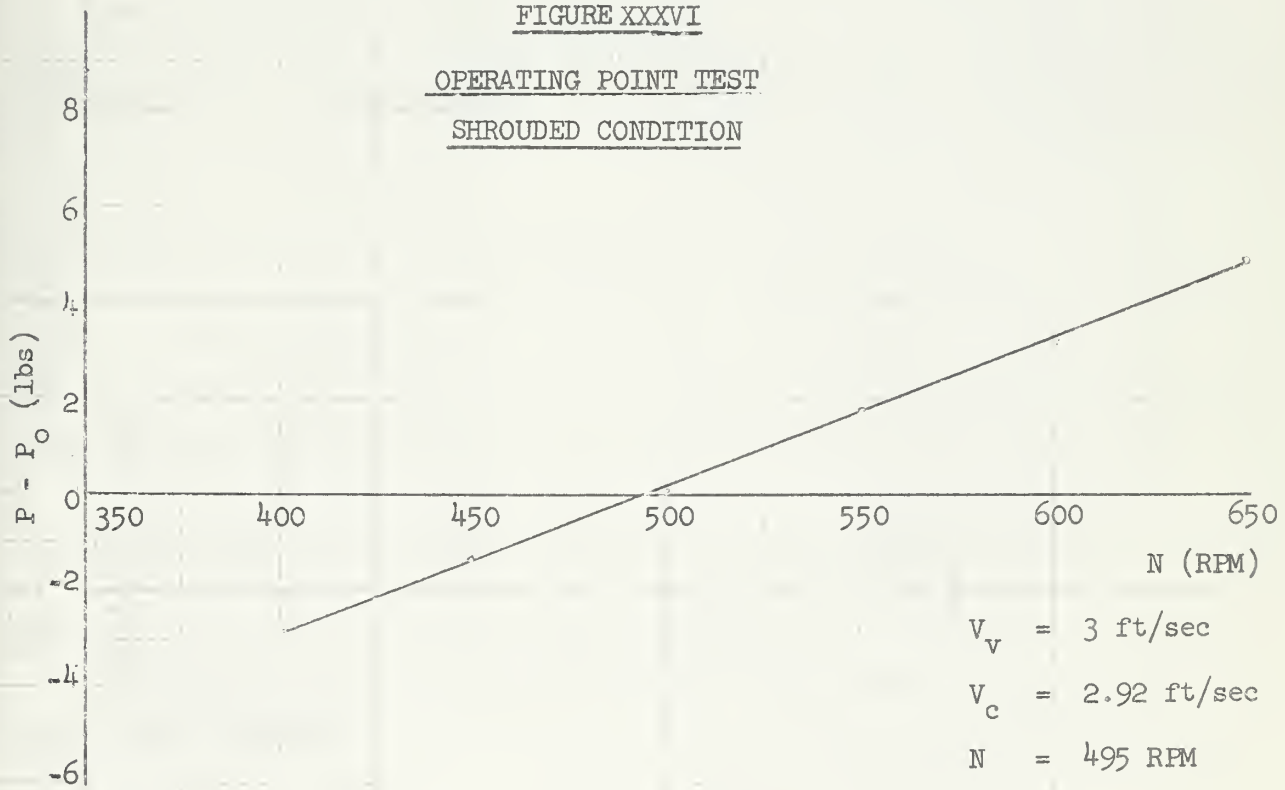

FIGURE XXXVII

OPERATING POINT TEST

SHROUDED CONDITION

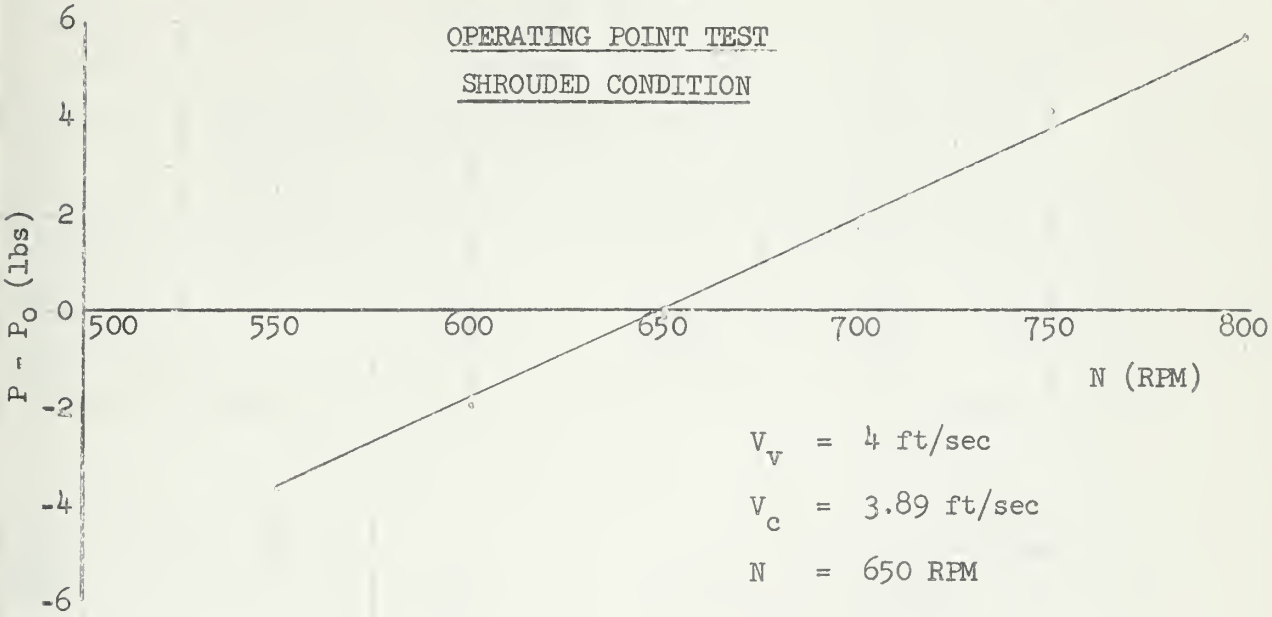

V_v = 4 ft/sec

V_c = 3.89 ft/sec

N = 650 RPM

FIGURE XXXVIII

OPERATING POINT TEST

SHROUDED CONDITION

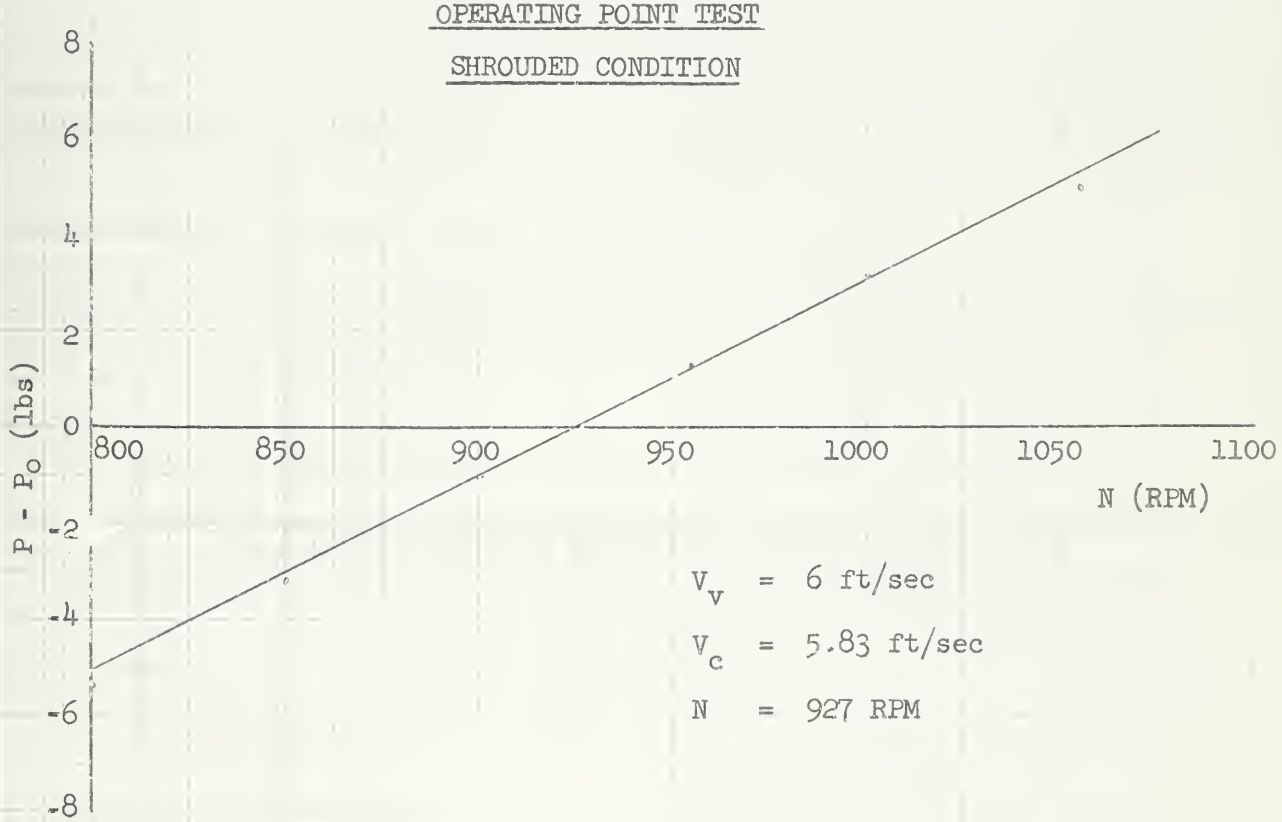

V_v = 6 ft/sec

V_c = 5.83 ft/sec

N = 927 RPM

FIGURE XXXIX

OPERATING POINT TEST

SHROUDED CONDITION

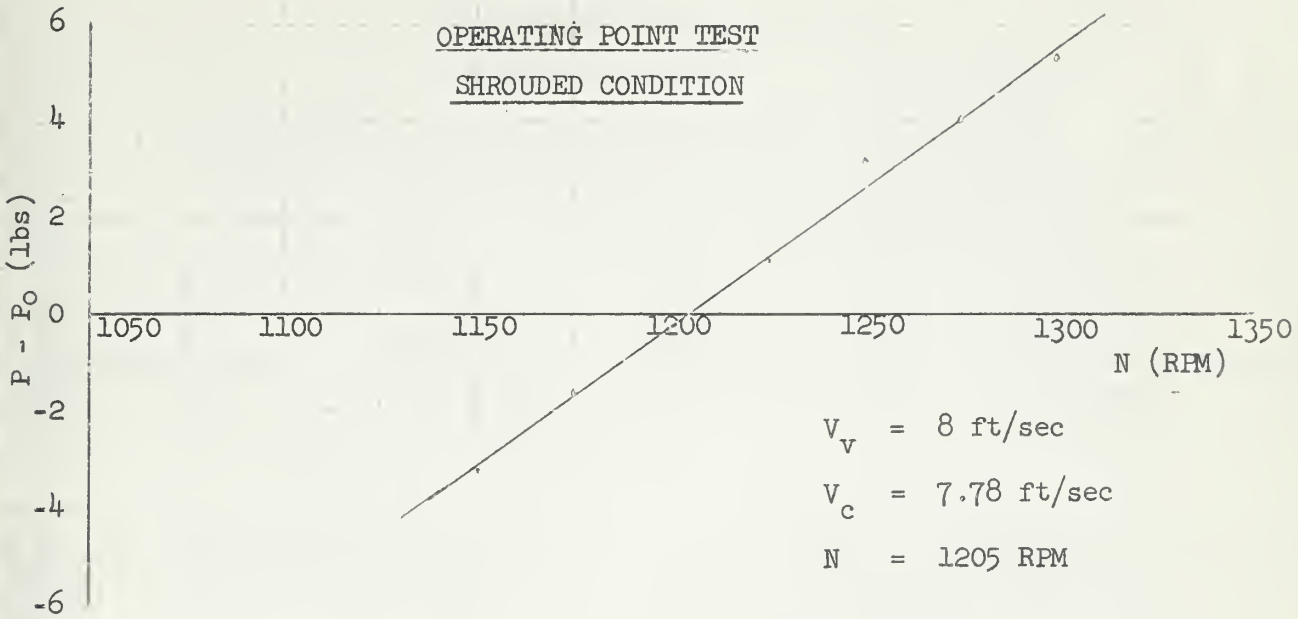

V_v = 8 ft/sec

V_c = 7.78 ft/sec

N = 1205 RPM

FIGURE XL

OPERATING POINT TEST

SHROUDED CONDITION

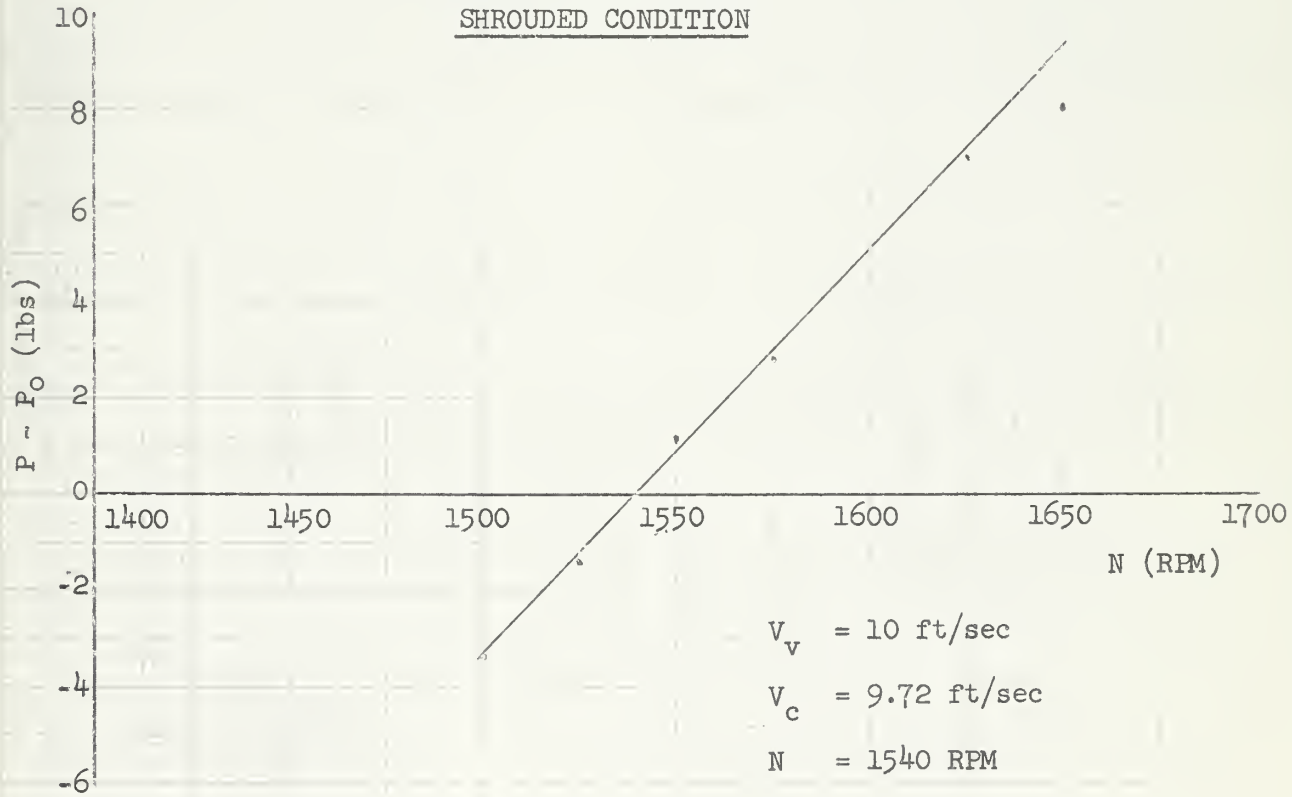

V_v = 10 ft/sec

V_c = 9.72 ft/sec

N = 1540 RPM

FIGURE XLI

COMPILATION OF OPERATING POINT DATA

(SHROUDED CONDITION)

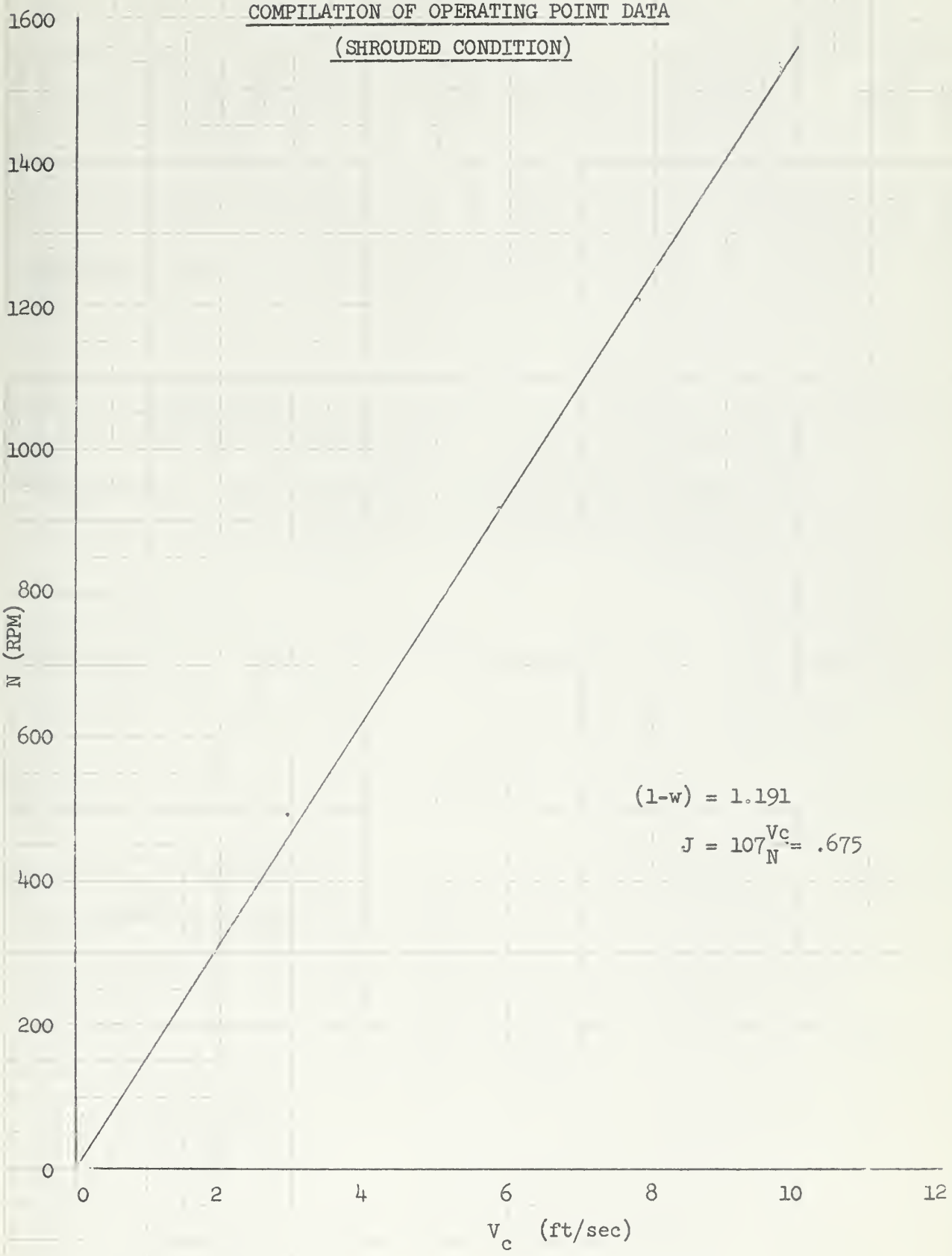

FIGURE XLII

PROPELLER TEST, SHROUDED

(WITH BODY DISTURBING FLOW)

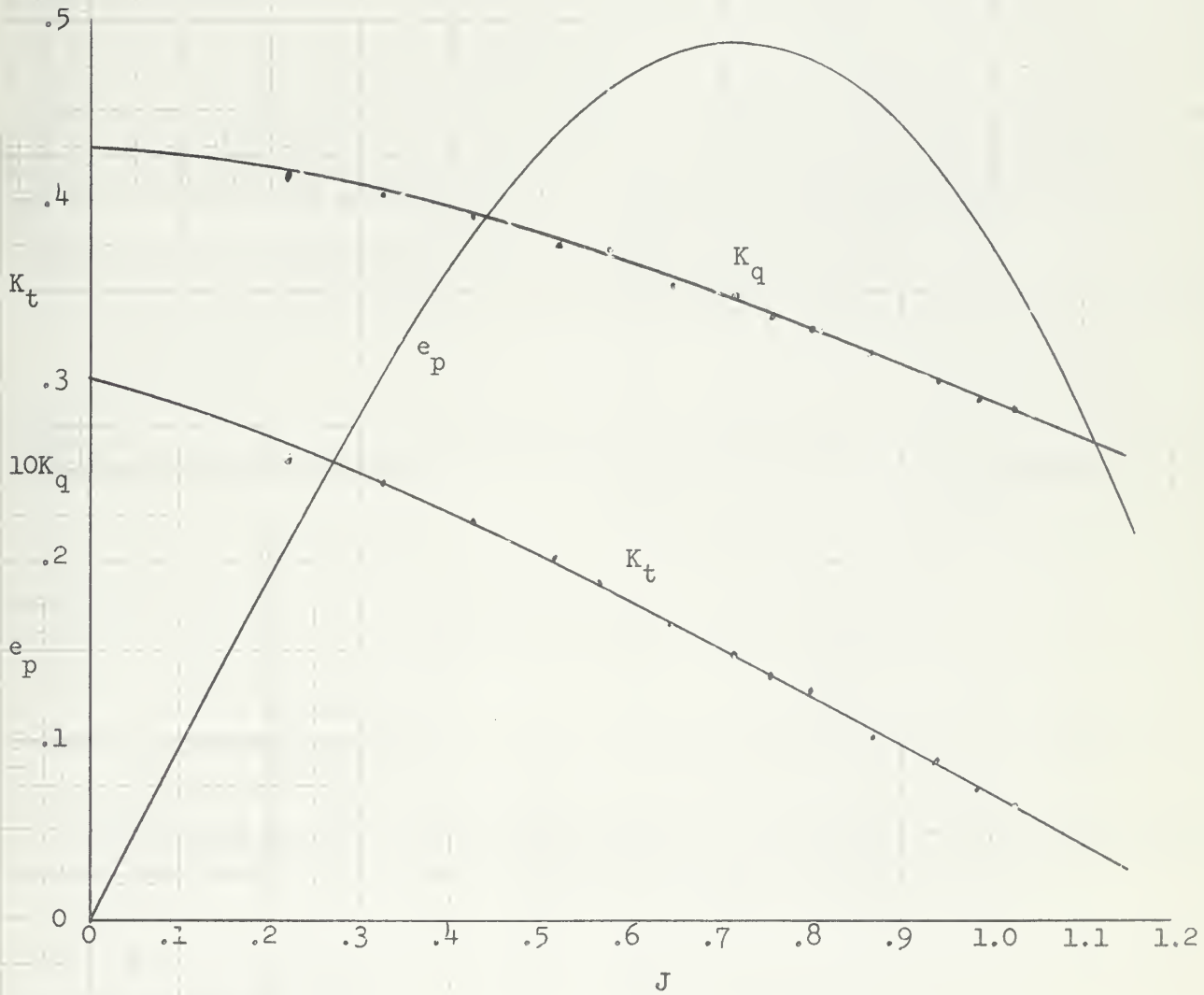

FIGURE XLIII

THRUST DEDUCTION

vs

EFFECTIVE FREE STREAM VELOCITY

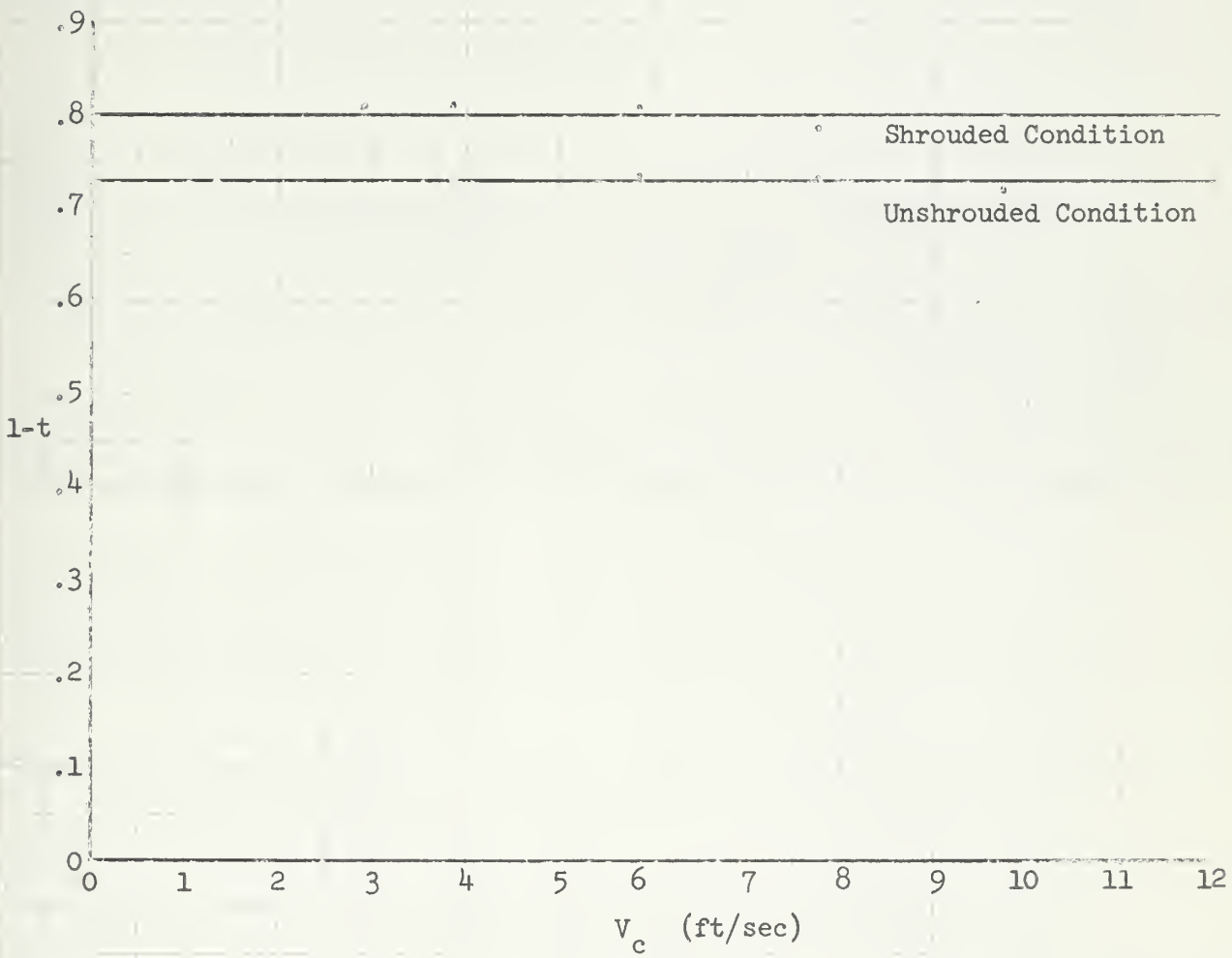

FIGURE XLIV

HULL EFFICIENCY

vs

EFFECTIVE FREE STREAM VELOCITY

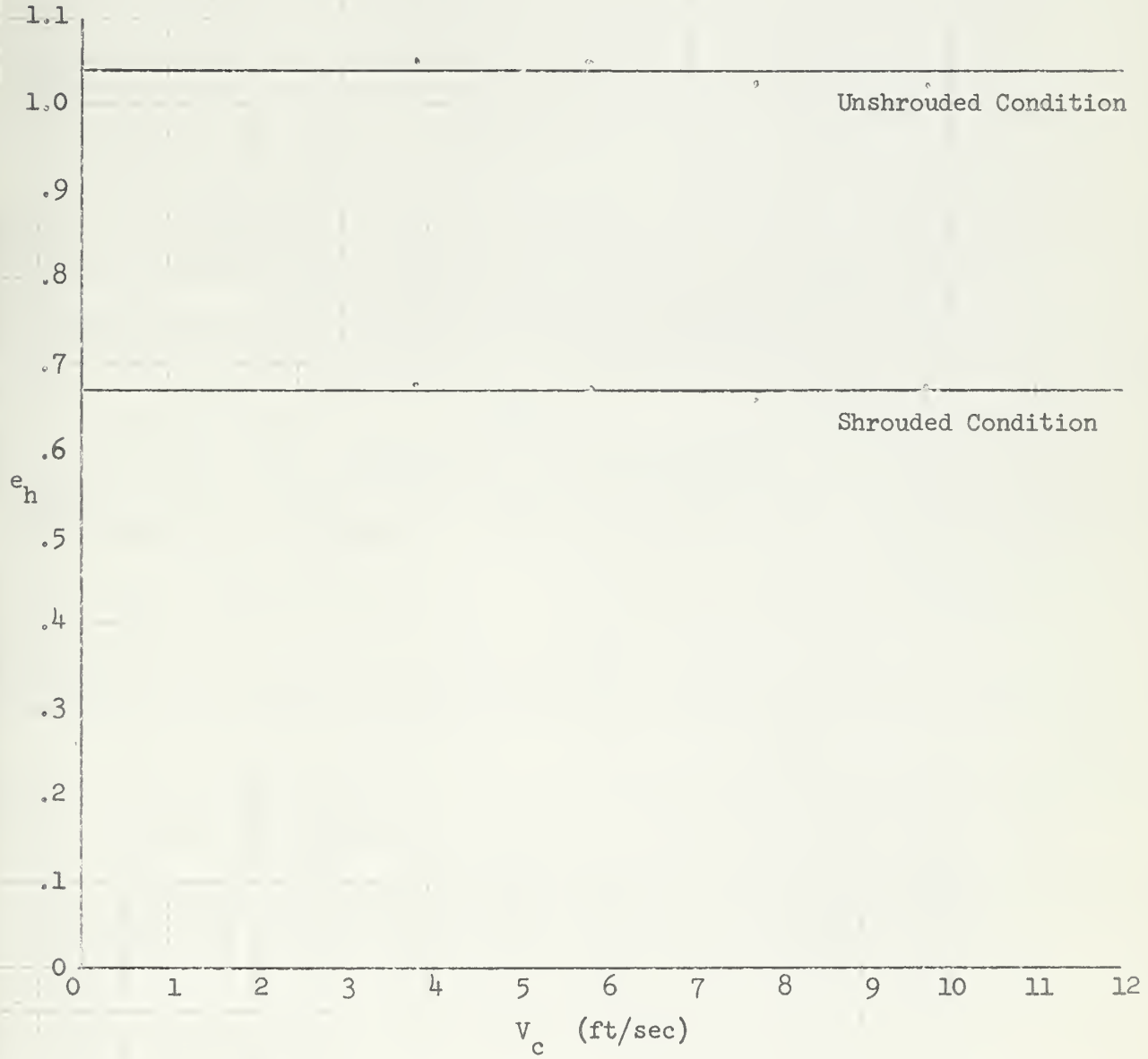

TABLE III

RESULTS FOR THE UNSHROUDED MODEL

Vc	w	T	R	t	e_h
ft/sec		lb_f	lb_f		
2.92	-	3.05	2.22	.272	-
3.89	.305	5.42	3.96	.270	1.050
5.83	.300	12.23	9.00	.265	1.050
7.78	.290	21.76	15.85	.270	1.025
9.72	.295	34.09	24.50	.280	1.020

TABLE IV

RESULTS FOR THE SHROUDED MODEL

Vc	w	T	R	t	e_h
ft/sec		lb_f	lb_f		
2.92	-	3.46	2.80	.190	-
3.89	-.195	6.05	4.89	.190	.667
5.83	-.205	13.42	10.83	.192	.671
7.78	-.195	23.79	18.61	.216	.656
9.72	-.188	36.31	28.22	.201	.673

TABLE V

DRAG COEFFICIENTS AND SURFACE AREA $(ft)^2$

	S	C_D	S_s	C_s
	Normal to Flow		Wetted Surface	
Unshrouded	.817	.328	5.41	.0495
Shrouded	.817	.366	8.56	.0349

TABLE VI

AVERAGE HULL EFFICIENCY PARAMETERS

	1-w	1-t	e_h
Unshrouded	.698	.729	1.060
Shrouded	1.191	.802	.669

CHAPTER V

DISCUSSION OF RESULTS

The final wake fraction and thrust deduction factor for the unshrouded configuration were both found to be approximately 0.3. This relatively unfavorable condition stems from the blunt hull shape of the model ($\frac{L}{D} = 1.97$) and the ensuing separation around the afterbody. It should be emphasized that the velocity survey was conducted in the absence of the propeller, and hence, the normal wake was established. In Figure XLV, the separation around the afterbody is clearly visible at a flow rate of six feet per second under the condition of a non-rotating propeller.

The wake fraction and thrust deduction factors are interrelated and can not be considered independently. In general, as the separation near the propeller increases the dependency of (1-t) on (1-w) also increases. The analysis of data to determine the thrust deduction factor was based on the normal wake fraction. With the propeller rotating as in Figure XLVI, the separation appears to be all but recovered, and subsequently, the velocity in the plane of the propeller is increased. Therefore, the effective wake should be less than 0.3 during the self-propulsion test. All other factors remaining constant, the advance coefficient corresponding to the operating point increases. Therefore, the actual thrust is less than the calculated thrust, which is based on the velocity survey. From the equation

$$t = 1 - \frac{R}{T} \qquad (6)$$

FIGURE XLV

MODEL ASSEMBLY WITH SEPARATION

V_v = 6 ft/sec. N = 0 RPM

Note separation along afterbody

FIGURE XLVI

MODEL ASSEMBLY WITH SEPARATION REDUCED

V_v = 6 ft/sec. N = 800 RPM

Note separation is reduced along afterbody

the decrease in the thrust deduction factor is inversely proportional to the decrease in thrust. Then it follows that (1-t) is proportional to (1-w), where the thrust coefficient is a linear function of the advance coefficient at the operating point.

A major factor influencing the propulsive coefficient, P.C., in an axisymmetric submarine with a centerline screw is the hull efficiency. This coefficient is a function of the ability of the propeller to recover a portion of the energy lost to separation around the afterbody of the hull. A compilation of hull efficiencies for submerged bodies of revolution having an axisymmetrically mounted screw has been assembled by Arentzen and Mandel (1) and leads to a significant relationship. In effect, the hull efficiency decreases as the propeller diameter to ship diameter increases.

The test results of Chapter IV apply to a propeller diameter to body diameter of 0.67. This ratio is relatively higher than the range of ratios for single screw submarines of the United States Navy. Accordingly, it might be expected from Figure XLVII, which is reproduced in part from reference (1), that the hull efficiency of this deep submergence hull form is considerably less than that of a typical submarine. Indeed, this is the case. The experimental results for the unshrouded configuration indicate that the hull efficiency is approximately unity.

Extrapolation of the (1-t) and (1-w) curves with appendages in Figure XLVII shows that these curves intersect for propeller diameter to ship diameter ratios in the vicinity of 0.65 to 0.70. Hence, the experimental hull efficiency in the unshrouded condition compares favorably with the extrapolated data of reference (1).

FIGURE XLVII

VARIATION OF WAKE COEFFICIENT
AND THRUST DEDUCTION COEFFICIENT

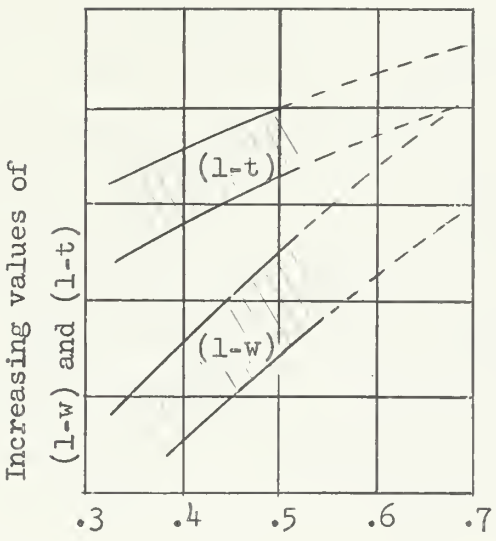

(Propeller/Ship) Diameter Ratio

Extrapolation of the (1-w) and (1-t)

Zones is Shown by Dash Lines

Attachment of the propeller-nozzle system to the body resulted in a negative wake fraction of 0.191. This result is substantiated by the fact that the fluid velocity in the plane of the propeller, V_o, increases due in part to the contraction of the fluid flow within the nozzle (13), while the effective free stream velocity remains essentially constant. Since the thrust deduction is directly influenced by the wake

fraction (21), it would be expected that the thrust deduction factor would decrease accordingly over the unshrouded propeller condition. The decrease of thrust deduction factor to about 0.20 does, in fact, confirm this hypothesis. However, while the wake fraction decreased by approximately 183 percent over the unshrouded condition, the corresponding thrust deduction decreased only 33 percent. This resulted in a hull efficiency of 0.67, which is considerably less than that for the unshrouded model configuration.

However, an evaluation of the hull efficiencies does not offer a totally conclusive comparison between the two model conditions. The more efficient system should be found by considering the propulsive coefficient and the corresponding propulsive power for each configuration. In the conventional manner, the propulsive coefficient is the product of the following components: relative rotative efficiency, hull efficiency and propeller efficiency. For the shrouded condition, one method of determining the propulsor (propeller and nozzle) efficiency is to use the total thrust coefficient, which can be determined by a summation of the propeller and nozzle thrust.

Furthermore, the propulsive power required is a major criterion in the selection of the best system for propelling a given hull form. This is because the optimum propulsive coefficient is dependent on the propeller diameter to body diameter ratio and the pitch to diameter ratio of the propeller (1). These optimum values are not necessarily the same for the shrouded and unshrouded cases. Using an assumed relative

rotative efficiency of 0.900, the hull efficiencies from Figures XLIV, and the respective propeller efficiencies from Figures XXXIII and XLII the propulsive coefficient for the unshrouded case was found to be 0.451 and for the shrouded case 0.293.

In Appendix K, the propulsive coefficients for the two systems have been tabulated and can be used for a general comparison. Nevertheless, the respective propulsive coefficients are not necessarily the optimum values and the analysis is valid only for a propeller diameter/body diameter of 0.67, a propeller pitch/diameter ratio of unity, and then only if the parameters of which the P.C. is composed are determined in the manner described in the preceding chapters.

For this particular system the fact that the nozzle does not contribute to an increase in propulsive efficiency may be attributed to several factors. Initially, the magnitude of the clearance between blade tip and nozzle wall markedly exceeds the tolerances predicted theoretically for this screw plus nozzle combination. In accordance with reference (11), the maximum clearance allowable is in the order of 0.04 inches so as to achieve an efficiency increase for a shrouded propeller of eight-inch diameter. Due to the complexity of installation and alignment of the propeller-nozzle combination in the test chamber and due to the inherent vibration of the torque shaft, it was necessary to use a significantly larger clearance. The actual clearance at the minimum nozzle diameter was 0.188 inches. With reference to van Manen (12) the efficiency loss due to this excessive blade clearance is in the order of ten percent.

The second reason for the efficiency loss in the shrouded condition is also highly significant. The fixed nozzle, despite its special from and the forward thrust which can be produced upon it, comprises a sizable appendage. Its fitting involves a considerable amount of added appendage resistance. The added friction is generally large enough so that it is balanced by the improved performance of the propeller only at high values of the thrust load factor, τ. As noted in reference (20), this occurs when τ is equal to or greater than four.

From the experimental shrouded propeller tests, the thrust load factor defined by the relation:

$$\tau = \frac{T}{\rho S V^2} \qquad (32)$$

was found to be about 1.04. Consequently, the addition of a shroud would not be expected to produce an increase in propulsive efficiency. A third reason for the low efficiency is attributed to the restricted fluid flow within the test chamber due to the relatively equal magnitude of the hull form and the tunnel nozzle. The boundary layer effects and excessive pressure gradients developed as a result of this phenomenon undoubtedly affect the circulation about the shroud, thereby affecting both hull parameters. In addition, the geometry of the test chamber required that the shroud extend about one inch into the exit nozzle of the tunnel. This factor also inhibits the contribution of the shroud to an increase in hull efficiency by inducing a greater wake and thrust deduction than the deep submersible would be likely to experience in an infinite fluid medium such as the ocean.

Finally, it is possible that the actual shroud and corresponding propeller did not actually form the integrated "optimum system".

Therefore, analysis of the experimental results does indicate that the attachment of a shroud assembly to the deep submergence hull form may, in some cases, be of benefit only as protection against environmental hazards and not as a means of improving propulsive efficiency.

CHAPTER VI

CONCLUSIONS

The most important conclusions to be derived from the preceding chapters may be summarized as follows:

1. The experimental values of wake fraction and thrust deduction were greater than anticipated for a body of revolution. This is attributed primarily to the large separation observed around the afterbody of the model.
2. The hull efficiency of the model in the unshrouded condition compares closely with published data, which is based on propulsion tests conducted on models of actual submarines and bodies of revolution.
3. The hull efficiency of the model in the shrouded condition is less than unity and the propeller efficiency is about one percent greater than that of the unshrouded propeller. In light of these facts, the relatively poor propulsive coefficient can be attributed to several significant factors; namely, clearance between blade tip and nozzle wall, light loading of the propeller, and the detrimental effects of the tunnel geometry on the fluid flow around the propeller-shroud system.

4. The use of a shrouded propeller did not result in greater efficiency than an open propeller for the hull form and the diameter of propellers tested. From the operating standpoint, the shrouded configuration is better adapted to heavily loaded propellers. Therefore, since deep submergence vehicles are, in general, lightly-loaded the primary purpose of the shrouded propeller is to provide protection against underwater obstructions.

CHAPTER VII

RECOMMENDATIONS

The era of deep submergence research is still in its infancy. Therefore, it seems important and necessary that further experimental work be undertaken in the study of deep submergence hull forms and their associated propulsive coefficient parameters.

With the construction of the new propeller tunnel at the Massachusetts Institute of Technology, the problems associated with determining hull efficiency should be greatly simplified. The installation of a new sting type dynamometer will improve significantly the sensitivity of thrust measurements, thereby permitting tests of models as small as six-inches in diameter. Models of this size will substantially alleviate the problem of tunnel wall boundary effects which up to now have been a major source of error.

In the future, it is suggested that the propeller-nozzle combination be tested as an integral unit. By using strain gages to measure the thrust developed by the nozzle, it should be possible to experimentally determine the total thrust actually developed during model tests. This improvement, together with closer clearances between the propeller and shroud, which will be possible in the renovated propeller tunnel, should provide more accurate experimental data.

Fur future investigation, it is highly recommended that a series of propellers using different pitch to diameter ratios and

various propeller diameters be tested behind a body of revolution. Correlation of such a series will provide a trend of hull and propeller efficiencies. In general, as the propeller efficiency increases, the hull efficiency will decrease allowing the determination of parameters which produce an optimum propulsive coefficient.

A series of propeller-nozzle systems could also be tested and analyzed. This work would permit more detailed comparison of the shroud effects on a deep submergence hull form.

BIBLIOGRAPHY

1. Arentzen, E. S. and Mandel, P., "Naval Architectural Aspects of Submarine Design", Transactions SNAME, Advance Copy of Paper presented Nov., 1960, pp. 13-14.

2. Beveridge, J. L., "Effect of Axial Position of Propeller on the Propulsion Characteristics of a Submerged Body of Revolution", DTMB Report 1456, March, 1963.

3. Eshbach, O. W., Handbook of Engineering Fundamentals, Wiley & Sons, Inc., Second Edition, 1952, Chapter VII.

4. Hunziker, R.R., "Hydrodynamic Influence of the Propeller on a Deeply Submerged Submarine", International Shipbuilding Progress, Volume 5, 1958, p. 166.

5. Kerwin J. E., "Linearized Theory for Propellers in Steady Flow", M.I.T. Department of Naval Architecture and Marine Engineering, July, 1963.

6. Koblyinski, L., "The Calculation of Nozzle Propeller Systems Based on the Theory of Thin Annular Airfoils with Arbitrary Circulation Distribution", International Shipbuilding Progress, Volume 8, No. 88, December 1961, pp. 495-514.

7. Korvin-Kroukovsky, B. V., "Stern Propeller Interaction with a Streamline Body of Revolution", International Shipbuilding Progress, Volume 3, 1956, pp. 3-24.

8. Lewis, F. M., "Propeller Testing Tunnel at the Massachusetts Institute of Technology", Transactions of SNAME, 1939.

9. Lewis, F. M., "Propeller Tunnel Notes", Transactions of SNAME, 1947, pp. 1-12.

10. Manen, J. D. van, "Effect of Radial Load Distributions on the Performance of Shrouded Propellers", International Shipbuilding Progress, Volume 9, No. 93, May 1962, pp. 185-196.

11. Manen, J. D. van, "Fundamentals of Ship Resistance and Propulsion, Part B: Propulsion", International Shipbuilding Progress, Reprinted by the Netherlands Ship Model Basin, Publication 132a, Sections III, V, VI, VII, and VIII.

12. Manen, J. D. van, "Open-water Test Series with Propellers in Nozzles", International Shipbuilding Progress, Volume 1, No. 2, 1954, pp. 83-108.

13. Manen, J. D. van, "Recent Research on Propellers in Nozzles", International Shipbuilding Progress, Volume 4, No. 36, August 1957, pp. 395-424.

14. Manen, J. D. van, and Superina, A., "The Design of Screw Propellers in Nozzles", International Shipbuilding Progress, Volume 6, No. 55, March 1959, pp. 95-113.

15. Manen, J. D. van, and Kamps, J., "The Effect of Shape of Afterbody on Propulsion", International Shipbuilding Progress, Volume 7, No. 70, June 1960, pp. 231-252.

16. Martinek, J., and Yeh, G. C. K., "On Potential Wake and Thrust Deduction", International Shipbuilding Progress, Volume 1, 1954, pp. 79-82.

17. Milne-Thomson, L. M., Theoretical Hydrodynamics, Macmillan Company, Fourth Edition, 1961, Chapter VIII.

18. Morgan, W. B., "A Theory of the Ducted Propeller with a Finite Number of Blades", University of California, Institute of Engineering Research, May, 1961.

19. Propeller Notebook, M.I.T. Department of Naval Architecture and Marine Engineering, September 1964.

20. Rossell, H. E. and Chapman, L. B., Principles of Naval Architecture, Society of Naval Architects and Marine Engineers, Volume II, 1941, Chapters II and III.

21. Saunders, H. E., "Hydrodynamics in Ship Design", Transactions SNAME, Volume 1, 1957.

22. Solovev, V. I. and Chumak, D. A., "Experimental Investigations of Propellers in Nozzles at the Central Aero-Hydrodynamic Institute (Moscow)", Translated from Russian by B. V. Nakonechny, DTMB Report T302, March 1961.

23. Wald, Q., "Performance of a Propeller in a Wake and the Interaction of Propeller and Hull", Journal of Ship Research, June 1965, pp. 1-8.

APPENDIX

APPENDIX A

Nomenclature

A	dimensionless fraction denoting a percentage of total sink strength
B	distance from point source (origin) to point sink
C	length of the line sink
C_D	drag coefficient of the model based on area normal to flow
C_o	voltmeter conversion factor
C_s	drag coefficient of model based on wetted surface area
C_1	$\frac{60(1-w)}{D}$
C_2	$3600\ \rho\ D^4$
D	propeller diameter
F	disc area of the propeller
F_i	inlet nozzle area
F_o	outlet nozzle area
F_p	nozzle area at minimum nozzle diameter
F_o/F_p	outlet coefficient
F_i/F_p	inlet coefficient
G	voltmeter thrust used to determine VMU conversion factor
G_c	adjusted voltmeter thrust $(G - G_o)$
G_o	voltmeter thrust zero reading used to determine VMU conversion factor
H	bromobenzene scale tunnel velocity

J	advance coefficient
K	constant thrust developed at zero velocity
K_q	torque coefficient of the propeller
K_t	thrust coefficient of the propeller
K_{tn}	thrust coefficient of the nozzle
K_1	conversion constant (305 mm/ft)
K_2	pitot tube calibration factor ≈ 1.0
L	model length
N	propeller revolutions per minute
P	$\left[3W_a - W_f + \frac{VMU}{C_o}\right]$
P.C.	propulsive coefficient, propulsive efficiency
P_o	value of P at zero flow velocity and zero propeller RPM
PHP	propeller horsepower
Q	propeller torque
R	body (or body and nozzle) drag
R_{mdc}	model cable drag
S	surface area of the model normal to the fluid flow
S_s	wetted surface area of the model (or model and nozzle)
T	thrust of the propeller (or propeller-nozzle system)
T_c	uncorrected thrust of the propeller (or propeller-nozzle system)
T_n	thrust of the nozzle
U	uniform free stream velocity
V	general velocity term

V_c	effective free stream velocity
V_o	average velocity in the plane of the propeller disc normal to the direction of flow
V_p	velocity along a streamline
V_{pt}	measured pitot tube velocity at maximum cross section of the body - used in free stream velocity correction
$V_{s.l.}$	potential flow at the maximum cross section of the body
V_v	propeller tunnel velocity
W	ordinate axis of the model development equation
W_f	weight acting to create CCW moment
W_a	weight acting to create CW moment
X	abscissa axis of the model development equation
X_i	nozzle inner wall offset (see Figure III)
X_u	nozzle outer wall offset (see Figure III)
X_l	unit distance
Y	propeller thrust developed
a_k	coefficients used in method of least squares
c	nozzle clearance
e_{rr}	relative rotative efficiency
e_p	propeller efficiency, propulsor efficiency (shroud and nozzle)
e_h	hull efficiency
f	camber of nozzle profile
g	gravitational constant

Δh	water manometer height difference
k	dimensionless constant $(\frac{V_c}{V_v})$
ℓ	length of nozzle
m	total source and total sink strength
n	propeller revolutions per second
o	subscript denotes zero reading
p	p^{th} multiple of unit distance (equation 12)
s	maximum thickness of nozzle profile
t	thrust deduction factor
v_o	velocity in the propeller plane
v_i	deviations or residuals in method of least squares
w	wake fraction
y	distance aft from foremost point on nozzle
α_i	angle of the nozzle profile relative to the shaft
f/ℓ	camber ratio
s/ℓ	thickness ratio
ρ	mass density of fluid medium
ρ'	mass density of manometer fluid
ψ	stream function

APPENDIX B

Body and Streamline Development Computer Program

Abstract

The development of the body through the superposition of sources and sinks was performed by the FORTRAN computer program listed in this appendix. The computer facilities at the Woods Hole Oceanographic Institution, Woods Hole, Massachusetts were used for this purpose in this project.

The program takes basic source-sink input data for a zero streamline and produces offsets which define the deep submersible hull form. It also develops a series of streamlines about the periphery of the hull form based on potential flow assumptions.

Input

The input consists of one general information card for the body development and any number of information cards for the streamline development.

Card Format

Columns	1-5:	Number of points on centerline (X) axis. (M)
Columns	6-10:	Number of points in plane normal to the flow at each point on centerline axis. (N)
Columns	11-15:	Initial coordinate on centerline axis. (X_o)
Columns	16-20:	Incremental changes in coordinate values on centerline axis. (DX)
Columns	21-25:	Initial coordinate in plane normal to the flow. (WO)

Columns 26-30: Incremental change in coordinate values in plane normal to the flow. (DW)

Columns 31-35: Ratio of point sink strength to total sink strength. (A)

Columns 36-40: Distance from point source to point sink. (B)

Columns 41-45: Length of line sink. (C)

Columns 46-50: Number of streamline. (D)

Output

The printed output consists of offsets from the centerline axis which define the profile of the hull form or the streamline of flow.

Potential Flow Streamlines

The actual potential flow streamlines around the deep submergence hull form developed from this computer program are given in Figure XLVIII.

FIGURE XLVIII

POTENTIAL FLOW STREAMLINES AROUND BODY

FIGURE XLVIII

POTENTIAL FLOW STREAMLINES AROUND BODY

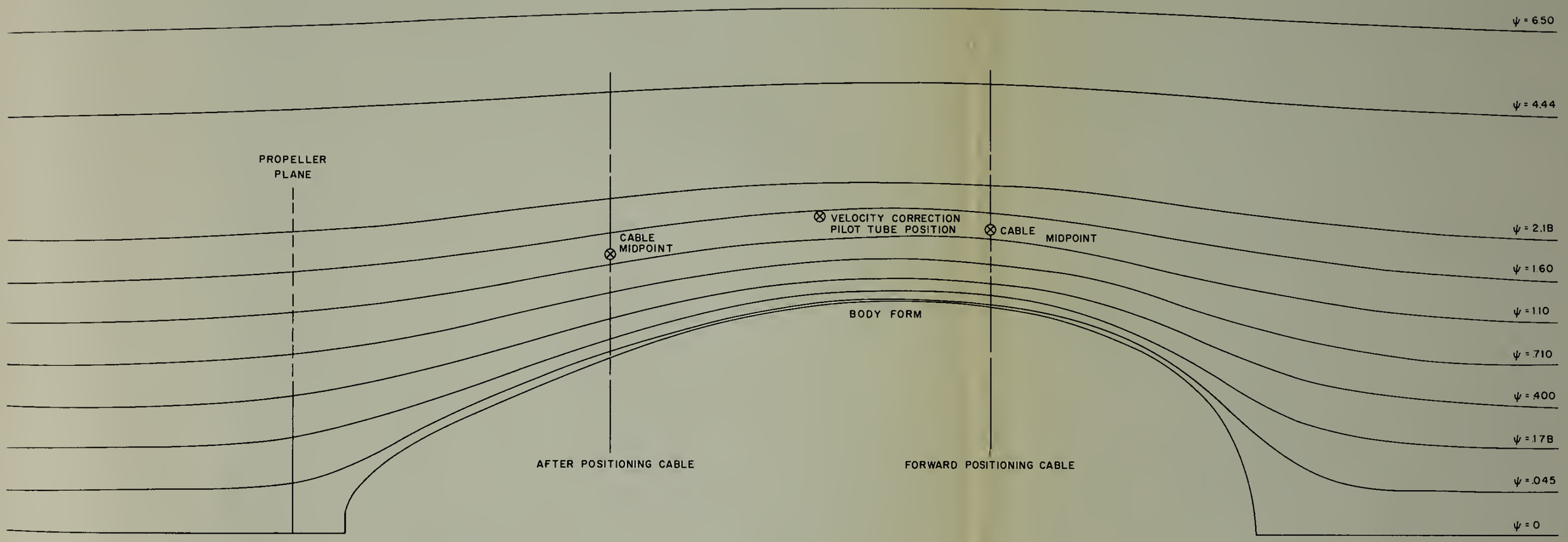

Body Development FORTRAN Program

```
C           Source Sink Program
      999   Read 1, M, N, XO, DX, WO, DW, A, B, C, D
            PRINT 4
            X = XO
            W = WO
            DO 3 J = 1, M
            DO 2 I = 1, N
            G = SQRTF ((X-B) ** 2 + W * W)
            H = SQRTF (W * W + X * X)
            E = SQRTF ((X-B-C) ** 2 + W * W)
            FV = X/H - 1.11 * W * W - (A/C) * (G-E) - (1.-A) * (X-B)/G-D
            PRINT 5, I, J, X, W, FV
        2   W = W + DW
            X = X + DX
        3   W = WO
            GO TO 999
        1   FORMAT (2I5, 8F5.3)
        4   FORMAT (/6X,1HI,7X,1HJ,10X,1HX,11X,1HW,11X,1HF..///)
        5   FORMAT (2(5X,113), 3(5X,F7.3))
            END
```

APPENDIX C

Propeller Tunnel Data Reduction Computer Program

The propeller performance data acquired during the open water test and the body disturbing flow test was reduced by the FORTRAN computer program listed in this appendix. This program was originated by Professor J. E. Kerwin. The IBM 7094 computer at the Massachusetts Institute of Technology was used for this purpose in the project.

Input

The initial data input consists of propeller dimensions, pressure and temperature conditions, plus thrust and torque parameters. Any number of cards may be added corresponding to the number of experimental runs conducted and should contain the shaft RPM, torque, and thrust observed.

Card Format

Card 1 Columns 1-6: Density (lbm/ft^3).

Columns 6-10: Kinematic viscosity (ft^2/sec).

Columns 15-16: Vapor pressure (P_v) at gage temperature.

Columns 18-19: Vapor pressure (P_v) at tunnel temperature.

Columns 21-25: Bromobenzene temperature correction.

Columns 28-31: Propeller diameter (inches).

Columns 33-37: Propeller chord at 0.7R.

Columns 39-41: Zero thrust reading.

Columns 43-45: $(P - P_v)$ at T_o.

Columns 47-49: Thrust sensitivity.

Columns 51-53: Zero torque reading.

Columns 55-59: Torque sensitivity.

Card 2 Columns 1-5: Shaft Revolution Rate (RPM)

Columns 6-8: Range of bromobenzene scale used

Columns 9-11: Bromobenze height (mm).

Columns 12-15: Atmospheric pressure (mm).

Column 16 : Large pan weights (#).

Column 18 : Small pan weights (#).

Columns 20-22: Thrust voltmeter reading (VMU).

Columns 24-26: Torque readings.

etc.

Output

The output consists of values for the thrust coefficient (K_t), torque coefficient (K_q), advance coefficient (J), and open water efficiency (e_p), which produce a fair curve between the experimental data points.

Propeller Tunnel Data Reduction Computer Program

```
      Propeller Tunnel Data Reduction Computer Program
      DIMENSION ARRAYA (40,5), ARRAYB (40,5), XKT (5),
     1 XKQ (5), SPACE (40), REMARK (12)
      E1 = .000001
      MGLSQ = 4
   16 READ 122, (REMARK (IMP), IMP = 1,12)
  122 FORMAT (12A6)
      PRINT 103, (REMARK (IMP), IMP = 1,12)
  103 FORMAT (1H1 /// 6X, 12A6 ///)
      PRINT 100
  100 FORMAT (/// 20X, 9HVAPOR BB, 9X, 24HO.7R
     1 THRUST TORQUE/6X, 59H*DENS*
     1 *VISC*PG PT CORRN DIAMT CHORD
     1 ZRO*SEN*)
      READ 101, RHO, GNU, NPVG, NPVW, BB,
     1 D, CHORD, NTZ, LZ, NTS, NQZ, QCONST
  101 FORMAT (R6.4, F7.4, 2I3, F6.3, F6.2, F6.3, 4I4, F6.3)
      IF (RHO) 11, 11, 14
   11 CALL EXIT
   14 PRINT 102, RHO, GNU, NPVG, NPVW, BB,
     1 D, CHORD, NTZ, LZ, NTS, NQZ, QCONST
  102 FORMAT (6X, F6.4, F7.4, 2I3, F6.3, F6.2,
     1 F6.3, 4I4, F6.3 ///)
```

```
      PRINT 110
110   FORMAT (21X, 6H THRUST/6X, 26H
     1 N R H P L S G Q, 484 J KT
     1 KQ E SN SV SB RN)
      TSENS = 15.0/FLOATF (NTS)
      SMALL = 10.0
      NPVQ = NPVW - NPVG
      IF (D-2.0) 1,1,2
    2 D = D/12.0
    1 QCON = 0.1*CONST
      K = 1
    3 READ 111, N, MRAN, M, L, NTA, NTB,
     1 NTC, NQ
111   FORMAT (I4, I2, 2I4, 2I2, 2I4)
      IF (N) 20, 20, 15
 15   IF (K-31) 17, 20, 20
 17   RAT = SQRTF (FLOATF(M))
      IF (MRAN-2) 4, 5, 6
    4 V = .424*BB*RAT
      GO TO 7
    5 V = .690*BB*RAT
      GO TO 7
    6 IF (MRAN-3) 8, 8, 9
    8 V = .964*BB*RAT
```

```
      GO TO 7
    9 V = 1.942*RAT
    7 RPS = FLOATF (N)/60.0
      AJ = V/(RPS*D)
      IF (AJ-SMALL) 22, 23, 23
   22   SMALL AJ
   23   VB = SQRTF (V**2+(6.2831853*0.35
     1 *RPS*D)**2)
      BUG = RHO*RPS**2*D**4
      T = 30.0*FLOATF(NTA) + 15.0*
     1 FLOATF(NTB) + FLOATF(NTC-NTZ)
     1 *TSENS + 0.00892 * FLOATF(L-LZ)
      AKT = (T + (V/21.0)**2)/BUG
      AKQ = (FLOATF(NQ-NQZ)*QCON)/
     1 (BUG * D)
      E = (AKT * AJ)/(6.2831853 * AKQ)
      L = L - NPVQ
      SIGN = FLOATF(L)/(0.1796 * RHO * RPS **
     1 2 * D ** 2)
      SIGV = SIGN/AJ**2
      SIGB = FLOATF(L)/(0.1796*RHO*VB**2)
      REYN = VB * CHORD/GNU
      PRINT 112, N, MRAN, M, L, NTA,
     1 NTB, NTC, NQ, AJ, AKT, AKQ, E, SIGN,
```

```
     1 SIGV, SIGB, REYN
112    FORMAT (6X, I4, I2, 2I4, 2I2, 2I4,
     1 3F7.4, 4F6.3, 4F6.2)
       ARRAYA (K,1) = 1.0
       ARRAYA (K,2) = AJ
       ARRAYA (K,3) = AJ**2
       ARRAYA (K,4) = AJ**3
       ARRAYA (K,5) = AKT
       ARRAYB (K,1) = 1.0
       ARRAYB (K,2) = AJ
       ARRAYB (K,3) = AJ**2
       ARRAYB (K,4) = AJ**3
       ARRAYB (K,5) = AKQ
       K = K + 1
       GO TO 3
20     K = K - 1
       CALL GLSQ (ARRAYA, XKT, SPACE, K,
     1 MGLSQ, ALPHA, E1, E1)
       CALL GLSQ (ARRAYB, XKQ, SPACE, K,
     1 MGLSQ, ALPHA, E1, E1)
       DO 12 J = 1, 40
       AJ = FLOATF(J)/20
       ARRAYA (J, 1) = AJ
       ARRAYA (J,2) = XKT(1) + (XKT(2)*AJ) +
```

```
     1 (XKT(3)*AJ**2) + (XKT(4)*AJ**3)
       ARRAYA (J,3) = XKQ(1) + (XKQ(2)*AJ) +
     1 (XKQ(3)*AJ**2) + (XKQ(4)*AJ**3)
       IF (ARRAYA (J,2)) 10,12,12
  12   CONTINUE
  10   J = J - 1
       PRINT 107
 107   FORMAT (/////// 40H    J          KT          KQ
     1 E    /)
       DO 13 I = 1,J
       EF = (ARRAYA (I,1)*ARRAYA(I,2))/
     1 (ARRAYA(I,3)*6.283189)
       IF (ARRAYA I,1) - SMALL + 0.04) 13,24,24
  24   PRINT 116, (ARRAYA(I,K), K = 1,3),EF
 116   FORMAT (F5.2, F12.4, F10.4, F9.3)
  13   CONTINUE
       GO TO 16
       END (1,1,0,0,0,0,0,1,0,1,0,0,0,0,0)
```

APPENDIX D

Pitot Tube Calibration

The pitot tube used to measure water velocities for the wake fraction calculations was initially calibrated against the bromobenzene gage permanently installed in the propeller tunnel. The pitot tube alone was placed in the water-filled test section just forward of and parallel to the propeller shaft. By regulating the impeller velocity from the tunnel control board, the circulation rate of the water was increased in incremental steps.

At each selected flow rate, the velocity was measured in millimeters on the bromobenzene gage and converted to units of feet per second through use of propeller tunnel conversion graphs. Simultaneously, the velocity at the pitot tube was measured in millimeters of water on the manometer to which it was connected. In order to convert the differences in height to standard units of velocity, the Bernoulli theorem was applied along a streamline.

FIGURE XLIX

PITOT TUBE SCHEMATIC

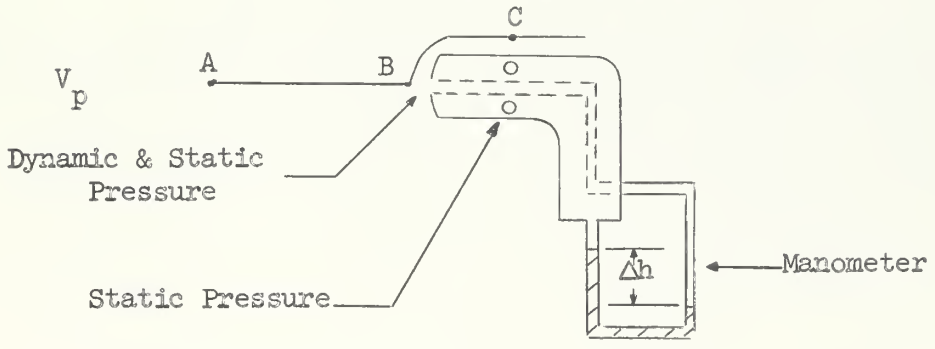

In the above figure A, B, and C are points in a streamline. Velocity and pressure at A are those obtaining in the fluid stream. The Bernoulli equation is:

$$p_A + \frac{1}{2g} \rho V_{PA}^2 = p_B \frac{1}{2g} \rho V_{PB}^2 = p_C + \frac{1}{2g} \rho V_{PC}^2 \qquad (33)$$

Since differences in level are insignificant:

$$p_A = p_C,\ V_{PB} = 0,\ V_{PA} = V_{PC} = V_P \qquad (34)$$

$$\text{Thus: } \frac{1}{2g} \rho V_{PC}^2 = \frac{1}{2g} \rho V_{PA}^2 = p_B - p_C = p_B - p_A \qquad (35)$$

$$V_P = \frac{2g\,(p_B - p_A)}{\rho} \qquad (36)$$

The difference in pressures is represented by the reading on the differential manometer. Thus the equation for velocity becomes:

$$V_P = \sqrt{\frac{2g\,\rho'}{K_1 \rho} \Delta h} \qquad (37)$$

where: K_1 = conversion constant ($305\ ^{mm}/_{ft}$)

(ρ' ≡ mass density of manometer fluid) = (ρ ≡ mass density of medium)

The equation is reduced to:

$$V_P = \sqrt{.211\ \Delta h}\ \ ^{ft}/_{sec} \qquad (38)$$

Hence, equation (38) permits conversion from manometer height differences to water flow velocity expressed in feet per second. The differences between the velocities V_P and V_C at each calibration point were then calculated.

The original data and corresponding results are tabulated below:

TABLE VII

PITOT TUBE CALIBRATION DATA

V_C (ft/sec)	Δh (mm H_2O)	V_P (ft/sec)	$V_C - V_P$ (ft/sec)
4.5	97	4.52	-.02
5.95	177	6.12	-.17
7.8	297	7.80	.00
8.3	343	8.53	-.23
9.35	406	9.27	.08
10.0	472	9.95	.05
11.25	594	11.20	.05
13.5	829	13.25	.25

The sum of the $\left[V_P - V_C\right]$ values were then averaged to determine the calibration factor, K_2, for the pitot tube.

$$V_C - V_P = .01$$

$$\left[V_P - V_C\right]_{\text{average}} = .00125$$

$$K_2 = .99875 \approx 1.0$$

APPENDIX E

Free Stream Velocity Correction

Velocity measurements in the propeller tunnel were obtained from a bromobenzene gage which was calibrated for open water propeller tests. When the model was mounted in the test chamber, the fluid flow became restricted because the model body and tunnel nozzle diameters were of the same magnitude; namely, twelve and twenty inches respectively. Consequently, the free stream velocity had to be corrected due to the boundary layer effect of the tunnel nozzle and the pressure gradient created in the open jet section of the test chamber.

In order to determine this correction, the water velocity was measured with a pitot tube positioned 2-3/8 inches radially outward from the body in the plane of the body's maximum cross section. This is approximately half the radial distance between the model surface and an imaginary extension of the nozzle wall.

Assuming that potential flow existed around the body from its nose aft to the maximum cross section, a relationship between the potential flow velocity at free stream, V_v, and the potential flow velocity at the maximum cross section, $V_{s.l.}$, was determined from the computer derived plot of streamlines.* The relation is expressed as follows:

$$\frac{V_{s.l.}}{V_v} = 1.45 \qquad (39)$$

---

* Refer to Appendix B

This assumption is based on the premise that the tunnel walls are an infinite distance from the body. However, tunnel walls actually do exist in the form of a pressure boundary. To compensate for this situation, actual measurements were made with a pitot tube positioned relative to the body at the same point at which $V_{s.l.}$ was determined from the streamline plot. It then followed from the potential flow assumption that an effective free stream velocity, V_c, must exist. Hence, the following equality resulted:

$$\frac{V_{p.t.}}{V_c} = \frac{V_{s.l.}}{V_v} \tag{40}$$

Tabulation of corrected velocity in feet per second is given in Table VIII.

TABLE VIII

EFFECTIVE FREE STREAM VELOCITY DATA

V_v	$V_{p.t.}$	V_c	$\frac{V_c}{V_v}$
3.0	4.83	3.33	1.110
4.0	5.73	3.95	.986
6.0	8.22	5.66	.944
8.0	11.1	7.65	.956
10.0	13.3	9.16	.916
12.0	16.1	11.10	.925

Taking the average of the $\frac{V_c}{V_v}$ ratios in Table VIII yields the constant used throughout this thesis to correct free stream velocity for the effects of the tunnel environment:

$$k = \frac{V_c}{V_v} = 0.972 \tag{41}$$

APPENDIX F

Voltmeter Unit Conversion Factor

In order to convert the voltmeter readings to units of force, a conversion factor expressed in voltmeter units per pound force is needed. Although there are several methods of determining this conversion factor, the method outlined in this appendix is most easily adapted to a straightforward analytical presentation.

Using the results of the unshrouded propeller test with the body disturbing flow for which data is given in Table XXV, the computer output arbitrarily selected for analysis is as follows:

N = 1204 PRM

D = 8 in. = 2/3 ft.

K_t = 0.1551

J = 0.7850

G = Thrust in voltmeter units = .380

G_o = Voltmeter units at zero thrust = .080

Using equation (8) to determine the thrust:

$$T = \rho n^2 D^4 K_t \qquad (8)$$

$$T = \left(1.938 \frac{\text{lbm}}{\text{Ft}^3}\right) \left[\frac{32.2 \text{ lbf ft/sec}^2}{32.2 \text{ lbm ft/sec}^2}\right] \left[\frac{1204 \text{ rev/min}}{60 \text{ sec/min}}\right]^2 \left[\frac{2}{3} \text{ ft}\right]^4 (.1551)$$

$$T = 24.0 \text{ lbf.}$$

Determining the adjusted thrust in voltmeter units, G_c:

$$G_c = G - G_o = .380 - .080$$

$$G_c = .300 \text{ VMU}$$

The conversion factor can now be calculated:

$$C_o = \frac{G_c}{T} = \frac{.300 \text{ VMU}}{24.0 \text{ lbs}}$$

$$C_o = 0.0125 \ {}^{\text{VMU}}/_{\text{lbf.}}$$

This conversion factor was verified frequently during the conduct of tests in the propeller tunnel.

APPENDIX G

Cable Drag Correction

During the thrust and drag tests, an error in measurement was introduced. This error was due to the drag imparted to the model by the six positioning cables. The following development serves to determine an analytical correction for this drag.

Recalling the equation for the drag on a body in a fluid

$$R = C_D \frac{1}{2} \rho S V_c^2 \qquad (4)$$

and estimating the velocity distribution around each cable, the cable drag can be calculated analytically once ρ, S, and C_D are determined. For simplicity, assume that the average velocity at each cable is at its midpoint and potential flow exists around each cable.

The forward and after cables were an average length of 4.0625 and 5.375 inches respectively and had a diameter of .0625 inches. From the plot of the potential flow streamlines, the velocity at the forward and after cables relative to the corrected open water velocity was found to be 1.620 and 1.335 respectively.

Equation (4) relates the cable drag as a function of C_D and V_c^2 since ρ and S are known constants. The drag coefficient for a cylinder normal to the flow is 1.2 for a cylinder $L/D > 20$.* However, the positioning cables are not without obstructions. Nico-press fittings concentric to the cables protrude from the body and adjusting

---

* O. W. Eshbach, HANDBOOK OF ENGINEERING FUNDAMENTALS, pp. 7-101 to 7-104.

screws project into the flow at the positioning bars.

The total cable drag on the six positioning cables is:

$$R_t = 3\,R_{f.c.} + 3\,R_{a.c.} \tag{42}$$

where $R_{f.c.}$ denotes the drag on one forward cable and $R_{a.c.}$ denotes the drag on one after cable. However, the total cable drag is proportionally transmitted to the model and the positioning bars. Therefore, let us assume that one half of this total drag is transferred to the model. Then the model drag correction becomes:

$$R_{mdc} = \frac{3}{2}\left[R_{f.c.} + R_{a.c.}\right] \tag{43}$$

where

$$R_{f.c.} = .00893\,V_c^{\,2} \tag{44}$$

and

$$R_{a.c.} = .00805\,V_c^{\,2} \tag{45}$$

By substituting equations (44) and (45) in equation (43), the model drag correction may be expressed as:

$$R_{mdc} = .0255\,V_c^{\,2} \tag{46}$$

A graphical plot of R_{mdc} vs V_c is shown in Figure L. From this figure the model cable drag at any likely model speed can be read. Hence, to reduce total measured drag or thrust to model drag or model thrust we need only subtract the model drag correction.

FIGURE L

CABLE DRAG ON HULL FORM

VS

EFFECTIVE OPEN WATER VELOCITY

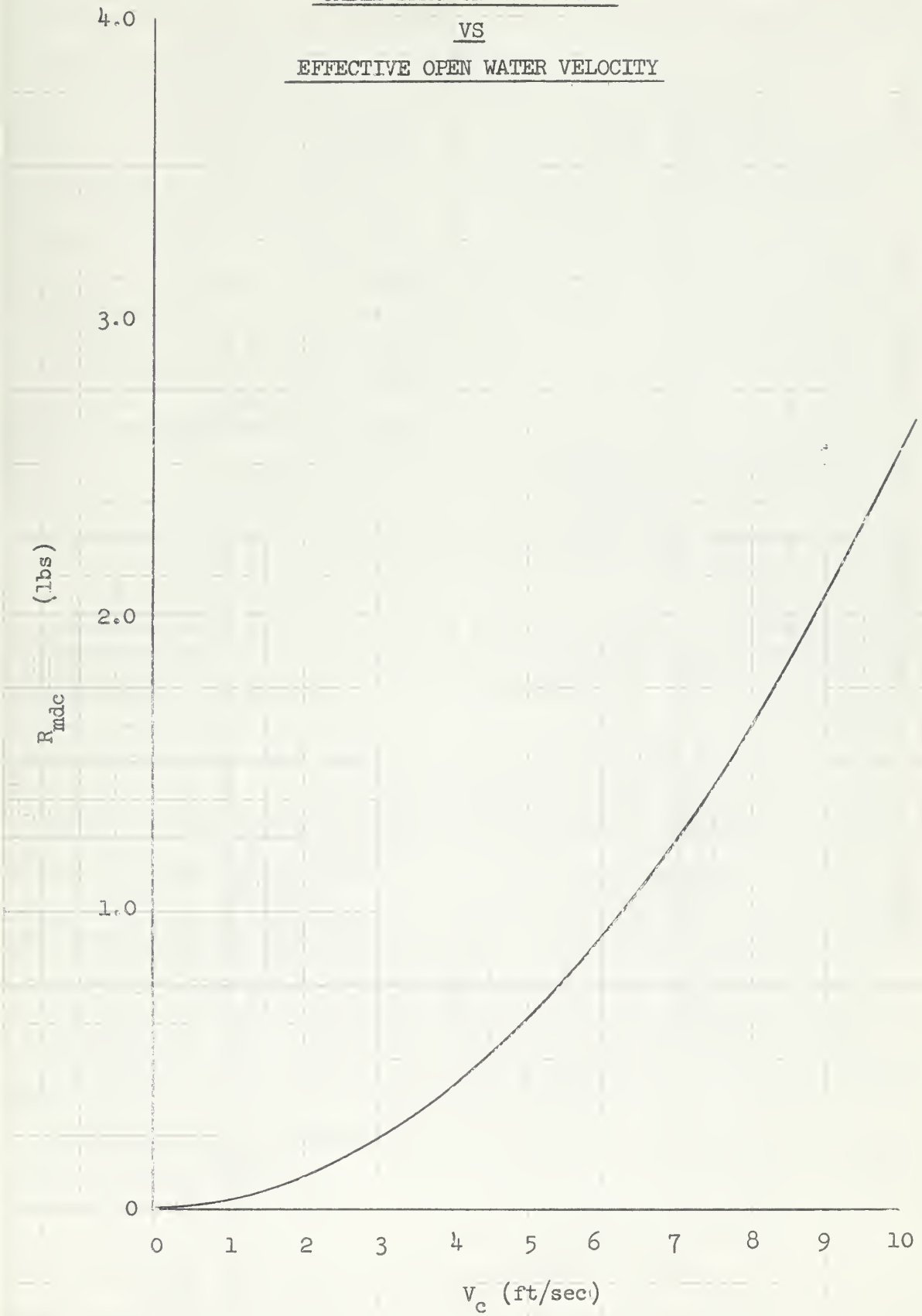

APPENDIX H

Method of Least Squares for Curve Fitting

It is often desirable to pass a curve, for which a mathematical equation is known, through a series of points. A process commonly used for this operation is the method of least squares.

The most direct manner by which to explain this process is by application to an actual problem. Considering the drag test as described in the main text of this thesis, a significant result of the test is the determination of the body drag coefficient, C_D.

It is known that the body resistance may be expressed by the drag equation:

$$R = \frac{1}{2} C_D \rho S V_c^2 \qquad (4)$$

From the drag test, there exists a measured drag for each fluid flow velocity. Hence, the method of least squares is chosen to produce a fair curve through these data points.

Since drag is proportional to the square of the velocity, a second degree polynomial equation is selected. The general form of the equation is as given in Chapter III, equation (27):

$$y = a_1 + a_2 x + a_3 x^2 \qquad (47)$$

where y represents the drag force and x denotes the corrected free stream velocity. Since the resulting curve will not pass through each data point exactly, deviations or residuals, v_i, will exist and are defined by the expression:

$$v_i = a_1 + a_2 x_i + a_3 x_i^2 - y_i \qquad (48)$$

From the preceding equation the following derivatives are obtained:

$$\frac{\partial v_i}{\partial a_1} = 1, \qquad \frac{\partial v_i}{\partial a_2} = x_i, \qquad \frac{\partial v_i}{\partial a_3} = x_i^2$$

and the sum of the squares of the deviations, S, are given by the relation:

$$S = \sum_{i=1}^{n} v_i^2 = \sum_{i=1}^{n} \left[f(x_i) - y_i \right]^2 \tag{49}$$

The unknown parameters, a_k, are then determined so that S is a minimum by the normal equation:

$$\frac{\partial S}{\partial a_k} = 2 \sum_{i=1}^{n} v_i \frac{\partial v_i}{\partial a_k} = 0 \tag{50}$$

For the specific case of the second degree polynomial with six points to fit the normal equations become:

$$\sum_{i=1}^{6} v_i \frac{\partial v_i}{\partial a_k} = 0 \qquad k = 1,2,3 \tag{51}$$

$$\sum_{i=1}^{6} (a_1 + a_2 x_i + a_3 x_i^2 - y_i) \cdot 1 = 0 \tag{52a}$$

$$\sum_{i=1}^{6} (a_1 + a_2 x_i + a_3 x_i^2 - y_i) \cdot x_i = 0 \tag{52b}$$

$$\sum_{i=1}^{6} (a_1 + a_2 x_i + a_3 x_i^2 - y_i) \cdot x_i^2 = 0 \qquad (53c)$$

On collecting the coefficients, a set of linear equations result:

$$6a_1 + \left[\sum_{i=1}^{6} x_i\right] a_2 + \left[\sum_{i=1}^{6} x_i^2\right] a_3 = \sum_{i=1}^{6} y_i \qquad (54a)$$

$$\left[\sum_{i=1}^{6} x_i\right] a_1 + \left[\sum_{i=1}^{6} x_i^2\right] a_2 + \left[\sum_{i=1}^{6} x_1^3\right] a_3 = \sum_{i=1}^{6} x_i y_i \qquad (54b)$$

$$\left[\sum_{i=1}^{6} x_i^2\right] a_1 + \left[\sum_{i=1}^{6} x_i^3\right] a_2 + \left[\sum_{i=1}^{6} x_i^4\right] a_3 = \sum_{i=1}^{6} x_i^2 y_i \qquad (54c)$$

Illustrating the use of these equations by applying actual data compiled during the unshrouded drag test:

TABLE IX

UNSHROUDED MODEL DRAG TEST DATA

Drag	0	3.21	8.33	16.06	23.99	35.73
V_c	0	3.89	5.83	7.78	9.72	11.66

Appropriate substitution yields:

$$\sum_{i=1}^{6} x_i = 38.87$$

$$\sum_{i=1}^{6} x_i^2 = 340.1$$

$$\sum_{i=1}^{6} x_i^3 = 3221.0$$

$$\sum_{i=1}^{6} x_i^4 = 32473.0$$

$$\sum_{i=1}^{6} y_i = 87.32$$

$$\sum_{i=1}^{6} x_i y_i = 834.9$$

$$\sum_{i=1}^{6} x_i^2 y_i = 8432.0$$

Hence, equations (54a), (54b), and (54c) become:

$$6\,a_1 + 38.87\,a_2 + 340.1\,a_3 = 87.32 \qquad (55a)$$

$$38.87\,a_1 + 340.1\,a_2 + 3221.0\,a_3 = 834.9 \qquad (55b)$$

$$340.1\,a_1 + 3221.0\,a_2 + 32473.0\,a_3 = 8432.0 \qquad (55c)$$

Solution of these equations yields:

$$a_1 = 0$$

$$a_2 = 0$$

$$a_3 = .2599$$

Then equation (47) simplifies to:

$$y = .2599\,x^2 \qquad (56)$$

and the drag equation becomes:

$$R = .2599\ V_c^2 \tag{57}$$

where R is the drag in pounds and V_c is the velocity in feet per second. Since,

$$R = \frac{1}{2}\ C_D\ \rho\ S\ V_c^2 \tag{4}$$

then,

$$C_D = \frac{2(.2599)}{\rho S}$$

where $S = .817\ ft^2$ and $\rho = 1.937$

Therefore, the unshrouded drag coefficient of the model based on the cross-sectional area is:

$$C_D = .328$$

The principle of least squares is applied throughout this thesis to produce accurate curve fit to plots of experimental data.

APPENDIX I

Sample Calculations

Wake Fraction

The determination of wake fraction at an uncorrected free stream velocity of 4 feet per second is used as an illustration.

Velocity in the plane of the propeller based on data from the velocity survey is plotted with respect to the distance of the pitot tube from the screw center line axis.

FIGURE LI

VELOCITY SURVEY CURVE

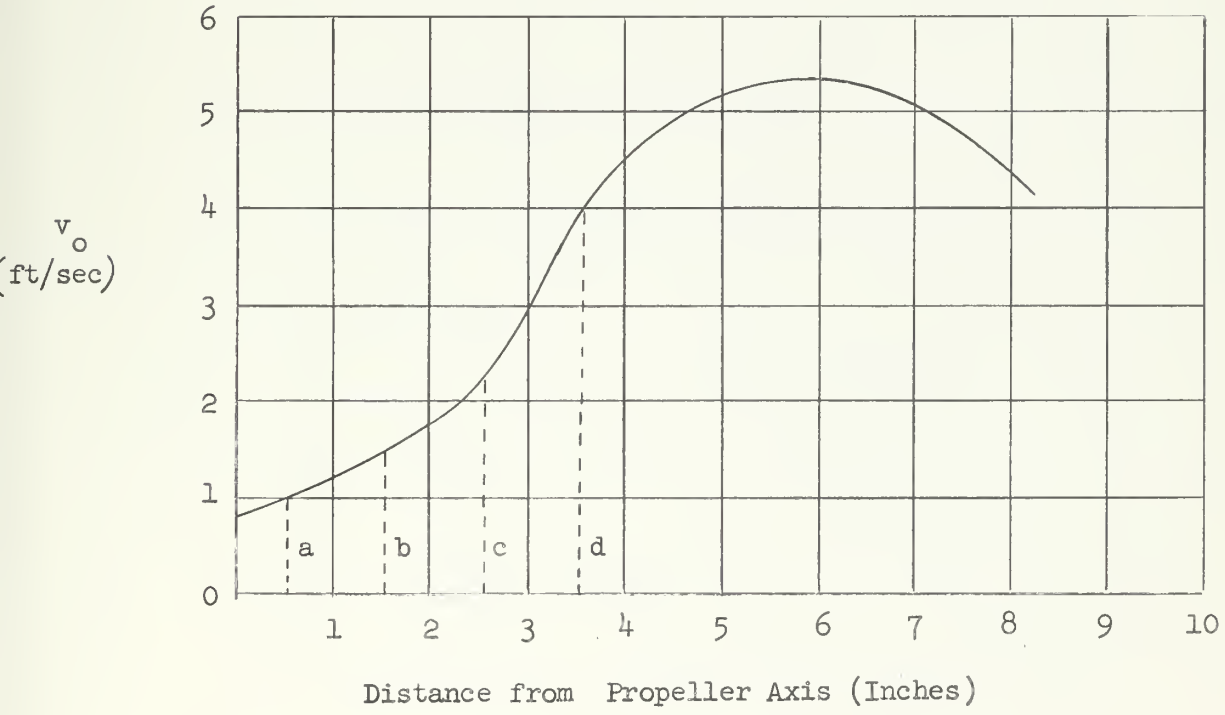

The propeller disc is divided into a series of concentric discs and the mean velocity is read graphically. Then it is weighed proportionately with its respective disc area.

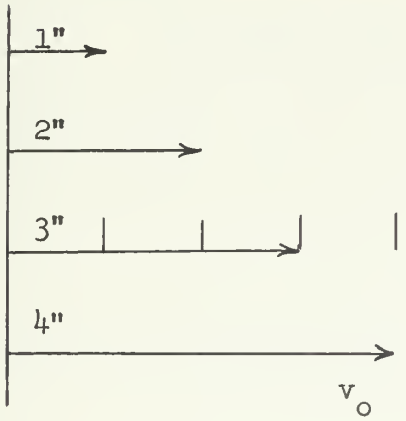

v_o	Area
a = 1.0	$1 - \pi$
b = 1.5	$2 - (4\pi - \pi) = 3\pi$
c = 2.2	$3 - (9\pi - 4\pi) = 5\pi$
d = 3.8	$4 - (16\pi - 9\pi) = 7\pi$

$$V_o = \frac{a + 3b + 5c + ... + (2p-1)m}{p^2} \qquad (14)$$

$$V_o = \frac{\left[1 + 3(1.5) + 5(2.2) + 7(3.8)\right] \pi}{16\pi}$$

$$V_o = 2.70 \ ^{ft}/_{sec}$$

With V_c also known, the wake fraction may be found:

$$1-w = \frac{V_o}{V_c} \qquad (5)$$

$$1-w = \frac{2.70}{3.89} = 0.695$$

$$w = 0.305$$

Thrust Deduction Factor

The determination of the thrust deduction factor at an uncorrected free stream velocity of 4 feet per second is used as an illustration.

From Figure XXVI, the zero value, P_o, is found to be 14.8 pounds. The value of P throughout a range of RPM values is found from equation (16).

$$P = 3W_A - W_F + \frac{VMU}{C_o} \qquad (16)$$

From data at N = 557 RPM: $W_F = W_A = 0$, VMU = .192

$$P = \frac{.192 \text{ VMU}}{.0125 \text{ VMU/lbs}} = 15.35 \text{ lbs.}$$

Now to find the thrust difference from equation (20):

$$Y - R = P - P_o \qquad (20)$$

$$P - P_o = 15.35 - 14.80 = 0.55 \text{ lbs.}$$

Similar calculations of $(P - P_o)$ are made across the range of shaft RPM analyzed resulting in an optimum operating shaft rotation rate, N.

Now to find the advance coefficient:

$$J = \frac{V_c (1-w)}{(N/60) D} \qquad (21)$$

$$J = \frac{(.972)(4)(0.695)(60)}{(535)(2/3)}$$

$$J = 0.460$$

Entering Figure XXXIII with this value of J:

$$K_t = .195$$

Hence, from equation (23) the thrust on the body and cables combined is found:

$$T_c = K_t \rho n^2 D^4 \qquad (23)$$

$$T_c = (.195)(1.9367)\left[\frac{1}{60}\right]^2 (535)^2 \left(\frac{2}{3}\right)^4$$

$$T_c = 5.81 \text{ lbs.}$$

Determining the corrected thrust by subtracting the cable drag (see Figure XLVI):

$$T = T_c - R_{mdc} \qquad (58)$$

$$T = 5.81 - .386 = 5.42 \text{ lbs.}$$

The body drag at the velocity analyzed is picked off Figure XXV.

$$R = 3.96 \text{ lbs.}$$

Now equation (6) may be solved for the thrust deduction factor:

$$1-t = \frac{R}{T} \qquad (6)$$

$$1-t = \frac{3.96}{5.42} = 0.730$$

$$t = 0.270$$

Hull Efficiency

$$e_h = \frac{1-t}{1-w} \qquad (31)$$

$$e_h = \frac{.730}{.698}$$

$$e_h = 1.04$$

APPENDIX J

Summary of Experimental Data

Velocity Survey Test - Unshrouded Condition

Test Facility - M.I.T. Propeller Tunnel

Test Date - December 23, 1965

Pitot Tube Location

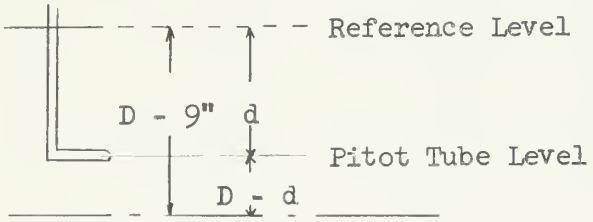

Air Temperature - 76°F

Water Temperature - 52°F

Barometric Pressure - 767.2 mm Hg.

TABLE X

V_v = 4 ft/sec = 35 mm B.B. V_c = 3.89 ft/sec				
Run	d	D - d	Δh	V_o
	inches	inches	mm H_2O	ft/sec
1	7 7/8	1 1/8	8	1.30
2	6 3/4	2 1/4	17	1.88
3	4 1/2	4 1/2	114	4.91
4	3 3/8	5 5/8	130	5.25
5	2 1/8	6 7/8	124	5.14
6	5/8	8 3/8	72	3.90
7	1 1/4	7 3/4	100	4.60
8	5 3/4	3 1/4	110	3.32

TABLE XI

V_v = 6 ft/sec = 75 mm B.B.			V_c = 5.83 ft/sec	
Run	d	D - d	Δh	v_o
	inches	inches	mm H_2O	ft/sec
1	7 7/8	1 1/8	19	2.0
2	6 3/4	2 1/4	24	2.25
3	4 1/2	4 1/2	236	7.06
4	3 3/8	5 5/8	257	7.40
5	2 1/8	6 7/8	252	7.31
6	5/8	8 3/8	135	5.35
7	1 1/4	7 3/4	200	6.50
8	6	3	80	4.10
9	5 1/2	3 1/2	179	6.15

TABLE XII

V_v = 8 ft/sec = 135 mm B.B.			V_c = 7.78 ft/sec	
Run	d	D - d	Δh	v_o
	inches	inches	mm H_2O	ft/sec
1	7 7/8	1 1/8	40	2.91
2	6 3/4	2 1/4	48	3.33
3	6	3	216	6.75
4	4 1/2	4 1/2	411	9.32
5	3 3/8	5 5/8	450	9.77
6	2 1/8	6 7/8	465	9.90
7	5/8	8 3/8	287	7.80
8	1 1/4	7 3/4	390	9.10

TABLE XIII

V_v = 10 $^{ft}/_{sec}$ = 200 mm B.B.			V_c = 9.72 $^{ft}/_{sec}$	
Run	d	D - d	Δh	v_o
	inches	inches	mm H_2O	ft/sec
1	7 7/8	1 1/8	46	3.12
2	6 3/4	2 1/4	78	4.06
3	5 3/4	3 1/4	430	9.52
4	4 1/2	4 1/2	632	11.53
5	3 3/8	5 5/8	686	12.03
6	2 1/8	6 7/8	693	12.10
7	5/8	8 3/8	447	9.75
8	1 1/4	7 3/4	574	11.0

TABLE XIV

V_v = 12 $^{ft}/_{sec}$ = 290 mm B.B.			V_c = 11.66 ft/sec	
Run	d	D - d	Δh	v_o
	inches	inches	mm H_2O	ft/sec
1	7 7/8	1 1/8	47	3.16
2	5 1/2	3 1/2	683	12.0
3	4 1/2	4 1/2	896	13.73
4	3 3/8	5 5/8	966	14.30
5	2 1/8	6 7/8	964	14.22
6	5/8	8 3/8	611	11.37
7	1 1/4	7 3/4	691	12.10

Velocity Survey Test - Shrouded Condition

Test Facility - M.I.T. Propeller Tunnel

Test Date - February 22, 1966

Pitot Tube Location

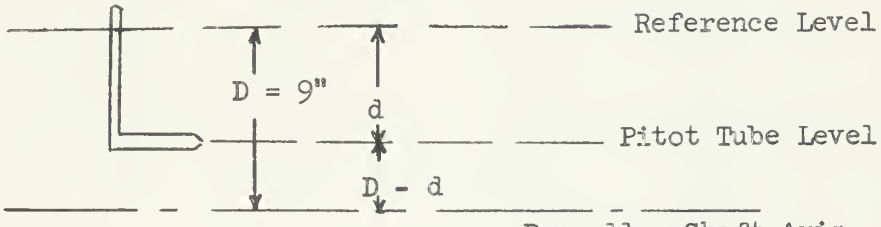

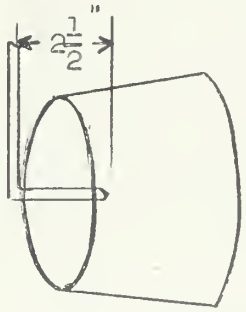

Pitot Tube Projection into the Shroud

Air Temperature - 70°F

Water Temperature - 52°F

Barometric Pressure - 767.0 mm Hg.

TABLE XV

V_v = 4 ft/sec = 35 mm B.B.			V_v = 3.89 ft/sec	
Run	d	D - d	Δh	v_o
	inches	inches	mm H_2O	ft/sec
1	9.00	0	57	3.48
2	7.80	1.20	86	4.27
3	7.05	1.95	100	4.60
4	6.29	2.71	105	4.71
5	5.84	3.16	109	4.80
6	5.25	3.75	111	4.83

TABLE XVI

V_v = 6 ft/sec = 75 mm B.B.			V_c = 5.83 ft/sec	
Run	d	D - d	Δh	v_o
	inches	inches	mm H_2O	ft/sec
1	9.00	0	118	4.99
2	7.80	1.20	178	6.15
3	7.05	1.95	211	6.70
4	6.29	2.71	239	7.11
5	5.84	3.16	260	7.41
6	5.25	3.75	265	7.50

TABLE XVII

V_v = 8 ft/sec = 135 mm B.B.			V_c = 7.78 ft/sec	
Run	d	D - d	Δh	v_o
	inches	inches	mm H_2O	ft/sec
1	9.00	0	197	6.45
2	7.80	1.20	327	8.32
3	7.05	1.95	386	9.05
4	6.29	2.71	417	9.40
5	5.84	3.16	430	9.55
6	5.25	3.75	471	9.98

TABLE XVIII

V_v = 10 ft/sec = 200 mm B.B. V_c = 9.72 ft/sec				
Run	d	D - d	Δh	v_o
	inches	inches	mm H_2O	ft/sec
1	9.00	0	336	8.41
2	7.80	1.20	530	10.58
3	7.05	1.95	609	11.32
4	6.29	2.71	650	11.70
5	5.84	3.16	668	11.87
6	5.25	3.75	680	11.98

TABLE XIX

V_v = 11 ft/sec = 240 mm B.B. V_c = 11.66 ft/sec				
Run	d	D - d	Δh	v_o
	inches	inches	mm H_2O	ft/sec
1	9.00	0	380	8.95
2	7.80	1.20	618	11.11
3	7.05	1.95	694	12.10
4	6.29	2.71	750	12.59
5	5.84	3.16	792	12.92
6	5.25	3.75	808	13.04

Drag Test - Unshrouded Condition

Test Facility - M.I.T. Propeller Tunnel

Test Date - December 23, 1965

Pitot Tube Location - d = 1 1/4 in. D = 7 3/4 in.

Voltmeter Constant - .0125 $^{VMU}/_{lb.}$

TABLE XX

Run	V_V	V_c	Δh	v_o	Pn. Wt.	Volt Wt	N
	ft/sec	ft/sec	mm H_2O	ft/sec	lbs.	VMU	RPM
1	4	3.89	100	4.60	50	.100	400
2	6	5.83	200	6.50	50	.170	405
3	8	7.78	390	9.10	50	.275	400
4	10	9.72	574	11.0	50	.385	400
5	12	11.66	691	12.1	50	.545	403

Zero Reading Calibration Data @ N = 400 RPM and V_V = 0

TABLE XXI

Pan Weights (lbs.)		0	10	20	30
VMU	Calibration 1	.690	.560	.440	.310
VMU	Calibration 2	.670	.550	.425	.295

Drag Test - Shrouded Condition

Test Facility - M.I.T. Propeller Tunnel

Test Date - February 19, 1966

Pitot Tube Location - same as unshrouded test

d = 1 1/4 in. D = 7 3/4 in.

Voltmeter Constant - .0125 $^{VMU}/_{lb.}$

TABLE XXII

Run	V_v	V_c	Pan Wt.	Volt Wt	Volt Wt	N
	ft/sec	ft/sec	lbs	VMU	lbs	RPM
1	2	1.94	0	.202	16.2	260
2	4	3.89	0	.227	18.1	262
3	6	5.83	0	.307	24.5	262
4	8	7.78	10	.288	23.0	261
5	10	9.72	20	.294	23.5	264
6	11	10.69	30	.240	19.2	264
7	12	11.66	40	.182	14.5	264

Zero Reading Calibration Data @ N = 260 RPM and V_v = 0

TABLE XXIII

Pan Weights (lbs)		0	5	10
VMU	Calibration 1	.171	.101	.040
VMU	Calibration 2	.151	.090	.020

Propeller Tests

TABLE XXIV

A. Open Water Propeller Test (Unshrouded)

Date: 17 November 1965						
Rng.	H	Prs.	Lrg. Wt.	Sml. Wt.	T_c	Q
#	mm B.B.	mm Hg.	#	#	VMU(10^{-3})	VMU(10^{-1})
1	41	779	1	1	185	151
1	107	775	1	0	308	148
1	163	773	1	0	250	146
1	192	773	1	0	220	145
1	257	769	0	1	363	142
1	288	767	0	1	340	141
1	320	774	0	1	320	140
1	397	777	0	1	275	140
1	493	779	0	1	200	138
1	534	779	0	1	185	137
2	240	776	0	1	135	135
2	308	776	0	0	245	131
2	382	775	0	0	165	128
2	480	774	0	0	75	124
2	518	773	0	0	20	122

TABLE XXV

B. Propeller with Body Disturbing Flow (Unshrouded)

Date: 30 December 1965						
Rng	H	Prs.	Lrg. Wt.	Sml. Wt.	T_c	Q
#	mm B.B.	mm Hg.	#	#	VMU(10^{-3})	VMU(10^{-1})
2	15	799	1	1	268	465
2	35	799	1	1	170	432
2	64	799	1	0	300	403
2	100	799	1	0	205	370
2	131	799	0	1	345	344
2	152	799	0	1	300	331
2	185	799	0	1	240	308
2	207	799	0	1	215	294
2	234	799	0	0	380	285
2	251	799	0	0	350	275
2	275	799	0	0	320	262
2	309	799	0	0	280	250
2	332	799	0	0	260	240
2	376	799	0	0	215	222

TABLE XXVI

C. Open Water Propeller Test (Shrouded)

Date: 26 February 1966						
Rng.	H	Prs.	Lrg. Wt.	Sml. Wt.	T_c	Q
#	mm B.B.	mm Hg.	#	#	VMU(10^{-3})	VMU(10^{-4})
2	19	780	2	0	235	178
2	33	780	2	0	157	176
2	58	780	2	0	77	173
2	73	780	1	1	259	171
2	103	780	1	1	155	167
2	125	780	1	1	112	166
2	140	780	1	0	288	164
2	175	780	1	0	218	162
2	210	780	1	0	144	160
2	269	780	1	0	41	157
2	303	780	0	1	218	154
2	375	780	0	0	339	150

TABLE XXVII

D. Propeller with Body Disturbing Flow (Shrouded)

Date: 22 February 1966						
Rng.	H	Prs.	Lrg. Wt.	Sml. Wt.	T_c	Q
#	mm B.B.	mm Hg.	#	#	VMU(10^{-3})	VMU(10^{-1})
2	14	797	1	0	340	167
2	30	797	1	0	315	166
2	51	797	1	0	270	164
2	75	797	1	0	228	163
2	90	797	1	0	199	162
2	117	797	1	0	146	160
2	143	797	0	1	320	159
2	163	797	0	1	292	158
2	180	797	0	1	271	157
2	217	797	0	1	215	155
2	245	797	0	1	183	153
2	270	797	0	0	365	152
2	295	797	0	0	340	152

TABLE XXVIII

General Propeller Test Data

Test Facility: M.I.T. Propeller Tunnel				
	A	B	C	D
Shaft Revolutions Rate (RPM)	1200	1200	1200	1200
Tunnel Temperature (°F)	62	68	58	50
Air Temperature (°F)	76	75	72	72
Mass Density (lbm/ft^3)	1.9379	1.9367	1.9386	1.9396
Kinematic Viscosity	1.1769	1.0836	1.2651	1.4080
Vapor Pressure at Tunnel Temp.	14	18	12	9
Vapor Pressure at Air Temp.	23	23	20	20
Bromobenzene Correction	0.996	0.995	0.997	0.997
Propeller Diameter (in)	8	8	8	8
Chord @ 0.7R	.250	.250	.250	.250
Thrust Zero	.043	.080	.223	.213
Thrust Sensitivity	.204	.192	.217	.212
Torque Zero	11.9	13.4	11.8	11.9
Torque Sensitivity	1.778	0.170	0.893	0.893
Barometric Pressure	770	764	754	768

Operating Point Test - Unshrouded Condition

Test Facility - M.I.T. Propeller Tunnel

Test Date - 17 February 1966

TABLE XXIX

Zero Point Readings for V_v = 3 ft/sec				
N	VMU	W_{fwd}	W_{aft}	P
RPM	+ voltmeter units	lbs	lbs	lbs
300	.148	0	0	11.83
258	.133	0	0	11.20
199	.128	0	0	10.22
150	.124	0	0	9.93
92	.115	0	0	9.21
60	.103	0	0	8.85
40	.102	0	0	8.35

TABLE XXX

Zero Point Readings for V_v = 4 thru 10 ft/sec				
N	VMU	W_{fwd}	W_{aft}	P
RPM	+ voltmeter units	lbs	lbs	lbs
300	.233	0	0	18.63
258	.218	0	0	18.20
199	.213	0	0	17.08
150	.209	0	0	16.73
92	.200	0	0	16.01
60	.188	0	0	15.70
40	.187	0	0	15.20

Operating Point Test - (Unshrouded Condition)

TABLE XXXI

V_v = 3 ft/sec		V_c = 2.92 ft/sec		
N	VMU	P	P_o	$P - P_o$
RPM	+ Voltmeter units	lbs	lbs	lbs
513	.200	16.00	8.0	+ 8.00
465	.160	12.80	8.0	+ 4.80
400	.105	8.40	8.0	+ 0.40
375	.077	6.15	8.0	- 1.85
340	.055	4.40	8.0	- 3.60

TABLE XXXII

V_v = 4 ft/sec		V_c = 3.89 ft/sec		
N	VMU	P	P_o	$P - P_o$
RPM	+ voltmeter units	lbs	lbs	lbs
650	.209	16.70	14.80	+ 1.90
600	.200	16.00	14.80	+ 1.20
557	.192	15.35	14.80	+ 0.55
505	.176	14.10	14.80	- 0.70
456	.169	13.55	14.80	- 1.25
400	.155	12.40	14.80	- 2.40

Operating Point Test - (Unshrouded Condition)

TABLE XXXIII

V_v = 6 ft/sec		V_c = 5.83 ft/sec		
N	VMJ	P	P_o	$P - P_o$
RPM	+ voltmeter units	lbs	lbs	lbs
864	.232	18.55	14.80	+ 3.75
800	.202	16.18	14.80	+ 1.38
763	.188	15.03	14.80	+ 0.23
722	.170	13.60	14.80	- 1.20
652	.136	10.90	14.80	- 3.90

TABLE XXXIV

V_v = 8 ft/sec		V_c = 7.78 ft/sec		
N	VMJ	P	P_o	$P - P_o$
RPM	+ voltmeter units	lbs	lbs	lbs
1160	.251	20.05	14.80	+ 5.25
1125	.228	18.23	14.80	+ 3.43
1048	.178	14.25	14.80	- 0.55
1004	.139	11.10	14.80	- 3.70
950	.115	9.20	14.80	- 5.60

TABLE XXXV

V_v = 10 ft/sec		V_c = 9.72 ft/sec		
N	VMJ	P	P_o	$P - P_o$
RPM	+ voltmeter units	lbs	lbs	lbs
1400	.229	18.33	14.80	+ 3.53
1284	.139	11.10	14.80	- 3.70
1208	.085	6.80	14.80	- 8.00
1157	.0417	3.30	14.80	-11.50

Operating Point Test - (Shrouded Condition)

Test Facility - M.I.T. Propeller Tunnel

Test Date - February 24, 1966

TABLE XXXVI

Zero Point Readings V_v = 3 thru 10 ft/sec				
N	VMU	W_{fwd}	W_{aft}	P
RPM		lbs	lbs	lbs
300	+ .125	0	0	10.0
251	+ .122	0	0	9.77
200	+ .120	0	0	9.60
147	+ .118	0	0	9.45
100	+ .116	0	0	9.30
50	+ .113	0	0	9.05

TABLE XXXVII

V_v = 3 ft/sec		V_c = 2.92 ft/sec		
N	VMU	P	P_o	$P - P_o$
RPM		lbs	lbs	lbs
650	+ .171	13.7	8.85	4.85
600	+ .150	12.0	8.85	3.15
550	+ .133	10.6	8.85	1.75
500	+ .110	8.90	8.85	+ 0.05
450	+ .094	7.50	8.85	- 1.35
400	+ .0731	5.85	8.85	- 3.00

Operating Point Test -(Shrouded Condition)

TABLE XXXVIII

V_v = 4 ft/sec		V_c = 3.89 ft/sec		
N	VMU	P	P_o	$P - P_o$
RPM	+ voltmeter units	lbs	lbs	lbs
800	.181	14.5	8.85	5.65
750	.163	12.1	8.85	4.20
700	.132	10.55	8.85	1.70
650	.110	8.8	8.85	- 0.05
600	.086	6.85	8.85	- 2.00
550	.064	5.13	8.85	- 3.73

TABLE XXXIX

V_v = 6 ft/sec		V_c = 5.83 ft/sec		
N	VMU	P	P_o	$P - P_o$
RPM	+ voltmeter units	lbs	lbs	lbs
1055	.173	13.80	8.85	4.95
1000	.150	12.00	8.85	3.15
956	.127	10.10	8.85	1.25
900	.098	7.80	8.85	- 1.05
850	.070	5.60	8.85	- 3.25
800	.042	3.34	8.85	- 5.51

Operating Point Test -(Shrouded Condition)

TABLE XL

V_v = 8 ft/sec			V_c = 7.78 ft/sec	
N	VMU	P	P_o	$P - P_o$
RPM	+ voltmeter units	lbs	lbs	lbs
1300	.178	14.2	8.85	5.35
1275	.161	12.9	8.85	4.05
1250	.152	12.1	8.85	3.25
1225	.125	10.0	8.85	1.15
1200	.104	8.32	8.85	- 0.53
1175	.091	7.27	8.85	- 1.59
1150	.069	5.52	8.85	- 3.33

TABLE XLI

V_v = 10 ft/sec			V_c = 9.72 ft/sec	
N	VMU	P	P_o	$P - P_o$
RPM	+ voltmeter units	lbs	lbs	lbs
1650	.210	16.80	8.85	7.95
1625	.194	15.50	8.85	6.65
1600	.173	13.80	8.85	4.95
1575	.144	11.50	8.85	2.65
1550	.126	10.10	8.85	1.25
1525	.093	7.44	8.85	- 1.41
1500	.068	5.45	8.85	- 3.40

APPENDIX K

Tabulation of Propeller Horsepower and Propulsive Coefficient

Propeller horsepower, PHP, is expressed by the equation:

$$PHP = .01142\ K_q\ \rho\ n^3\ D^5 \qquad (59)$$

A tabulation of PHP over a range of tunnel velocities based on the advance coefficient at the operating point is presented below.

TABLE XLII

UNSHROUDED CONDITION

V_v	n	J	K_q	PHP
3	6.62	.460	.0310	.0263
4	8.92	.460	.0310	.0645
6	13.25	.460	.0310	.2110
8	17.80	.460	.0310	.5130
10	22.20	.460	.0310	1.000

$$P.C. = e_p\ e_h\ e_{rr} \qquad (60)$$

$$P.C. = (.472)\ (1.060)\ (.900)$$

$$P.C. = .451$$

TABLE XLIII

SHROUDED CONDITION

V_v	n	J	K_q	PHP
3	7.75	.675	.0353	.0484
4	10.30	.675	.0353	.1130
6	15.40	.675	.0353	.3780
8	20.10	.675	.0353	.8390
10	25.35	.675	.0353	1.680

$$P.C. = e_p \, e_h \, e_{rr}^{*} \qquad (60)$$

$$P.C. = .487 \; (.669)(.900)$$

$$P.C. = .293$$

---

* e_p in the shrouded configuration is the propulsor efficiency and includes both the nozzle and propeller.